**Contract No:**

This document was prepared in conjunction with work accomplished under Contract No. DE-AC09-08SR22470 with the U.S. Department of Energy (DOE) Office of Environmental Management (EM).

**Disclaimer:**


# Defense Waste Processing Facility Simulant Chemical Processing Cell Studies for Sludge Batch 9

**Tara E. Smith**
**J. David Newell**
**Wesley H. Woodham**

August 2016
SRNL-STI-2016-00281, Revision 0

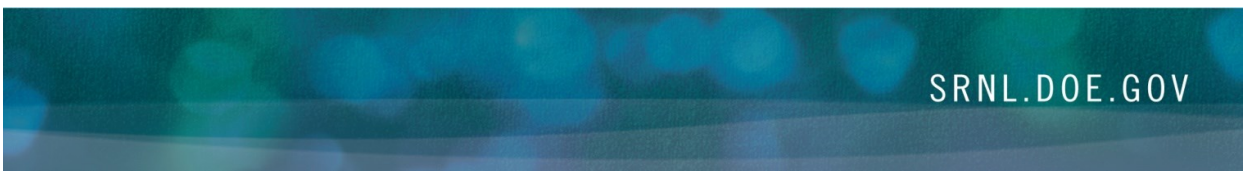

**DISCLAIMER**



**Printed in the United States of America**

**Prepared for**
**U.S. Department of Energy**

**Keywords:** *DWPF, SB9*

**Retention:** *Permanent*

# Defense Waste Processing Facility Simulant Chemical Processing Cell Studies for Sludge Batch 9

Tara E. Smith
J. David Newell
Wesley H. Woodham

August 2016

Prepared for the U.S. Department of Energy under contract number DE-AC09-08SR22470.

Savannah River National Laboratory™
OPERATED BY SAVANNAH RIVER NUCLEAR SOLUTIONS

# REVIEWS AND APPROVALS

AUTHORS:

Tara E. Smith, Separation & Actinide Science Programs Date

J. David Newell, Process Technology Programs Date

Wesley H. Woodham, Process Technology Programs Date

TECHNICAL REVIEW:

Christopher J. Martino, Process Technology Programs, Reviewed per E7 2.60 Date

APPROVAL:

Frank M. Pennebaker, Manager Date
Process Technology Programs

David E. Dooley, Director Date
E&CPT Research Programs

Eric J. Freed, Manager Date
DWPF and Saltstone Engineering

# EXECUTIVE SUMMARY

The Savannah River National Laboratory (SRNL) received a technical task request from Defense Waste Processing Facility (DWPF) and Saltstone Engineering to perform simulant tests to support the qualification of Sludge Batch 9 (SB9) and to develop the flowsheet for SB9 in the DWPF. These efforts pertained to the DWPF Chemical Process Cell (CPC). CPC experiments were performed using SB9 simulant (SB9A) to qualify SB9 for sludge-only and coupled processing using the nitric-formic flowsheet in the DWPF.

Two simulant batches were prepared, one representing SB8 Tank 40H and another representing SB9 Tank 51H [1]. The simulant used for SB9 qualification testing was prepared by blending the SB8 Tank 40H and SB9 Tank 51H simulants. The blended simulant is referred to as SB9A.

Eleven CPC experiments were run with an acid stoichiometry ranging between 105% and 145% of the Koopman minimum acid equation (KMA), which is equivalent to 109.7% and 151.5% of the Hsu minimum acid factor. Three runs were performed in the 1L laboratory scale setup, whereas the remainder were in the 4L laboratory scale setup. Sludge Receipt and Adjustment Tank (SRAT) and Slurry Mix Evaporator (SME) cycles were performed on nine of the eleven. The other two were SRAT cycles only. One coupled flowsheet and one extended run were performed for SRAT and SME processing. Samples of the condensate, sludge, and off-gas were taken to monitor the chemistry of the CPC experiments.

Experimental results indicate that 105% - 120% of the KMA is an acceptable acid window for SB9. Hydrogen exceeded (SB9A-1A 145%, SB9A-3A/SB9A-4A 130%) or approached (SB9A-5A 125%) the DWPF limit, which is established to protect the lower flammability limit (LFL), during experimental runs above 120% of the KMA. In all experiments, nitrite was destroyed to below the detectable level. Mercury appears to have been stripped to below the target of 0.45 wt.% (total solids basis) within the given conflux time for all 4L laboratory scale runs. The differences in 1L laboratory scale (i.e. reduced heat transfer coefficient, longer scaled off-gas flow path, different agitator configuration, etc.) appear to cause greater retention of mercury in the sludge, which caused SB9A-4A to not attain the mercury target within the given time. Hydrogen generation is influenced by a multitude of factors, such as heating rate, mixing, noble metal solubility, volume, etc. As a result, variation is seen between reproduced runs. Differences in the equipment scale are not the primary source of hydrogen variation between experimental runs. The REDuction/OXidation (REDOX) target was 0.15 based on DWPF and Saltstone Engineering's input for unbubbled operations. The measured and calculated (Mn electron equivalent (EE) term = 5) REDOX for SB9A-6A, 0.169 and 0.10 respectively, and SB9A-2A, 0.153 and 0.17 respectively, were near the target. Meeting the REDOX target indicated that SB9A-6A 120% KMA and SB9A-2A 105% KMA bound the SB9 acid window. If extending the acid window is desired, additional testing could be performed at lower stoichiometry. Nitrogen off-gas species, particularly $N_2O$ were significantly higher than seen in SB8 simulant testing and similar to SB7 simulant testing [2]. The waste loading was low for the sludge-only flowsheet, ranging from 27.75% to 32.17%. The coupled run, SB9A-9A, contained the greatest total solids in the SRAT (27.4%) and the greatest waste loading (36.75%). Excluding rheology, the coupled run did not adversely impact results and was bounded by the sludge-only flowsheet. The coupled flowsheet resulted in greater shear stress likely due to a higher total solids and increased sodium content.

SB9A-11A was performed similarly to SB9A-6A, but using $RuCl_3$ instead of $Ru(NO)(NO_3)_3$ as a ruthenium precursor. Noble metals are added at 125% of target, thus both catalysts provide conservative $H_2$ generation during testing. Previous sludge batch simulant studies used $RuCl_3$; however, chloride can form compounds with mercury such as calomel ($Hg_2Cl_2$), which deters mercury stripping and is not representative of DWPF feed. It was noted that SB9A-11A produced conservative levels of hydrogen; however, it was less than the hydrogen generated in SB9A-6A. Analytical results indicate that the

difference in $RuCl_3$ solubility correlates with reduced hydrogen production, which is consistent with the hypothesis that less ruthenium in solution causes less formation of hydrogen via formic acid catalysis.

# TABLE OF CONTENTS

# LIST OF TABLES

# LIST OF FIGURES

# LIST OF ABBREVIATIONS

| | |
|---|---|
| ACTL | Aiken County Technology Laboratory |
| AD | Analytical Development |
| AF C | Antifoam Carbon Contribution |
| ARP | Actinide Removal Process |
| CPC | Chemical Process Cell |
| CSTR | Continuously Stired Tank Reactor |
| CVAA | Cold Vapor Atomic Absorption Spectrometry |
| DWPF | Defense Waste Processing Facility |
| EE | Electron Equivalence |
| ELN | Electronic Laboratory Notebook |
| FAVC | Formic Acid Vent Condenser |
| FT-HNMR | Fourier Transform Hyrdogen Nuclear Magnetic Resonance |
| FTIR | Fourier Transform Infrared Spectroscopy |
| GC | Gas Chromatography |
| HMDSO | Hexamethyldisiloxane |
| HPLC | High Proformance Liquid Chromotography |
| IC | Ion Chromatography |
| ICPAES | Inductively Coupled Plasma Atomic Emission Spectroscopy |
| IOF | Input-Output Failure |
| KMA | Koopman Minimum Acid |
| M&TE | Measuring and Test Equipment |
| MAR | Measurement Acceptability Region |
| MCU | Modular Caustic Side Solvent Extraction Unit |
| MS | Mass Spectrometry |
| MS&E | Measurement Systems and Equipment |
| MST | Monosodium Titante |
| MWWT | Mercury Water Wash Tank |
| NGS | Next Generation Solvent |
| PI | Principal Investigator |
| PID | Proportional–Integral–Derivative |
| PRFT | Precipitate Reactor Feed Tank |
| PSAL | Process Science Analytical Laboratory |
| QA | Quality Assurance |
| REDOX | REDuction/OXidation |

| | |
|---|---|
| RSD | Relative Standard Deviation |
| SB9 | Sludge Batch 9 |
| SEFT | Strip Effluent Feed Tank |
| SME | Slurry Mix Evaporator |
| SRAT | Sludge Receipt and Adjustment Tank |
| SRNL | Savannah River National Laboratory |
| SRR | Savannah River Remediation |
| SVOA | Semi-Volatile Organic Analysis |
| TGA | Thermogravimetric Analysis |
| TIC | Total Inorganic Carbon |
| TMS | Trimethylsilanol |
| TOC | Total Organic Carbon |
| TS | Total Solids |
| TTQAP | Task Technical and Quality Assurance Plan |
| TTR | Technical Task Request |
| UV | Ultraviolet |
| VOA | Volatile Organic Analysis |
| WAC | Waste Acceptance Criteria |

## 1.0 Introduction

Sludge Batch 9 (SB9) simulant testing was performed using the nitric-formic flowsheet as requested by the DWPF Technical Task Request (TTR) X-TTR-S-00005, Rev. 2 and as described in SRNL-RP-2014-01059, Rev. 1 [3, 4]. The objective of this work was to perform DWPF Chemical Process Cell (CPC) Sludge Receipt and Adjustment Tank (SRAT) and Slurry Mix Evaporator (SME) simulant flowsheet testing to validate the sludge-only flowsheet and establish a coupled operation flowsheet for use with SB9 using the new antifoam addition strategy and existing nitric-formic flowsheet. Objectives were achieved by monitoring the chemistry of the CPC experiments through sampling the condensate, sludge, and off-gas. Separate studies were conducted for frit development and glass properties.

Eleven CPC experiments were run with an acid stoichiometry ranging between 105% and 145% of the Koopman minimum acid (KMA) equation, which is equivalent to 109.7% and 151.5% of the Hsu minimum acid factor, using a sludge batch 9 simulant (SB9A). Separate simulants of SB9-Tank 51 and SB8-Tank 40 were prepared and then blended to generate SB9A. Prior to each experiment, the noble metals were blended into the sludge.

Complete SRAT and SME cycles were performed in experiments SB9A-1A through SB9A-6A to validate the sludge-only flowsheet. All sludge-only flowsheet runs, except SB9A-4A, were performed at the 4L laboratory setup scale. SB9A-4A was performed at a 1L laboratory setup scale. Differences seen between the hydrogen generation seen in SB9A-3A and SB9A-4A required additional study. Thus, the SRAT cycle was only performed on SB9A-7A and SB9A-8A in the 1L laboratory scale setup to better understand the effects, if any, of the scale of the laboratory equipment used on off-gas analysis. SB9A-9A through SB9A-11A runs were performed at the 4L laboratory setup scale. The experiment SB9A-9A was performed to validate the coupled operations, in which Actinide Removal Process (ARP) simulant without monosodium titanate (MST) was added at the beginning of the SRAT cycle, and Modular Caustic Side Solvent Extraction Unit (MCU) simulant additions were added after dewater in the SRAT cycle. SB9A-10A was performed at half the boil up rate of the DWPF design basis, unlike the other experiments, and included six canister decontamination simulant additions that were added at the start of the SME cycle. SB9A-11A repeated experiment SB9A-6A using a ruthenium chloride solution instead of ruthenium nitrosyl nitrate. Previous sludge batch simulant qualifications used the ruthenium chloride. SB9A used ruthenium nitrosyl nitrate, since chloride may interfere with mercury reduction chemistry and stripping. All experiments added undiluted antifoam followed by a flush of the line with water.

A recommendation for the performance of the SRNL Shielded Cells qualification SRAT and SME run(s), with a blend of actual waste SB9 Tank 51 and SB8 Tank 40 samples, was based on the conditions used in test SB9A-6A [5]. The results of the SRNL Shielded Cells qualification SRAT and SME run(s), including glass preparation and testing, are documented in a separate series of memorandums and a final report.

## 2.0 Experimental Procedure

Eleven lab-scale CPC runs were performed with a blend of Tank 51H and Tank 40H simulants denoted as SB9A. Testing was completed at the Aiken County Technology Laboratory (ACTL). The 4L laboratory scaled CPC runs were performed in pairs; all runs were performed using 24 hour operations. Nine of the eleven SB9A experiments were complete SRAT and SME runs; whereas the other two were SRAT cycles only. Three of the eleven runs were performed in the 1L laboratory scaled setup instead of the 4L laboratory scaled setup. In SB9A-9A, the coupled flowsheet, ARP simulant without monosodium titanate and MCU simulant were added. SB9A-10 was scaled to better mimic the DWPF processing conditions by using a reduced boil up rate and adding six canister decontamination blast simulant additions.

## 2.1 Simulant Makeup

Four different simulants were generated to meet the objectives of the study: slurry, ARP, MCU, and canister decontamination. These simulants are outlined below.

### *2.1.1 Sludge Batch 9 Simulant*

Two simulant batches were prepared, one representing SB8 Tank 40H and another representing SB9 Tank 51H [1]. The simulant used for SB9 qualification testing was prepared by blending the SB8 Tank 40H and SB9 Tank 51H simulants. The blended simulant is referred to as SB9A. Inputs to the Measurement Acceptability Region (MAR) assessment included the projected chemical compositions of SB9 Tank 51H and SB9 Tank 40H, the targeted blend ratio was provided by Savannah River Remediation (SRR), and the Tank 51/Tank 40 insoluble solids ratio targeted in the "September 1, 2015 Restart (Case 1)" for nominally a 1.0 M Na end point of washed Tank 51H [6]. That case assumed consumption of SB8 at the rate of 150 canisters per year at 36% waste loading between September 1, 2015 and June 1, 2016 [7].

The simulant development was completed during a six step process:

1. **Manganese Dioxide ($MnO_2$) Preparation:** $MnO_2$ was prepared by feeding potassium permanganate at 40°C to a manganese nitrate solution at 40°C

2. **Metal Nitrate Solution Precipitation in Continuously Stirred Tank Reactor (CSTR):** The metal oxides were co-precipitated in the CSTR. A 50 wt.% NaOH solution and combined $MnO_2$ and metal nitrate solutions were fed to the CSTR at a rate sufficient to produce a precipitate at a pH of ~9.5

3. **Precipitation of Insoluble Carbonate Species:** Sodium carbonate was added to precipitate the insoluble carbonate species.

4. **Washing and Concentration Adjustment of Slurry:** The slurry was batch washed in a 55 gallon drum with inhibited water (0.001 M NaOH and 0.001 M $NaNO_2$).

5. **Add Final Insoluble Compounds to the Washed Slurry:** The remaining insoluble species were added to the washed slurry.

6. **Add Final Soluble Compounds to the Concentrated Washed Slurry:** The remaining soluble species that would have been removed during washing were added to the washed slurry.

Samples were obtained and analyzed during the preparation process as required to meet the SRR System Planning projections seen in 7.1 Appendix A: Sludge Batch 9.

Noble metals are added into the sludge immediately before each experiment at 125% of the projection. Mercury is added at 105% of the projected mercury concentration, as seen in Table 2-1.

**Table 2-1. Trim Addition of Noble Metals**

| Target Noble Metals | | |
|---|---|---|
| Trimmed Sludge Target Ag metal content | 0.0139 | total wt.% dry basis after trim |
| Trimmed Sludge Target wt.% Hg dry basis | 2.4800 | total wt.% dry basis after trim |
| Trimmed Sludge Target Pd metal content | 0.0037 | total wt.% dry basis after trim |
| Trimmed Sludge Target Rh metal content | 0.0156 | total wt.% dry basis after trim |
| Trimmed Sludge Target Ru metal content | 0.0762 | total wt.% dry basis after trim |

Each individual noble metal was weighed out dry, then slurried using DI water and a vortex mixer. The metal slurry was then poured into the vessel. The bottle was then flushed with DI water that is added to the vessel as well.

*2.1.2 ARP Simulant*

ARP simulant was generated to mimic the Precipitate Reactor Feed Tank (PRFT) addition to the SRAT. ARP was made by slowly combining the compounds in Table 2-2, then mixing for 1+ hours. MST was not added to the ARP simulant, because currently integrated salt disposition processing is running the "No MST" flowsheet. MST does not impact CPC chemistry, but it could change rheology and glass properties.

**Table 2-2. ARP Simulant**

| Compound | Molecular Formula | Target wt.% |
|---|---|---|
| DI Water | $H_2O$ | 90.28% |
| Sodium Hydroxide | NaOH | 4.82% |
| Aluminum Nitrate | $Al(NO_3)_3.9H_2O$ | 1.19% |
| Sodium Carbonate | $Na_2CO_3$ | 0.69% |
| Sodium Sulfate | $Na_2SO_4$ | 0.13% |
| Sodium Oxalate | $Na_2C_2O_4$ | 0.84% |
| Sodium Nitrate | $NaNO_3$ | 1.57% |
| Sodium Nitrite | $NaNO_2$ | 0.47% |

*2.1.3 MCU Simulant*

An MCU simulant was developed to mimic Strip Effluent Feed Tank Additions (SEFT), per Table 2-3.

**Table 2-3. MCU Simulant**

| Compound | Molecular Formula | Target wt.% |
|---|---|---|
| Water | $H_2O$ | 99.94% |
| Boric Acid | $H_3BO_3$ | 0.06% |

The 0.01 M $H_3BO_3$ solution was titrated with 50 wt.% NaOH to target a pH of 8.7 (69.5 mg/L Na). The 50/50 blended BOBCalixC6-Next Generations Solvent (NGS) (i.e. "Blended Solvent"), which was utilized in the 2012 NGS flowsheet testing, was used. The solvent addition was targeted to result in a concentration of 117.9 mg/L of total solvent in the SEFT (87 mg/L Isopar-L). Analysis was performed to

update solvent constituent levels after four years of aging and chemical degradation, in addition to quantifying any extracted elements in the solvent.

*2.1.4 Canister Decontamination Simulant*

Canister decontamination simulant was added to the SME. The laboratory simulant contains only DI water, and does not contain frit. DWPF adjusts the frit added later in the SME to account for the frit previously added during decontamination additions. The simulant experiment added the same amount of scaled frit; however, only during the frit addition portion of the SME cycle.

## 2.2 Equipment Set-up

Two 4L runs were performed at the same time using separate hoods located in 999-W Lab 132, whereas the 1L run was performed individually in 999-W Lab 134 or in parallel with a 4L run. Lab view was used to automate the CPC experiments and record real time data. Collected data includes:

- SRAT slurry temperature
- Bath temperatures for the cooling water to the SRAT condenser and Formic Acid Vent Condenser (FAVC)
- Slurry pH
- SRAT mixer speed and torque
- Air and helium purge flows (He is used as an internal standard and is set to 0.5% of the nominal SRAT air purge flow)
- Raw GC data
- Heating rod temperature and power
- Heat transfer coefficient of the heating rods
- Hood temperature
- Scrubber temperature
- Condenser flowrates
- MWWT temperature

Two heating rods were used for each CPC run. During heating to 93°C a proportional–integral–derivative PID algorithm is used to reach the temperature set point, while limiting the temperature differential between the hottest rod and the sludge to 30°C. Above 93°C, a PID algorithm is used to target a wattage set point. The wattage is adjusted by personnel to target the desired boil-up rate. Boil-up rate was determined using the graduated markings on the MWWT and a stopwatch. The pH of the sludge was monitored and the automation temperature-corrected the pH to 25°C. The 4L laboratory scale CPC setup is shown in Figure 2-1. The 1L laboratory scale CPC setup is shown in Figure 2-2


**Figure 2-1. CPC 4L setup**

**Figure 2-2. CPC 1L setup**

During CPC processing, acid and antifoam are added to the system, and samples are removed through stopcocks in an attempt to not bias the gaseous environment in the system.

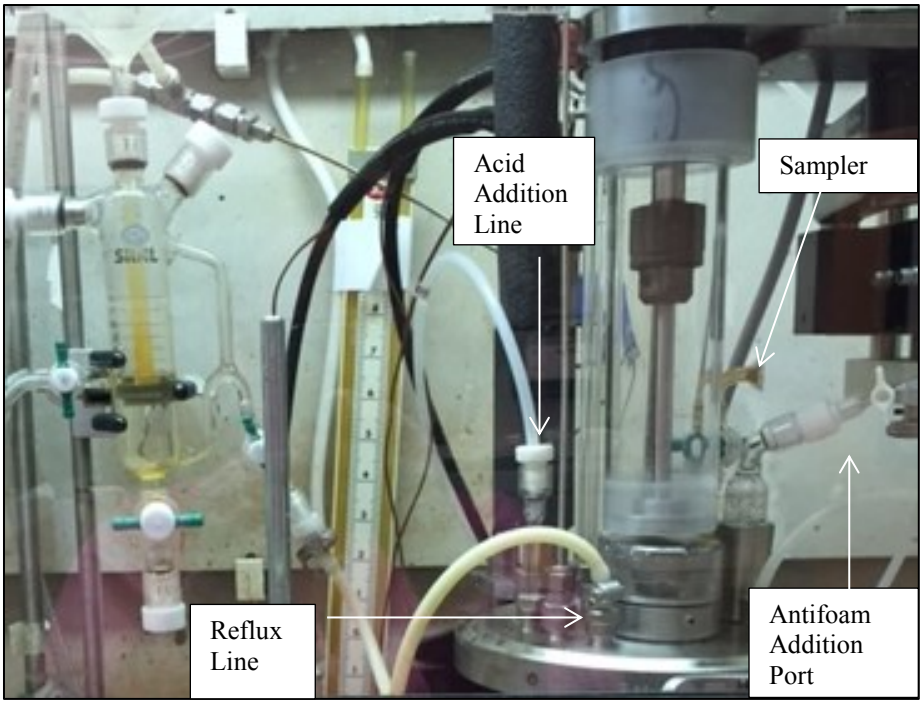


**Figure 2-3. SRAT Lid**

Off-gas passes through the SRAT/SME vessel, then passes through a condenser operated at 25°C that drops any SRAT/SME condensate vertically into the MWWT. The MWWT is filled with ~30 mL of DI water (for both the 1L and 4L) prior to starting the run. For the 4L laboratory scale setup, off-gas flows from the condenser through the ammonia scrubber. The reservoir below the ammonia scrubber was charged with a solution of 749 g of de-ionized water and 1 mL of 50 wt.% nitric acid. The dilute acid reservoir solution was recirculated by a MasterFlex driven Micropump gear pump at 120 mL per minute, to a spray nozzle at the top of the packed section. The lab-scale ammonia scrubber collects ammonia vapor in the SRAT/SME condenser off-gas for quantification of ammonia generation. For both the 4L and 1L laboratory scale setups, the off-gas next passes through the formic acid vent condenser, which is operated at 4°C. The off-gas then passes through the Nafion dryer after which the gas is sampled for analysis before exhausting to the hood. Off-gas is analyzed by gas chromatography (GC) for all runs, mass spectrometry (MS) for all 4L laboratory scale setups, and Fourier Transform Infrared (FTIR) spectroscopy for half of the 4L laboratory scale setups. The FTIR was switched from SB9A-9A to SB9A-10A, after SB9A-9A completed.

## 2.3 Experimental Run Parameters

The chemistry and DWPF processing parameters described below were used to develop the R&D directions based on mass balances that are scaled to the DWPF process. The total acid was calculated based on the KMA requirement equation (all terms have units of moles/L slurry).

$$\frac{moles\ acid}{L\ slurry} = \ base\ equivalents + Hg + soluble\ TIC + NO_2 + 1.5(Ca + Mg + Mn) \quad \text{Equation 1}$$

In the case of the coupled flowsheet, it is important to note that the calculated stoichiometry is based on the sum of the sludge simulant acid demand and the ARP simulant acid demand.

The mass balance then adjusts the ratio of formic acid to total acid to meet a target REDOX, given the input parameters. The input parameters are the assumptions for destruction and/or conversion of the acids. The input parameters are adjusted as needed between experimental runs to meet the REDOX target and ensure processability.

*2.3.1 Input Parameters*

Acid stoichiometry of experiments ranged from 105% to 145% of the KMA equation, which is equivalent to a range of 109.7% to 151.5% of the Hsu minimum acid factor. All experiments targeted a REDOX ratio of 0.15, 100% destruction of nitrite, SRAT product total solids of 25 wt.%, and SME product total solids of 48 wt.%. The assumed values for the conversion of nitrite to nitrate, destruction of formic acid, and destruction of nitrate are also listed in Table 2-4. Assumptions were adjusted as needed to meet the REDOX target. The REDOX calculation (see Equation 18) was performed using a Mn electron equivalence term of 5.

**Table 2-4. Experimental Matrix**

| Run ID # | Acid in Excess Stoichiometric Ratio | | Vessel Size | Conversion of Nitrite to Nitrate in SRAT | Destruction of Formic acid charged in SRAT | Destruction of Formic acid charged in SRAT | Destruction of Nitrate |
|---|---|---|---|---|---|---|---|
| | Koopman | Hsu | | | SRAT Cycle | SME Cycle | SME Cycle |
| SB9A-1A | 145% | 151.5% | 4L | 25% | 20% | 1.50% | 0.50% |
| SB9A-2A | 105% | 109.7% | 4L | 25% | 20% | 1.50% | 0.50% |
| SB9A-3A | 130% | 135.9% | 4L | 28.6% | 36% | 1.50% | 0.50% |
| SB9A-4A | 130% | 135.9% | 1L | 28.6% | 36% | 1.50% | 0.50% |
| SB9A-5A | 125% | 130.6% | 4L | 25% | 20% | 1.50% | 0.50% |
| SB9A-6A | 120% | 125.4% | 4L | 25% | 20% | 1.50% | 0.50% |
| SB9A-7A[a] | 120% | 125.4% | 1L | 25% | 20% | N/A | N/A |
| SB9A-8A[a] | 120% | 125.4% | 1L | 25% | 20% | | |
| SB9A-9A[b] | 120% | 125.4% | 4L | 25% | 20% | 1.50% | 0.50% |
| SB9A-10A[c] | 120% | 125.4% | 4L | 25% | 20% | 1.50% | 0.50% |
| SB9A-11A[d] | 120% | 125.4% | 4L | 25% | 20% | 1.50% | 0.50% |

[a]SRAT cycle only
[b]Coupled run (ARP and MCU included)
[c]Extended run
[d]Ruthenium chloride used in lieu of ruthenium nitrosyl nitrate

The REDOX of SB9A-1A and SB9A-2A were close to target, thus the analytical results were used to adjust the inputs for SB9A-3A and SB9A-4A. However, it was determined that the initial inputs for SB9A-1A and SB9A-2A provided more accurate targets. SB9A-9A, the coupled run, consisted of adding the ARP simulant scaled to a DWPF volume of 1,250 gallons and a MCU simulant scaled to a DWPF volume of 12,000 gallons [8, 9]. The MCU simulant targeted 0.01 M boric acid titrated with NaOH to a pH of 8.7 (69.5 mg/L Na) and 117.9 mg/L of Blended Solvent (87 mg/L Isopar-L). Solvent was added by a syringe pump immediately before the MCU simulant was pumped into the SRAT, through a port in the lid of the kettle. SB9A-10A, the extended run, was performed at a reduced boil-up rate equivalent to 2,500 lbs/hr of steam, and included six canister decontamination simulant additions. All other runs were performed at the DWPF design basis boil-up rate equivalent to 5,000 lbs/hr of steam, and canister decontamination simulant additions were not performed [10].

During SB9A-4A, the 1L was stopped slightly early (100 grams of dewater still needed in the SME) to ensure the heating rods stayed covered. The lid was redesigned to allow a greater starting volume in the future.

*2.3.2 Scaled Parameters*

Purge rates, acid addition flow rates, and boil-up rates were scaled by mass to the DWPF rates used for a DWPF SRAT receipt volume of 6,000 gallons. The DWPF SME purge rates and antifoam additions are scaled to the predicted SME starting volume. DWPF inputs used for scaling and limits are in Table 2-5. The predicted SME starting volume accounts for the starting mass of the trimmed sludge after acid addition, nitrite destruction, conversion of nitrite to nitrate, formic destruction, nitrate destruction, dewatering, and sampling. Thus, the predicted SME volume is highly dependent on the input parameters. It is important to note that after performing the experiment and receiving all results, a mass balance is performed to better estimate the SME starting volume, since the original predictions only account for the theoretical gas generation losses, which are often lower than actual.

**Table 2-5. DWPF Processing Parameters**

| DWPF Scale | | |
|---|---|---|
| SRAT Starting Volume | 6,000 | gallons |
| ARP Addition Volume | 1,250 | gallons |
| MCU Addition Volume | 12,000 | gallons |
| Volume of Water per Decon. Canister Addition | 1,000 | gallons |
| SRAT Air Purge | 230 | scfm |
| SME Air Purge | 74 | scfm |
| DWPF Nitric Acid Design Basis Addition Rate | 2.0 | gallons per minute |
| DWPF Formic Acid Design Basis Addition Rate | 2.0 | gallons per minute |
| SRAT Design Basis Boil-up Rate | 5,000 | lbs/hr |
| SME Design Basis Boil-up Rate | 5,000 | lbs/hr |
| SRAT Total Boil-up (reflux) | 60,000 | lbs |
| SRAT Mercury Product Target Concentration | 0.45 | wt.% total solids basis |
| SRAT Steam Stripping Factor | 750 | (g steam/g mercury) |
| SRAT Hydrogen Limit | 0.65 | lbs/hr |
| SME Hydrogen Limit | 0.223 | lbs/hr |

During SB9A-10A, the extended run, the boil-up rate was reduced to half of the DWPF design basis.

Antifoam additions were scaled from the DWPF addition size for a 6,000 gallon SRAT receipt, to the starting mass of the material in the laboratory scaled setup. Antifoam 747 (Lot # 110684-0413), manufactured by Siovation, was used for all additions. The DWPF 100 gallon antifoam flush that follows the antifoam addition was also scaled to the laboratory size. SME antifoam additions and the flush water are scaled to the predicted SME starting volume. The planned antifoam additions during the SRAT and SME cycle are detailed in Table 2-6.

**Table 2-6. Planned Antifoam Additions**

| | | Antifoam Addition | | | | | |
|---|---|---|---|---|---|---|---|
| | | DWPF Scale, gal | | Approximate 4L Lab Scale, g | | Approximate 1L Lab Scale, g | |
| Addition Timing | Temperature, °C | Antifoam | Flush | Antifoam | Flush | Antifoam | Flush |
| ARP Addition | 93 | 0.5 | 100 | 0.28 | 44.1 | N/A | |
| Post Nitric Acid Addition | 93 | 1.5 | | 0.77 | 51.4 | 0.32 | 21.5 |
| Post Formic Addition | 93 | 1.5 | | 0.77 | 51.4 | 0.32 | 21.5 |
| 12-Hour/Emergency Addition | Boiling (~102) | 1 | | 0.52 | 51.4 | 0.11 | 21.5 |
| Frit Cycle Addition | 95 | 1 | | 0.43 | 44.1 | 0.17 | 16.9 |
| Addition prior to SME Boiling | 93 | 0.5 | | 0.22 | 44.1 | N/A | |
| Canister Decontamination Addition | Boiling (~102) | 0.5 | | 0.22 | 44.1 | | |

### *2.3.3 Chemical Process Cell Processing*

CPC experiments are performed by R&D directions to supplement L29 ITS-0094, Laboratory Scale Chemical Process Cell Simulations. Sludge is added to the kettle. The mixer is started, and then noble metals and mercury are trimmed uniquely into the sludge at the beginning of each SRAT run. Ag, Pd, Rh, and Ru were trimmed to 125% of the target. The trimmed SRAT receipt volume was ~3.1 L in the 4 L laboratory scale and 1.3 - 1.4 L in the 1L laboratory scale. The trimmed sludge is allowed to mix for a minimum of thirty minutes prior to sampling and beginning the SRAT cycle. The sequence of steps performed is listed below. Experiments used concentrated acids and frit 803.

SRAT Cycle

- Sludge and noble metals are added to the vessel
- Trimmed sludge is mixed for 30 minutes then sampled
- Purge gases are turned on
- Ammonia scrubber recirculation pump started
- Heating rods used to heat sludge to 93°C
- ARP addition (if applicable)
    - Add antifoam
    - Heat to boiling
    - Add ARP simulant while dewatering
- Cool to 93°C
- Nitric acid addition
- Add antifoam
- Formic acid addition
- Sample
- Add antifoam
- Heat to boiling
- Dewater
    - Sample dewater
- Sample
- Reflux
    - MCU addition (if applicable)
        - Add MCU simulant and then dewater
    - Sample typically after 5 hours
    - Sample typically after 8 hours
    - Sample typically after 10 hours
    - Sample typically 30 minutes before ending
- Cool to < 50°C
- SRAT product samples
- Drain MWWT and FAVC condensate

SME Cycle

- Adjust purge rates
- Heat the sludge to 93°C
- Canister decontamination addition(s) (if applicable)
    - Add antifoam
    - Heat to boiling
    - Add Canister Decontamination Simulant
    - Dewater
    - Add Antifoam
    - Add Canister Decontamination Simulant
    - Dewater
    - Repeat antifoam, canister decontamination simulant addition, and dewater as needed
- Add frit (not at boiling)
- Add formic acid
- Add water
- Add antifoam at ~95°C
- Go to boiling
- Dewater
- Frit addition
- Heat to boiling
- Dewater (sample dewater)
- Add frit (not at boiling)
- Add formic acid
- Add water
- Add Antifoam at ~95°C
- Go to boiling
- Dewater (sample dewater)
- Cool to < 50°C
- SME product samples
- Turn off purges
- Deinventory MWWT, FAVC, Sludge

Antifoam was also added if excessive foaming occurred, and also every 12 hours from the last addition. Typically two 12 hour additions were added based on the predicted run time of the standard CPC experiments. In the case of the extended run, about four 12 hour additions were planned. CPC personnel handle samples requiring sludge to be cooled, prior to pulling large samples.

*2.3.4 Selection of Ruthenium Catalyst*

Historically, SRNL uses $RuCl_3$ as the ruthenium precursor. This introduces a greater concentration of chlorides in simulant sludge than is present in the real waste. Chlorides are known to form complexes with mercury such as calomel ($Hg_2Cl_2$). In the case of calomel, its solubility is believed to hinder stripping of mercury, thus negating proper evaluation of the processing time required to remove mercury from the SRAT. Therefore, it was previously recommended to minimize chlorides in simulant waste to improve reduction and stripping of mercury [11, 12]. Thus, for SB9A testing $Ru(NO)(NO_3)_3$ was used. $Ru(NO)(NO3)_3$ was not expected to have a significant impact on CPC chemistry given the amount of nitrogen species present in the simulant prior to noble metal addition. After comparing the results of SB9A testing, specifically SB9A-6A (120%), to SB8 simulant testing (specifically D3 120%), it was determined that hydrogen was being produced greater than expected. Hydrogen generation is influenced by a multitude of factors, such as heating rate, mixing, noble metal solubility, starting masses, etc. As a result, variation is seen between reproduced runs. The type of ruthenium precursor was adjusted to evaluate the potential impact on hydrogen generation. It was determined by SRNL and SRR to use $RuCl_3$ in SB9A-11A for comparison. Further evaluation is recommended to determine parameters affecting hydrogen generation and nitrogen chemistry.

## 2.4 Off-gas Analysis

Off-gas was monitored by GC, MS, and/or FTIR. The specific off-gas analysis used is detailed in Table 2-7.

**Table 2-7. Off-gas Monitoring Used**

| | GC | MS | FTIR |
|---|---|---|---|
| SB9A-1A | X | X | X |
| SB9A-2A | X | X | |
| SB9A-3A | X | X | X |
| SB9A-4A | X | | |
| SB9A-5A | X | X | X |
| SB9A-6A | X | X | |
| SB9A-7A | X | | |
| SB9A-8A | X | | |
| SB9A-9A | X | X | X[e] |
| SB9A-10A | X | X | X[e] |
| SB9A-11A | X | X | |

[e]Used for Portion of Experiment

Raw chromatographic data was acquired by GC on samples of the FAVC off-gas stream using a separate computer interfaced to the data acquisition computer. The chilled off-gas leaving the FAVC was passed through a Nafion dryer in counter-current flow with a dried air stream to reduce the moisture content at the GC inlet. Sampling frequency was approximately one chromatogram every 4.5 minutes. Each experiment had a dedicated Agilent (or Inficon) 3000A dual column micro GC. Column-A can collect data related to He, $H_2$, $O_2$, $N_2$, NO, and CO, while column-B can collect data related to $CO_2$, $N_2O$, and water. GC data was reprocessed after each experiment to bring the observed readings in-line with the known compositions of the calibration gas and room air, and to offset small drifts in calibration. GC's were calibrated with a standard calibration gas containing 0.510 vol.% He, 1.000 vol.% $H_2$, 20.10 vol.% $O_2$, 50.77 vol.% $N_2$, 25.1 vol.% $CO_2$ and 2.52 vol.% $N_2O$. The calibration was verified prior to starting the

SRAT cycle and after completing the SME cycle. Room air was used to give a two point calibration for $N_2$. As established previously, no evidence for CO generation has been obtained while examining the region of the chromatogram where it would elute. The GC's were baked out before and between runs to remove any potential preexisting contaminents.

The Extrel Core MS also sampled chilled off-gas leaving the FAVC that was passed through the Nafion dryer in counter-current flow with a dried air stream to reduce the moisture. A single MS was used to monitor off-gas data from the pair of CPC runs performed simultaneously with an automated sampling system. The MS sampler cycles back and forth between the off-gas streams from the two hoods taking readings every 6-7 seconds. The MS was set to scan for specific molecular weights associated with the fragments of hexamethyldisloxane (HMDSO) (mass 73 and mass 147) and off-gas compounds ($H_2$, He, $N_2$, $O_2$, NO, $NO_2$, $CO_2$, and Ar) resulting from the CPC chemistry.

A MKS FTIR was manually valved into one or the other CPC off-gas systems for the duration of the run. Since two CPC runs occurred in parallel at a time, the FTIR was typically used on the higher acid stoichiometry run of the pair. The FTIR gives $CO_2$, NO, $NO_2$, $N_2O$, $H_2O$, and HMDSO concentrations, as currently configured. HMDSO is a volatile marker for decomposed antifoam. Although the GC detects water, the FTIR gives a quantitative concentration for moisture in the chilled off-gas leaving the Nafion drier. The FTIR obtained data roughly every 19 seconds (about 7400 data sets for SB8-D4 vs. 600 GC data sets).

The purge gas for the SRAT and SME was 99.5 vol.% air and 0.5 vol.% helium (He). The He tracer enabled comparison between the GC and MS readings and allowed for instrument drift during the experiment to be corrected. The helium tracer is also used to determine the total gas flowing through the system. Because the gas components are converted from a volume basis to a mass basis using the total gas determined, leaks or ingresses of air are corrected during this calculation process. When the system is completely opened, the volume percent of He drops to zero and these data points are removed from the processed gas data. The purge rate was scaled from a DWPF SRAT purge rate of 230 scfm for 6,000 gallons of SRAT receipt and a DWPF SME purge of 74 scfm to the laboratory scale. The gas flow standard conditions for both the DWPF and laboratory scales were 21.1°C and 1 atm.

A summary of which gas species are monitored by the GC, MS, and FTIR is seen in Table 2-8.

**Table 2-8. Off-gas Analysis**

| | GC | MS | FTIR |
|---|---|---|---|
| $H_2$ | X | X | |
| $CO_2$ | X | X | X |
| NO | | X | X |
| $NO_2$ | | X | X |
| $N_2$ | X | X | |
| $N_2O$ | X | | X |
| $O_2$ | X | X | |
| He | X | X | |
| Ar | | X | |
| $NH_3$ | | | X |
| HMDSO | | | X |

2.5 Liquid Sampling

Samples were analyzed by SVOA, VOA, ICPAES, IC Cations, IC, ICPAES, TIC, TOC, UV-Vis, weight, and rheology. Condensate samples were taken from the MWWT, FAVC, ammonia scrubber, and the SRAT/SME dewater material in addition to slurry samples taken during the SRAT/SME sludge and its product. Fewer samples were planned for the 1L laboratory scale setup during the SRAT cycle to ensure the heating rods remained covered.

Samples taken during the SRAT cycle were used to monitor mercury and the progress of major reactions. Samples to be analyzed for mercury were pulled directly into digestion vials to eliminate potential segregation of mercury during sub-sampling steps. Major anions in the slurry were evaluated immediately after acid addition. Selected cations were evaluated in the SRAT supernate and the SRAT condensates. The SRAT and SME product slurries were sampled once the vessel contents had cooled slightly, but still while mixing. SRAT and SME product samples were analyzed for cation and anion composition, in addition to solids analyses and rheological characterization. The MWWT and FAVC were drained after both the SRAT and SME cycles. The condensates were weighed and elemental mercury was separated from the aqueous phase in the post-SRAT MWWT sample, and the mass of the mercury-rich material was determined.

Although there was some variation in the sample plan between runs, the basic sample plan can be seen in Table 2-9. The sample plan is consistent with previous simulant flowsheet work and what has been specified in the Task Technical and Quality Assurance Plan (TTQAP) [4]. Based on findings from additional study of mercury within the liquid waste flowsheet, it is recommended that future simulant work include cold vapor atomic absorption (CvAA Hg) to compare method sensitivities during simulant tests.

**Table 2-9. Sample Plan**

| Vessel | Sample Description | Analysis |
|---|---|---|
| SRAT | SRAT post noble metals Addition (Mixing >30 min) | Hg (digest then ICPAES), ICPAES |
| MWWT | MWWT post formic addition | SVOA, VOA |
| SRAT | SRAT post acid mercury sample | Hg (digest then ICPAES) |
| SRAT | SRAT post acid slurry (NaOH quench) | IC |
| SRAT | SRAT post acid: supernate | ICPAES |
| SCRUBBER | Post acid ammonia scrubber solution | IC Cations- $NH_4$ |
| Dewater (SMECT) | SRAT dewater condensate | SVOA, VOA, TOC, IC, ICPAES |
| SRAT | SRAT Post dewater Hg sample (from SRAT) | Hg (digest then ICPAES) |
| SRAT | SRAT slurry 5 hrs into reflux (NaOH quench) | IC |
| SRAT | SRAT 5 hrs into reflux: supernate | ICPAES |
| SRAT | SRAT 8 hrs into reflux Hg sample | Hg (digest then ICPAES) |
| SRAT | SRAT slurry 10 hrs into reflux (NaOH quench) | IC |
| SRAT | SRAT 30 minutes before end of reflux (NaOH quench) | IC |
| SRAT | SRAT product | ICPAES, IC, pH, density, TS, IS, SVOA, VOA, TIC/TOC, IC Cations- $NH_4$, rheology, Hg |
| MWWT | MWWT dewater | TS, ICPAES, SVOA, VOA |
| MWWT | MWWT (mercury bead phase) | weight |
| FAVC | SRAT FAVC | SVOA, VOA |
| SCRUBBER | Ammonia scrubber at end of SRAT | SVOA, VOA, IC Cations- $NH_4$ |
| Dewater (SMECT) | SME 1st Frit dewater | SVOA, VOA |
| Dewater (SMECT) | SME 2nd Frit dewater | SVOA, VOA |
| SME | SME product | TS, IS, SS, pH, density, ICPAES, TIC/TOC, IC Cations- $NH_4$, SVOA, VOA, rheology, Hg, REDOX |
| SCRUBBER | Ammonia scrubber acid at end of SME | SVOA, VOA, IC Cations- $NH_4$ |

All analytical instruments used were Measurement Systems and Equipment (MS&E). Balances and pipettes used are a part of the Measuring and Test Equipment (M&TE) program.

Total solids, soluble solids, and calcined solids were analyzed in the slurry. Total solids content was determined by weighing a 5 - 10 g aliquot of the slurry sample, after it was dried in a platinum crucible at 110°C in an oven for about 12 hours. The dried total solids are then calcined in an 1100°C furnace for 1 hour to determine the amount of calcined solids. Soluble solids content was determined by weighing a dried 5-10 g of 0.45 μm filtered, centrifuged slurry sample. The filtered sample was also dried in a platinum crucible at 110°C in an oven for about 12 hours. Insoluble solids are calculated by taking the difference between total solids and soluble solids.

An Agilent 730 ES ICPAES was used to analyze for metals in the supernate, slurry, and dewater using L29, ITS-0079. The ICPAES was calibrated before each run and NIST certified standards were analyzed with each set of samples to verify the calibration. Dewater samples were diluted as needed prior to performing ICPAES. Mercury was determined by ICPAES after digesting the sludge with aqua regia and diluting. Slurry samples are eluted through a 0.45 μm filter, and then diluted as needed, before being analyzed to determine Ag, Al, B, Ba, Ca, Cr, Cu, Fe, K, Li, Mg, Mn, Na, Ni, P, Pd, Rh, Ru, S, Si, Sn, Ti, Zn, and Zr in the supernate. If solids were still visible, aqua regia was performed on the filtrate prior to analysis. To determine metals in the slurry, the calcined solids were ground with a mill grinder, and then sieved to collect a powder that is less than 149 μm particle size. The powder was digested by peroxide fusion (L29 IST-0040) to determine B and Li, and also by lithium metaborate (L29 ITS-0071) and lithium tetraborate (L29 ITS-0070) to determine all other metals.

Dionex DX-500 and ICP-5000 IC were used to measure anions in the slurry and dewater via L29 ITS-0027. The IC was calibrated before each set of samples being run, and NIST certified standards were run with each set to verify the calibration. Dewater was diluted as needed prior to IC. Two grams of 50 wt.% NaOH was added to a 10 g aliquot of slurry if the sample wasn't immediately caustically quenched after being pulled. At points in the process when a significant amount of chemistry is occurring, CPC personnel add 1 mL of 50 wt.% NaOH to the sample to prevent the chemical reactions from continuing further. The aliquot was then diluted 100x, 500x, and 5000x and filtered with a 0.45μm filter prior to being analyzed for F, Cl, $NO_2$, $NO_3$, $SO_4$, $C_2O_4$, and $HCO_2$.

The SME product was converted to glass per L29 ITS-0052 after adding 50 g of 50 wt.% NaOH per kilogram of product to account for the difference in insoluble sodium between the simulant and the projections. The SME product was dried at 40-50°C until resembling a thick paste without freestanding liquid, and then placed in a sealed crucible. The crucibles are then added to a furnace at 1100°C for at least 1 hour to vitrify the material. The glass was then submitted for iron analysis by UV-Vis to determine REDOX using L29 ITS-0042. UV-Vis is used to determine the $Fe^{+2}$ content and total iron content. The $Fe^{+2}$ was subtracted from the total iron to determine the $Fe^{+3}$ in the glass. A blank is run to validate the calibration.

Dionex ICS-3000 Reagent-Free IC was used to analyze for ammonia via L16.1 ADS-2310. The sample was diluted with DI water to within the calibration curve range of 1-50 mg/L prior to being run through the IC. Calibration is performed prior to performing analysis, and a quality control sample is run with each sample set.

TIC and TOC was analyzed using L16.1 ADS-2292 by OI Analytical solids TOC to determine carbon content in the slurry and the dewater. Total carbon is found by placing the sample into a quartz cup that is sealed within the instrument. Using zirconium, carbon is catalytically oxidized and gasified. The gaseous species pass through a condenser prior to being sent to the $CO_2$ specific non-dispersive infrared detector for quantification. To determine TOC, samples were acidified with 5-7 % $H_3PO_4$, and then heated to 250°C to purge TIC. The TIC free solution was then heated to 900°C to analyze for TOC. TIC is found by subtracting the TOC from total carbon.

### 2.6 Quality Assurance

Procedures relevant to this task are outlined in the quality assurance (QA) matrix of the approved TTQAP [4]. Details of simulant preparation and lab-scale process simulations were recorded in the electronic laboratory notebook (ELN). These notebooks contain sufficient data to reproduce the simulant preparation and simulant testing, as well as containing processing data recorded manually every twenty minutes during DWPF process simulations. A higher data logging rate is typically achieved with the automated process control system (e.g. data every minute on most temperatures, agitator speeds, gas chromatograph and mass spectrometry scans, etc.), but space considerations (the electronic data would run to many hundreds of pages) preclude placing hard copies of the data in the laboratory notebooks. Instead this data is placed on the CPC database server, where they are backed-up daily by Information Technology. Details of sample analyses (final results only presented in this report) were recorded in controlled laboratory notebooks or ELN, held by either the Process Science Analytical Laboratory (PSAL) or SRNL Analytical Development (AD). Special data not recorded by the above methods, such as rheological flow curves, are included in the main body or the appendix of this report.

Requirements for performing reviews of technical reports and the extent of review are established in manual E7 2.60. SRNL documents the extent and type of review using the SRNL Technical Report Design Checklist contained in WSRC-IM-2002-00011, Rev. 2.

## 3.0 Results and Discussion

Eleven CPC experiments with an acid stoichiometry ranging between 105% and 145% of the KMA equation, equivalent to 109.7% and 151.5% of the Hsu minimum acid factor, using SB9A were performed. Separate simulants of SB9-Tank 51H and SB8-Tank 40H were prepared, then blended and trimmed to generate SB9A. All experiments utilized a new antifoam strategy, where antifoam was added undiluted, then the line was flushed with water. Prior to each experiment, the noble metals were blended into the sludge. The experiments performed were used to validate the sludge-only and coupled flowsheets.

### 3.1 Simulants Used

The Tank 51H and 40H simulants were sampled and analyzed by the PSAL. The results of these analyses are summarized and compared to their respective compositional targets in Table 3-1. The final SB9A simulant used in testing is presented in Table 3-2. Anion and physical property data are presented in Table 3-3 and Table 3-4.

**Table 3-1. SB9 Tank 51H and SB8 Tank 40H Elemental Calcined Solids**

| Calcine Solids | Normalized Target for SB9 Tank 51H Waste, wt.% | SB9 Tank 51H Simulant Waste, wt.% | Normalized Target for SB8 Tank 40H, wt.% | SB8 Tank 40 Simulant Waste, wt.% |
|---|---|---|---|---|
| Al | 9.65 | 9.83 | 10.0 | 8.97 |
| B | - | <0.100 | - | - |
| Ba | - | <0.100 | 0.122 | 0.119 |
| Ca | 1.43 | 1.66 | 1.39 | 1.42 |
| Ce | 0.245 | <0.100 | 0.304 | 0.246 |
| Cr | - | 0.203 | 0.104 | 0.086 |
| Cu | - | 0.146 | 0.100 | 0.149 |
| Fe | 24.7 | 24.4 | 24.2 | 23.8 |
| K | 0.147 | <0.100 | 0.152 | <0.100 |
| La | - | <0.100 | 0.074 | <0.100 |
| Li | - | <0.100 | 0.020 | <0.100 |
| Mg | 0.299 | 0.272 | 0.328 | 0.283 |
| Mn | 8.10 | 8.48 | 7.58 | 7.57 |
| Na | 20.4 | 14.4 | 20.8 | 15.6 |
| Ni | 1.06 | 0.843 | 2.35 | 2.22 |
| Pb | - | <0.100 | 0.049 | <0.100 |
| S | 0.223 | 0.104 | 0.493 | 0.433 |
| Si | 2.41 | 2.91 | 1.58 | 1.92 |
| Ti | - | <0.100 | 0.020 | <0.100 |
| Zn | - | <0.100 | 0.038 | <0.100 |
| Zr | - | 0.161 | 0.094 | <0.100 |

**Table 3-2. SB9A Blended Tank 40H Elemental Calcined Solids**

| Calcine Solids | Normalized Target for SB9A Blended Waste, wt.% | SB9A Simulant Waste, wt.% |
|---|---|---|
| Al | 9.78 | 9.83 |
| B | 0.016 | <0.100 |
| Ba | 0.066 | 0.094 |
| Ca | 1.40 | 1.53 |
| Ce | 0.275 | 0.162 |
| Cr | 0.057 | 0.132 |
| Cu | 0.054 | 0.098 |
| Fe | 24.3 | 25.2 |
| K | 0.149 | <0.100 |
| La | 0.040 | <0.100 |
| Li | 0.011 | <0.100 |
| Mg | 0.313 | 0.293 |
| Mn | 7.77 | 8.74 |
| Na | 20.5 | 15.0 |
| Ni | 1.76 | 1.78 |
| Pb | 0.026 | <0.100 |
| S | 0.368 | 0.263 |
| Si | 1.94 | 2.41 |
| Ti | 0.011 | <0.100 |
| Zn | 0.021 | <0.100 |
| Zr | 0.051 | <0.100 |

Except for Ba, Ce, Cr, Cu, Mn, Na, S and Si, all species are within 10% of target. Ba, Ce, Cr, and Cu are minor components of the sludge. Sulfur is difficult to measure. Silicon remains inert during SRAT and SME processing. Manganese is 12.5% over target, which will cause increased acid consumption. There is an obvious difference in the projected sodium concentrations and measured concentrations in the simulants. This difference results from the amount of insoluble sodium present in the sludge. Currently, there is no strategy for simulating insoluble sodium. Therefore, the supernatant sodium concentration was targeted. Insoluble sodium does not contribute to the chemical reactions occurring during CPC processing. It does, however, have an impact on glass formulation of the SME product. For this reason, it was decided that sodium hydroxide would be trimmed into the SME product prior to making glass in order to achieve a final sodium concentration comparable to the targeted concentration. Sodium hydroxide was selected to add sodium because it would not adversely affect glass chemistry, like sodium chloride or sodium nitrate, and would not significantly cause off-gasing during simulated melter work like sodium carbonate.

**Table 3-3. Anion Composition, mg/kg slurry**

| | Tank 51H Target | Tank 51H Actual | Tank 40H Target | Tank 40H Actual | SB9A Target | SB9A Actual |
|---|---|---|---|---|---|---|
| $NO_2$ | 12090 | 12900 | 12010 | 12750 | 10640 | 10200 |
| $NO_3$ | 7085 | 7595 | 7262 | 7140 | 6318 | 5725 |
| $SO_4$ | 1175 | 639 | 2330 | 2230 | 1619 | 1235 |
| $C_2O_4$ | 3495 | 3265 | 1591 | 4720 | 2062 | 3980 |
| Na | 19010 | 22240 | 20000 | 21470 | 17280 | 18200 |
| TIC | 1391 | 2303 | 1180 | 1186 | 1292 | 1619 |

**Table 3-4. Physical Properties of Tank 51H, Tank 40H and SB9A Sludge Simulant**

| | Tank 51H Target | Tank 51H Actual | Tank 40H Target | Tank 40H Actual | SB9A Target | SB9A Actual |
|---|---|---|---|---|---|---|
| Total Solids, wt.% | 18.97 | 20.44 | 17.21 | 17.61 | 15.94 | 15.3 |
| Insoluble Solids, wt.% | 13.74 | 12.03 | 11.32 | 9.06 | 10.79 | 10.6 |
| Calcined Solids, wt.% | 12.35 | 15.24 | 13.13 | 13.25 | 12.35 | 11.74 |
| Soluble Solids, wt.% | 5.15 | 8.41 | 5.89 | 8.55 | 5.15 | 4.70 |
| Slurry Density, g/mL | 1.14 | 1.16 | 1.16 | 1.15 | 1.13 | 1.12 |
| Supernate Density, g/mL | 1.05 | 1.05 | 1.06 | 1.05 | 1.05 | 1.04 |

Using the SB9A simulant analytical data, the inputs in Table 3-5 were developed for use in the acid calculation.

**Table 3-5. Target Sludge Simulant Parameters**

| Parameter | SB9A Simulant | Parameter | SB9A Simulant |
|---|---|---|---|
| Target Sludge (untrimmed) added to 4L vessel, g | 3,330 | Fresh Sludge Nitrite, mg/kg | 10,200 |
| Trimmed Sludge Target Ag metal content, wt.% | 0.0139 | Fresh Sludge Nitrate, mg/kg | 5,725 |
| Trimmed Sludge Target wt.% Hg dry basis | 2.48 | Fresh Sludge Sulfate, mg/kg | 1,235 |
| Trimmed Sludge Target Pd metal content, wt.% | 0.0037 | Fresh Sludge Oxalate, mg/kg | 3514 |
| Trimmed Sludge Target Rh metal content, wt.% | 0.0156 | Fresh Sludge Manganese (% of Calcined Solids) | 8.74 |
| Trimmed Sludge Target Ru metal content, wt.% | 0.0762 | Fresh Sludge Calcium (% of Calcined Solids) | 1.53 |
| Fresh Sludge Weight % Total Solids | 15.25 | Fresh Sludge Magnesium (% of Calcined Solids) | 0.293 |
| Fresh Sludge Weight % Calcined Solids | 11.74 | Fresh Sludge Slurry TIC, mg/kg slurry | 1,619 |
| Fresh Sludge Weight % Insoluble Solids | 10.55 | Fresh Sludge Base Equivalent molarity pH = 7 | 0.483 |
| Fresh Sludge Density, g/mL | 1.1215 | Fresh Sludge Supernate TIC, mg/L Supernate | 1,671 |

The BOBCalixC6-NGS solvent used in SB9A-9A was previously used for NGS flowsheet testing at SRNL. Analysis, seen in Table 3-6, indicates that the solvent density is within the MCU operating range of 0.82 - 0.85 g/cc and near nominal concentrations. TiDG has undergone chemical degradation for four years and is thus lower than nominal (1.44E+05 mg/L, i.e. 3 mM). Typically titration is considered a more accurate measurement and has a 10% analytical uncertainty compared to 20% for FT-HNMR. The FT-HNMR can bias high, due to the interference of other amines resulting from degradation products, and/or impurities in the solvent. The lower FT-HNMR measurement may point to issues with the FT-HNMR standards. Further investigation of the standards was inconclusive. However, SRNL recently studied the chemical degradation of TiDG in non-radioactive solvent standards over time resulting in the development of a first and second order rate equations [13]. These rate equations predict TiDG levels at 26.9% ($1^{st}$ order) and 57.0% ($2^{nd}$ order) of nominal after 4 years. The second order rate law is statistically similar to the FT-HNMR measurement. Therefore, the TiDG is likely at ~52% of nominal, which is

within the typical bounds of MCU operating conditions. Cesium was present at 11.83 mg/L in the solvent, assuming Cs-137 only, this would be equivalent to 3.89 Ci/gal, which is significantly below the current DWPF WAC limit of 16.2 Ci/gal. The pH of the MCU facility BOBCalixC6-NGS solvent is typically around 6. The pH of the used BOBCalixC6-NGS simulant indicates that the material did not undergo stripping. Thus, the pH of the solvent was more basic, ~12.9, than typically sent to DWPF and has minimal impact on acid consumption. Analysis was not performed for Na or K to determine if the solvent was scrubbed. A carbon steel tank is used at EDL for flowsheet testing, which is likely why some metals (like Cu) are higher than expected. The acidity and metal content in the solvent are expected to have negligible impact on the CPC chemistry due to the amount of solvent added.

**Table 3-6. BOBCalixC6-NGS Solvent Analysis**

| Analysis | | Results, mg/L | 50/50 Blend Target, mg/L | % of Nominal |
|---|---|---|---|---|
| Isopar-L | FT-HNMR | 6.23E+05 | 6.23E+05 | 100.0% |
| | TGA | 6.31E+05 | | 101.2% |
| Modifier | HPLC | 1.65E+05 | 1.69E+05 | 97.6% |
| | FT-HNMR | 1.71E+05 | | 101.0% |
| | TGA | 1.67E+05 | | 98.5% |
| TiDG | Titration | 1.29E+03 | 1.44E+03 | 83.8% |
| | FT-HNMR | 7.49E+02 | | 52.0% |
| TOA | Titration | 4.80E+02 | 5.30E+02 | 90.6% |
| MaxCalix | FT-HNMR | 4.84E+04 | 4.44E+04 | 109.0% |
| | TGA | 4.15E+04 | | 93.4% |
| BOBCalixC6 | HPLC | 4.46E+03 | 4.03E+03 | 109.0% |
| Solvent Density | | 0.8333 | 0.8384 | N/A |
| Solvent pH | | 12.87 | ~ 6 | N/A |
| Cs | ICPMS | 11.83 | N/A | N/A |
| Cu | ICPMS | 2.35 | N/A | N/A |
| Sr | ICPMS | 0.32 | N/A | N/A |
| Zr | ICPMS | 0.20 | N/A | N/A |
| Mo | ICPMS | 0.34 | N/A | N/A |
| Sn | ICPMS | 0.15 | N/A | N/A |
| Ba | ICPMS | 0.47 | N/A | N/A |
| Pb | ICPMS | 0.28 | N/A | N/A |

The ARP simulant results can be seen below. MST was not added to the ARP simulant.

**Table 3-7. ARP Simulant Anions and Cations**

| Al, mg/Kg | Ca, mg/Kg | Cu, mg/Kg | K, mg/Kg | Na, mg/Kg | S, mg/Kg | $NO_2$, mg/Kg | $NO_3$, mg/Kg | $SO_4$, mg/Kg | $C_2O_4$, mg/Kg |
|---|---|---|---|---|---|---|---|---|---|
| 899 | 1.73 | 0.21 | 1.69 | 41,570 | 315 | 3,517 | 17,570 | 847 | 5,492 |

**Table 3-8. ARP Simulant Properties**

| Total Solids, wt.% | Soluble Solids, wt.% | Insoluble Solids, wt.% | pH | Density, g/cc |
|---|---|---|---|---|
| 7.57% | 7.53% | <0.10% | 13.71 | 1.056 |

## 3.2 Results from Flowsheet Simulant Testing

Eleven CPC experiments with an acid stoichiometry ranging between 105% and 145% of the KMA equation, which is equivalent to 109.7% and 151.5% of the Hsu minimum acid factor using SB9A were performed.

### *3.2.1 Acid Stoichiometry*

The experiments, described in Table 2-4, were performed to support SB9 qualification with the SB9A simulant. All experiments targeted a REDOX ratio (measured using $Fe^{+2}$/Total Fe analytical results) of 0.15, 100% destruction of nitrite, SRAT product total solids of 25%, SME product total solids of 48%, and a sludge oxide contribution (waste loading) of 36%. After loading the SB9A sludge simulant into the vessel the noble metals and mercury were blended into the sludge. A summary of the run results can be seen in Table 3-9 and Table 3-10. The data will be discussed in detail in the following subsections.

**Table 3-9. Summary of Actual SB9A-1A through SB9A-6A Results**

| | Vessel | SB9A-1A | SB9A-2A | SB9A-3A | SB9A-4A | SB9A-5A | SB9A-6A |
|---|---|---|---|---|---|---|---|
| **Acid Stoichiometry** | SRAT | 145% | 105% | 130% | 130% | 125% | 120% |
| **Untrimmed Sludge, g** | SRAT | 3299.8 | 3299.5 | 3298.6 | 1362.7 | 3297.1 | 3296.5 |
| **Ratio of Formic to Total Acid** | SRAT | 0.847 | 0.884 | 0.907 | 0.909 | 0.862 | 0.867 |
| **Formic Acid Added, moles** | SRAT | 4.68 | 3.54 | 4.46 | 1.86 | 4.11 | 3.96 |
| **Nitric Acid Added, moles** | SRAT | 0.84 | 0.47 | 0.46 | 0.19 | 0.65 | 0.61 |
| **Total Acid Added, moles** | SRAT | 5.52 | 4.00 | 4.92 | 2.04 | 4.76 | 4.57 |
| **Nitrate Removal in Dewater** | SRAT | 0.6% | 6.6% | 1.6% | 7.0% | 3.2% | 1.4% |
| **Nitrate Loss** | SRAT | 13.3% | -14.4% | 7.4% | -4.7% | -4.1% | -4.7% |
| | SME | 7.5% | 10.0% | 8.6% | 0.5% | 10.4% | 0.0% |
| **Remaining Nitrite, mg/Kg** | SRAT | < 100 | < 100 | < 100 | < 100 | < 500 | < 500 |
| **Formate Removal in Dewater** | SRAT | 1.8% | 0.3% | 1.1% | 0.8% | 0.7% | 0.4% |
| **Loss of Formic acid charged** | SRAT | 51.8% | 35.1% | 38.4% | 40.5% | 43.9% | 36.9% |
| | SME | 12.5% | 8.3% | 9.2% | 0.1% | 13.0% | 5.2% |
| **Conversion of Nitrate to Ammonium** | SRAT | 0.00% | 0.00% | 11.68% | 10.09% | 4.70% | 3.79% |
| | SMR | 4.90% | 0.38% | 11.82% | 12.07% | 3.93% | 3.48% |
| **REDOX ($Fe^{+2}/Fe^{Total}$)** | SME | All $Fe^{+3}$ | 0.153 | 0.210 | 0.373 | 0.094 | 0.169 |
| **Total Solids wt.%** | SRAT | 22.6% | 24.3% | 24.3% | 22.8% | 24.3% | 24.9% |
| | SME | 45.7% | 47.5% | 47.6% | 41.6% | 46.6% | 48.9% |
| **Sludge Oxide Contribution (Waste Loading) based on $Fe_2O_3$** | SME | 30.94% | 30.51% | 28.62% | 27.26% | 31.96% | 32.17% |
| **Max $CO_2$ lb/hr, MS** | SRAT | 701.99 | 679.33 | 719.65 | N/A | 748.30 | 710.03 |
| | SME | 135.11 | 46.63 | 82.72 | | 123.96 | 83.08 |
| **Max $CO_2$ lb/hr, FTIR** | SRAT | 736.57 | N/A | 751.47 | N/A | 783.05 | N/A |
| | SME | 138.09 | | 82.57 | | 126.93 | |
| **Max $CO_2$ lb/hr, GC** | SRAT | 698.16 | 754.94 | 717.49 | 697.02 | 730.14 | 734.25 |
| | SME | 107.71 | 47.97 | 68.74 | 49.61 | 112.94 | 72.25 |
| **Max $N_2O$ lb/hr, GC** | SRAT | 37.69 | 31.77 | 39.36 | 49.02 | 34.93 | 38.07 |
| | SME | 0.00 | 0.00 | 0.00 | 0.00 | 0.00 | 0.00 |
| **Max $N_2O$ lb/hr, FTIR** | SRAT | 39.44 | N/A | 37.54 | N/A | 35.81 | N/A |
| | SME | 0.04 | | 0.03 | | 0.02 | |
| **Max $H_2$ lb/hr, MS** | SRAT | 1.33 | 0.02 | 0.69 | N/A | 0.48 | 0.33 |
| | SME | 0.16 | 0.00 | 0.18 | | 0.22 | 0.12 |
| **Max $H_2$ lb/hr, GC** | SRAT | 1.142 | 0.023 | 0.656 | 0.413 | 0.432 | 0.323 |
| | SME | 0.151 | 0.007 | 0.177 | 0.067 | 0.208 | 0.127 |
| **Max NO lb/hr, MS** | SRAT | 7.02 | 2.02 | 2.84 | N/A | 3.85 | 1.64 |
| | SME | 0.08 | 0.10 | 0.09 | | 0.13 | 0.17 |
| **Max NO lb/hr, FTIR** | SRAT | 4.15 | N/A | 1.98 | N/A | 2.44 | N/A |
| | SME | 0.01 | | 0.02 | | 0.07 | |
| **Max $NO_2$ lb/hr, MS** | SRAT | 20.99 | 17.12 | 24.83 | N/A | 24.69 | 26.37 |
| | SME | 0.16 | 0.18 | 0.15 | | 0.21 | 0.20 |
| **Max $NO_2$ lb/hr, FTIR** | SRAT | 17.09 | N/A | 20.17 | N/A | 18.59 | N/A |
| | SME | 0.01 | | 0.02 | | 0.06 | |

N/A is based on Table 2-4, Table 2-7, and Table 2-8

**Table 3-10. Summary of Actual SB9A-7A through SB9A-11A Results**

| | Vessel | SB9A-7A | SB9A-8A | SB9A-9A | SB9A-10A | SB9A-11A |
|---|---|---|---|---|---|---|
| **Acid Stoichiometry** | SRAT | 120% | 120% | 120% | 120% | 120% |
| **Untrimmed Sludge, g** | SRAT | 1271.5 | 1271.8 | 3298.7 | 3299.2 | 3300.0 |
| **Ratio of Formic to Total Acid** | SRAT | 0.862 | 0.862 | 0.887 | 0.876 | 0.869 |
| **Formic Acid Added, moles** | SRAT | 1.58 | 1.57 | 4.46 | 3.99 | 3.97 |
| **Nitric Acid Added, moles** | SRAT | 1.83 | 1.82 | 5.02 | 4.56 | 4.57 |
| **Total Acid Added, moles** | SRAT | 1.58 | 1.57 | 4.46 | 3.99 | 3.97 |
| **Nitrate Removal in Dewater** | SRAT | 1.1% | 6.7% | 10.5% | 2.4% | 5.7% |
| **Nitrate Loss** | SRAT | 7.2% | 11.3% | -7.6% | -4.8% | -4.5% |
| | SME | N/A | N/A | 12.3% | 8.7% | 0.0% |
| **Remaining Nitrite, mg/Kg** | SRAT | < 500 | < 500 | < 500 | < 500 | < 500 |
| **Formate Removal in Dewater** | SRAT | 0.7% | 1.0% | 0.5% | 0.0% | 0.0% |
| **Loss of Formic acid charged** | SRAT | 44.4% | 52.2% | 36.5% | 48.8% | 32.3% |
| | SME | N/A | N/A | 20.8% | 19.8% | 10.0% |
| **Conversion of Nitrate to Ammonium** | SRAT | 0.0% | 3.03% | 1.48% | 5.09% | 0.82% |
| | SME | N/A | N/A | 1.95% | 2.94% | 0.95% |
| **REDOX ($Fe^{+2+}/Fe_{Total}$)** | SME | | | 0.152 | 0.021 | 0.181 |
| **Total Solids wt.%** | SRAT | 21.6% | 21.3% | 27.4% | 24.2% | 24.6% |
| | SME | N/A | N/A | 49.3% | 45.0% | 47.2% |
| **Sludge Oxide Contribution (Waste Loading) based on $Fe_2O_3$** | SME | N/A | N/A | 36.75% | 30.45% | 33.29% |
| **Max $CO_2$ lb/hr, MS** | SRAT | N/A | N/A | 692 | 674 | 687 |
| | SME | | | 41.2 | 37.0 | 0.00 |
| **Max $CO_2$ lb/hr, FTIR** | SRAT | N/A | N/A | 714.59 | N/A | N/A |
| | SME | | | N/A | 41.5 | |
| **Max $CO_2$ lb/hr, GC** | SRAT | 648 | 694 | 630 | 707 | 692 |
| | SME | N/A | N/A | 35.0 | 38.4 | 0.00 |
| **Max $N_2O$ lb/hr, GC** | SRAT | 28.6 | 25.9 | 15.7 | 19.6 | 11.0 |
| | SME | N/A | N/A | 3.45 | 0.00 | 0.00 |
| **Max $N_2O$ lb/hr, FTIR** | SRAT | N/A | N/A | 16.4 | N/A | N/A |
| | SME | | | N/A | 0.00 | |
| **Max $H_2$ lb/hr, MS** | SRAT | N/A | N/A | 0.232 | 0.312 | 0.083 |
| | SME | | | 0.082 | 0.097 | 0.000 |
| **Max $H_2$ lb/hr, GC** | SRAT | 0.204 | 0.304 | 0.226 | 0.309 | 0.083 |
| | SME | N/A | N/A | 0.070 | 0.096 | 0.000 |
| **Max NO lb/hr, MS** | SRAT | N/A | N/A | 2.06 | 1.83 | 1.02 |
| | SME | | | 0.36 | 0.05 | 0.00 |
| **Max NO lb/hr, FTIR** | SRAT | N/A | N/A | 2.36 | N/A | N/A |
| | SME | | | N/A | 0.00 | |
| **Max $NO_2$ lb/hr, MS** | SRAT | N/A | N/A | 26.4 | 20.6 | 46.9 |
| | SME | | | 0.17 | 0.14 | 0.00 |
| **Max $NO_2$ lb/hr, FTIR** | SRAT | N/A | N/A | 21.88 | N/A | N/A |
| | SME | | | N/A | 0.01 | |

N/A is based on Table 2-4, Table 2-7, and Table 2-8

### 3.3 Process Data

Lab View was used to record process data for all runs. The temperature trends can be seen in Figure 3-1. During SRAT processing acid addition is performed at 93 +/- 2 °C. Dewater and reflux were performed at boiling. SB9A-1A and SB9A-2A were stopped to replace the mixer coupling, which was found to have a shorter life span than expected. After completing acid addition in SB9A-7A, the automation of the mixer resulted in an input-output failure (IOF) on the backshift. SRAT personnel notified the PI and the experiment was placed in a safe state at room temperature until process control personnel could correct the automation. Because acid addition was completed, the chemistry was proceeding, although the kinetics were likely different. Therefore, it was uncertain that analytical results and observations would be indicative of normal processing. The run was restarted to view the hydrogen generated from the Rh and Ru catalysts, then shut down and repeated as SB9A-8A. SB9A-8A was stopped after viewing the hydrogen generated from the Ru and Rh catalysts. SB9A-7A and SB9A-8A were performed to collect additional peak hydrogen generation data in the 1L laboratory setup due to variations seen between SB9A-3A and SB9A-4A. At the beginning of SB9A-9A, the glass off-gas leg was leaking and turned out to be damaged. The sludge was cooled so that the off-gas leg could be replaced. The helium tracer was used to determine the total gas flowing through the system. Because the gas components were converted from volume to mass using the total gas determined, leaks or ingresses of air were corrected. When the system is completely opened, the percent He drops to zero, and these data points are removed from the processed gas data.

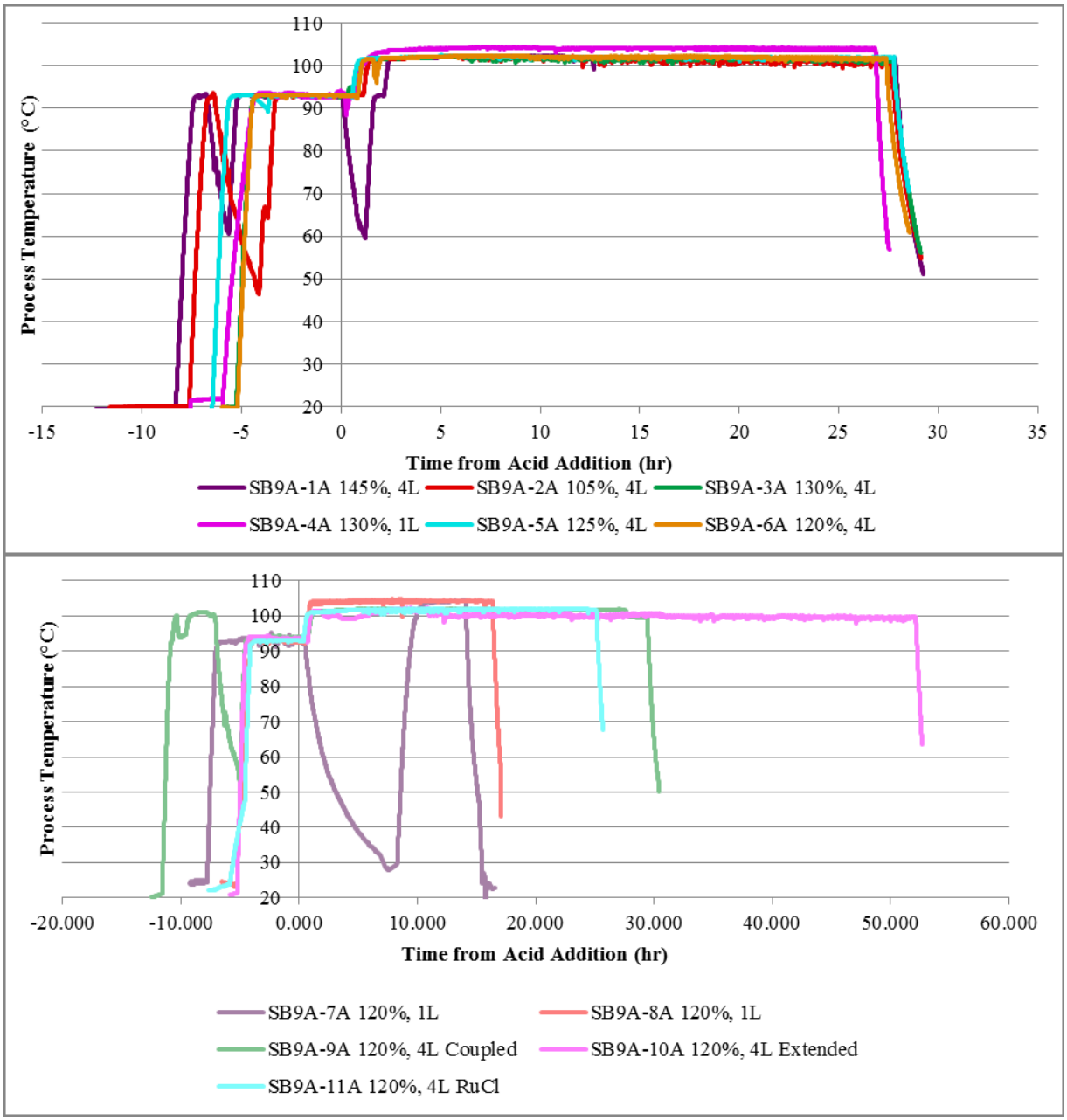


**Figure 3-1. Temperature of Sludge during SRAT Cycle**

Upon completion of the SRAT cycle, the sludge was cooled to below 50°C, then sampled. The MWWT and FAVC were drained. The purge gases were reduced, and then the SME cycle was started. Frit, formic acid, water and antifoam were added. The sludge was brought to boiling for dewatering. The sludge was then cooled to allow the second frit addition to be added before repeating the dewater.

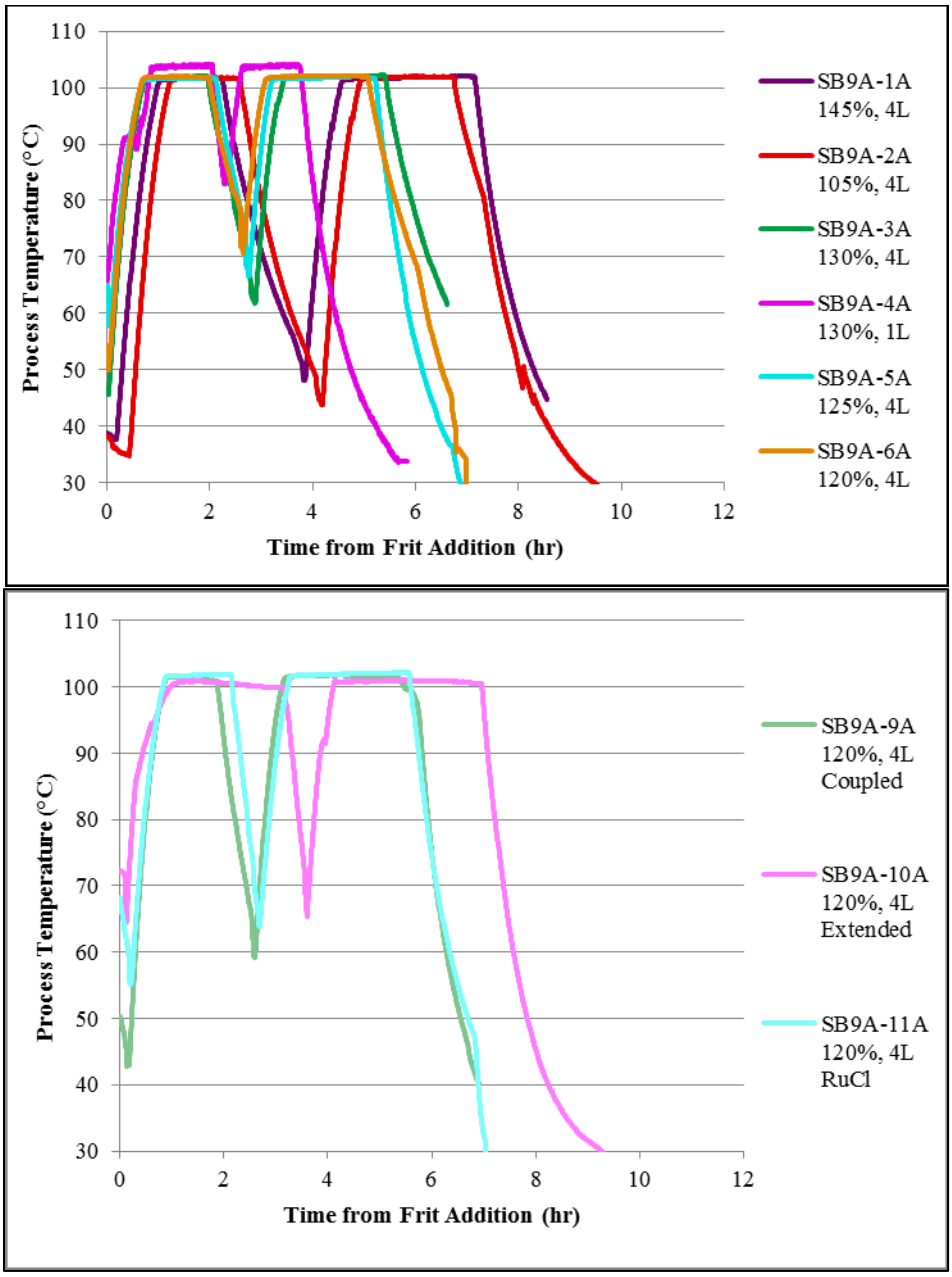


**Figure 3-2. Temperature of Sludge during SME Cycle**

SB9A-10A also included six canister decontamination additions prior to the two frit additions. Figure 3-3 contains the temperature profile for run SB9A-10A.

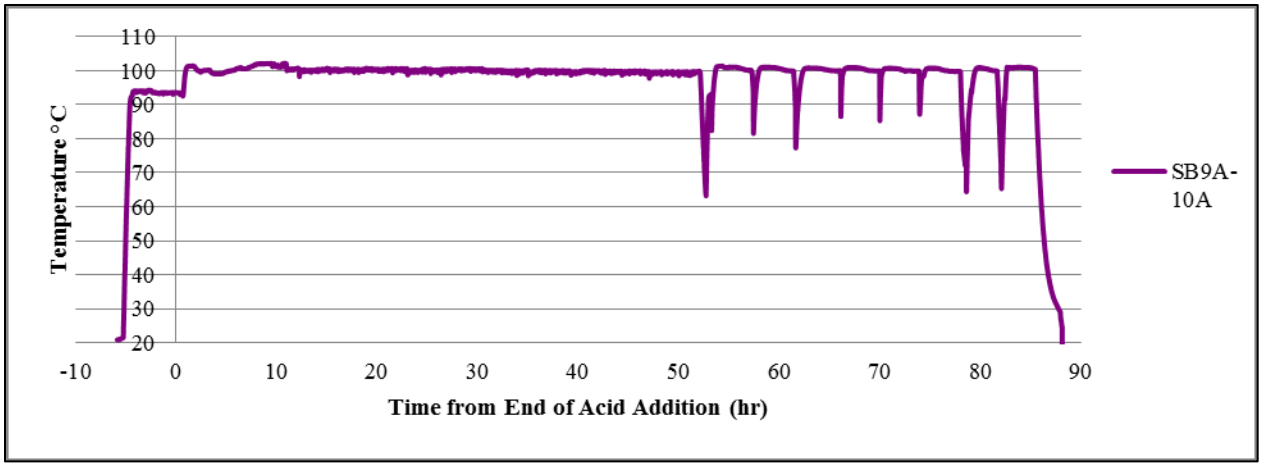


**Figure 3-3. SB9A-10A Temperature**

Mixer speed, seen in Figure 3-4, was adjusted as needed to ensure thorough mixing. As the sludge thickened, the mixer speed was increased. In simulant runs, the initial mixing speed was set to a speed such that mixing was clearly visible. Typically the mixer speed was not increased above 1000 rpm to ensure optimum mixing.

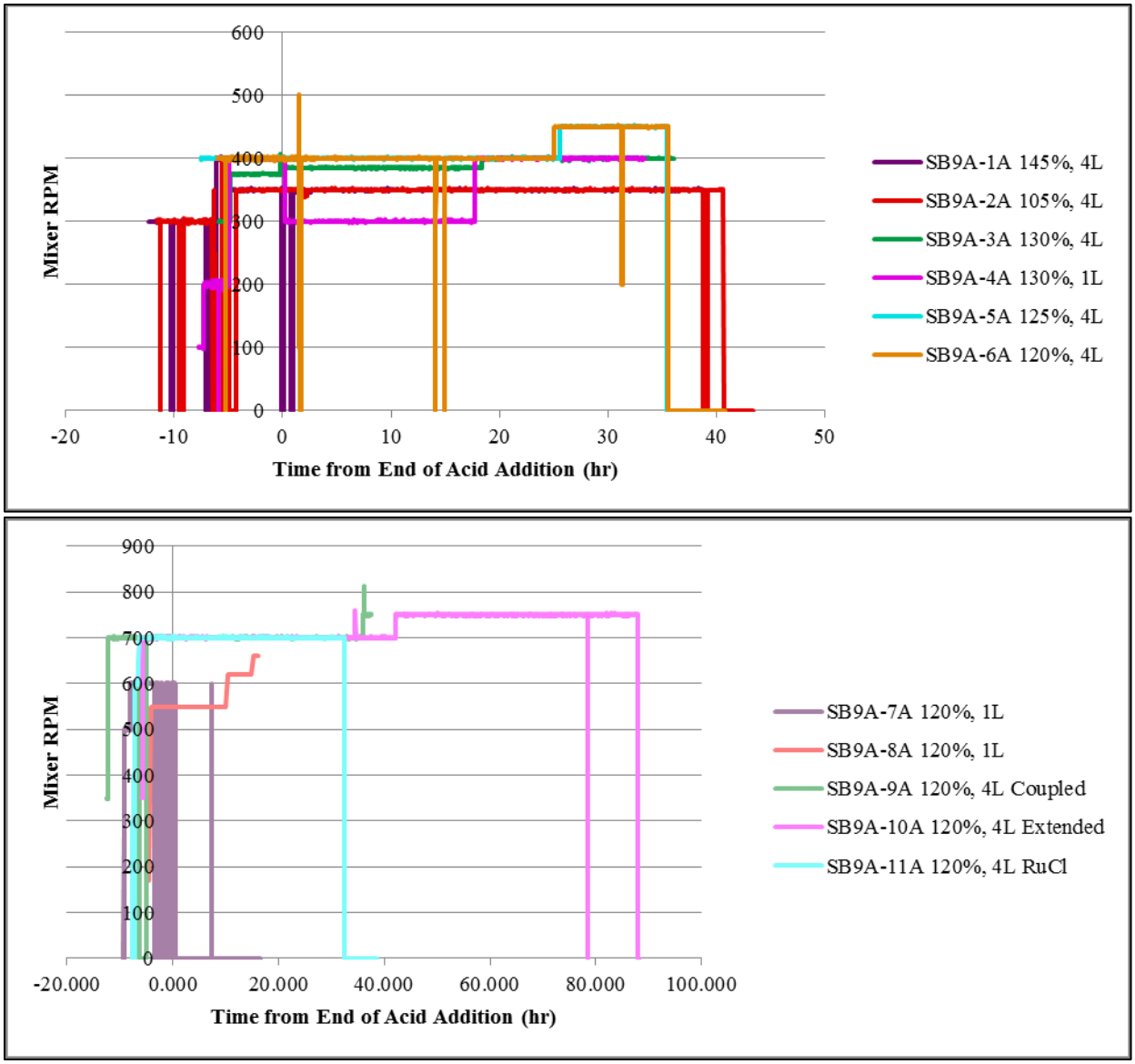


**Figure 3-4. Mixer Speed**

During acid addition, a PID algorithm was used to target a temperature set point. Upon going to boiling, another PID algorithm was used to target a wattage input ('power mode'). The difference in gains seen in Figure 3-5 indicates the PID algorithm seeking wattage is better tuned than the algorithm targeting a temperature set point. The heat transfer is calculated based on the limiting rod, i.e. the lowest temperature differential between the rod temperature and the sludge.

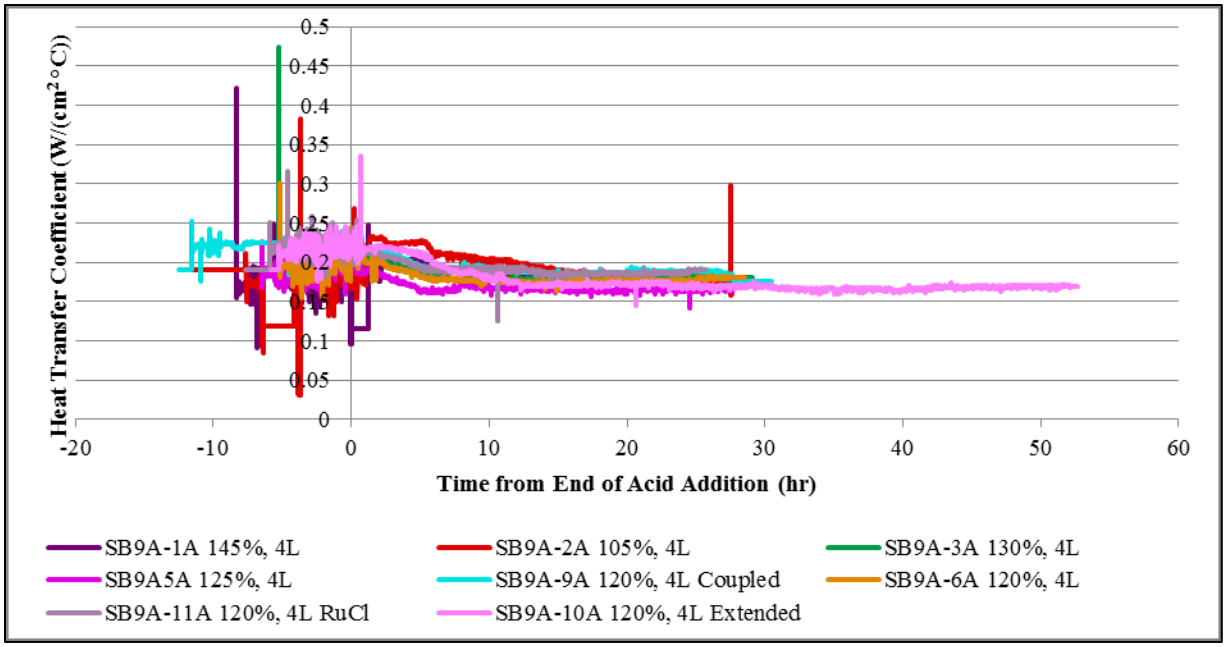


**Figure 3-5. Heat Transfer Coefficient in SRAT**

Viewing the heat transfer coefficient during conflux allows the heat transfer to be better compared. As seen in Figure 3-6, the 1L laboratory scale setup trends slightly lower than the 4L setup. The difference may be a result of different heating rod sizes and/or heat dissipation from the vessel.

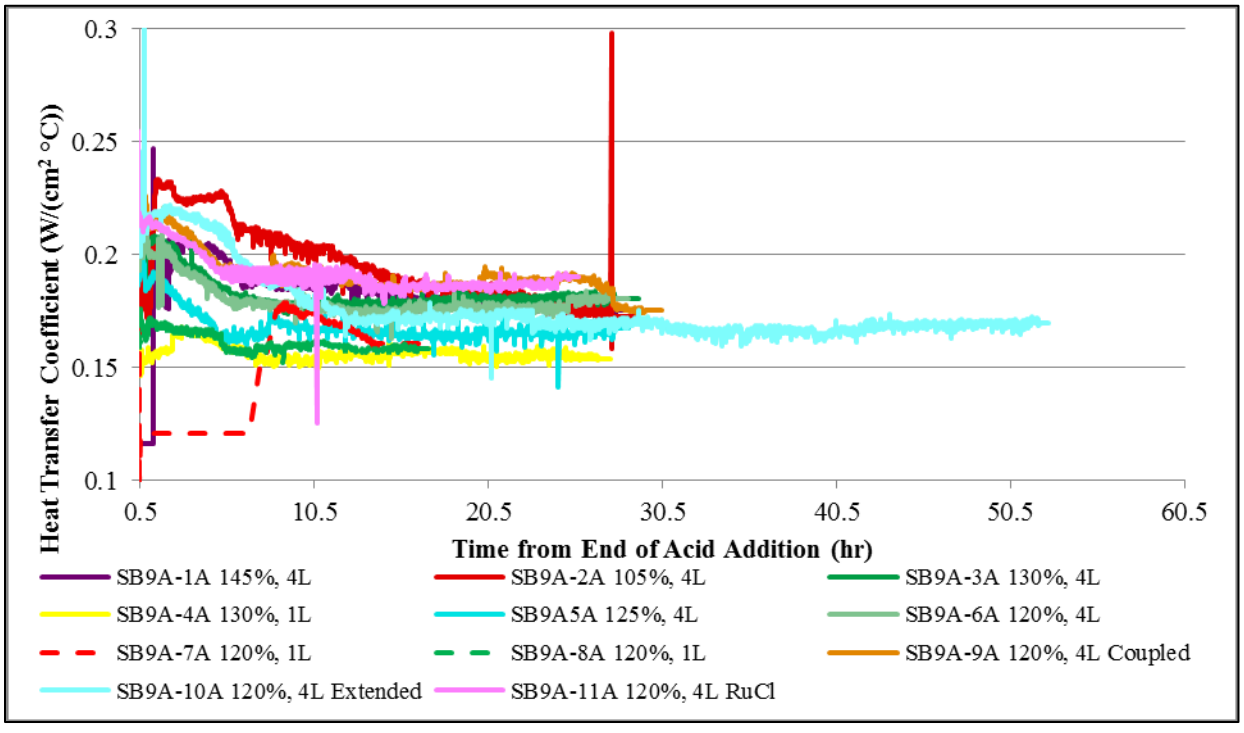


**Figure 3-6. Heat Transfer Coefficient in POWER mode**

The heat transfer coefficient during the SME cycle can be seen in Figure 3-7. During SB9A-9A, one of the two heating rods started to foul as seen in the drop off of the pink dashed line in Figure 3-7. The last ~20 grams of dewater was performed with only one heating rod. Although the boil-up rate slowly decreased since less heat was being added, there was minimal effect on off-gas and chemistry. In addition, the post SB9A-9A leak check indicated a leak in the system occurred, which resulted in faster concentration of the slurry.

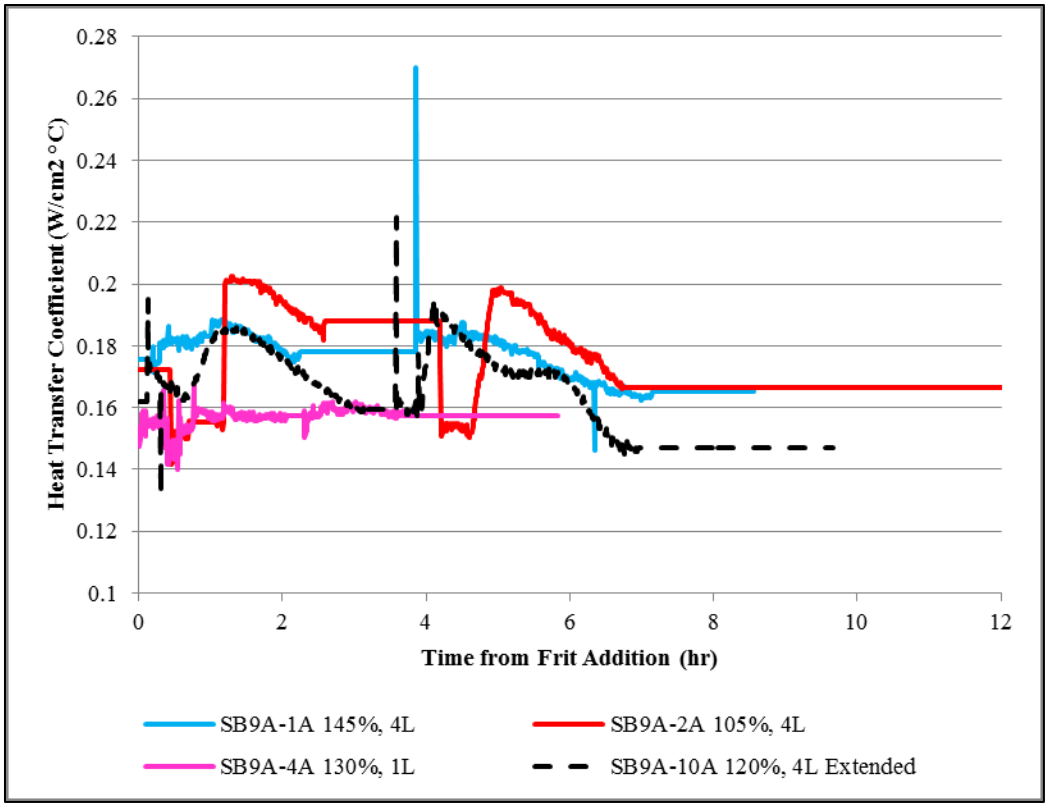


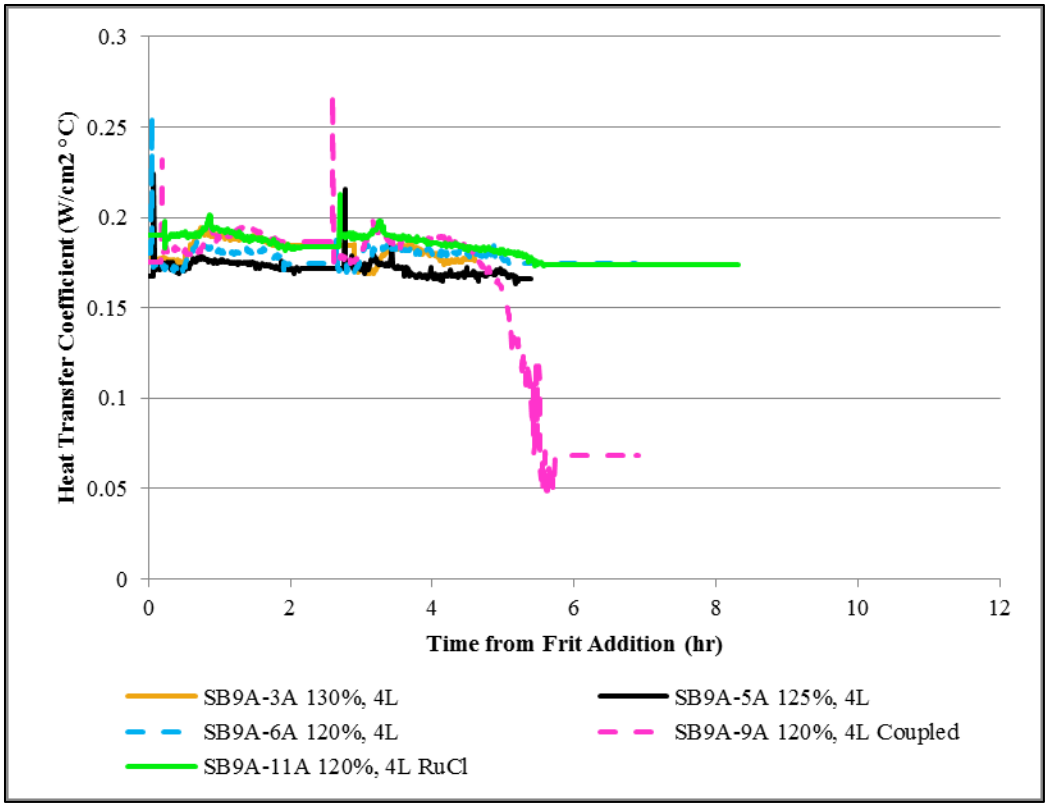


**Figure 3-7. Heat Transfer Coefficient in SME**

Acid addition and SRAT chemistry shift the pH from alkaline to acidic, and then to near neutral. The pH profiles can be seen in Figure 3-8.

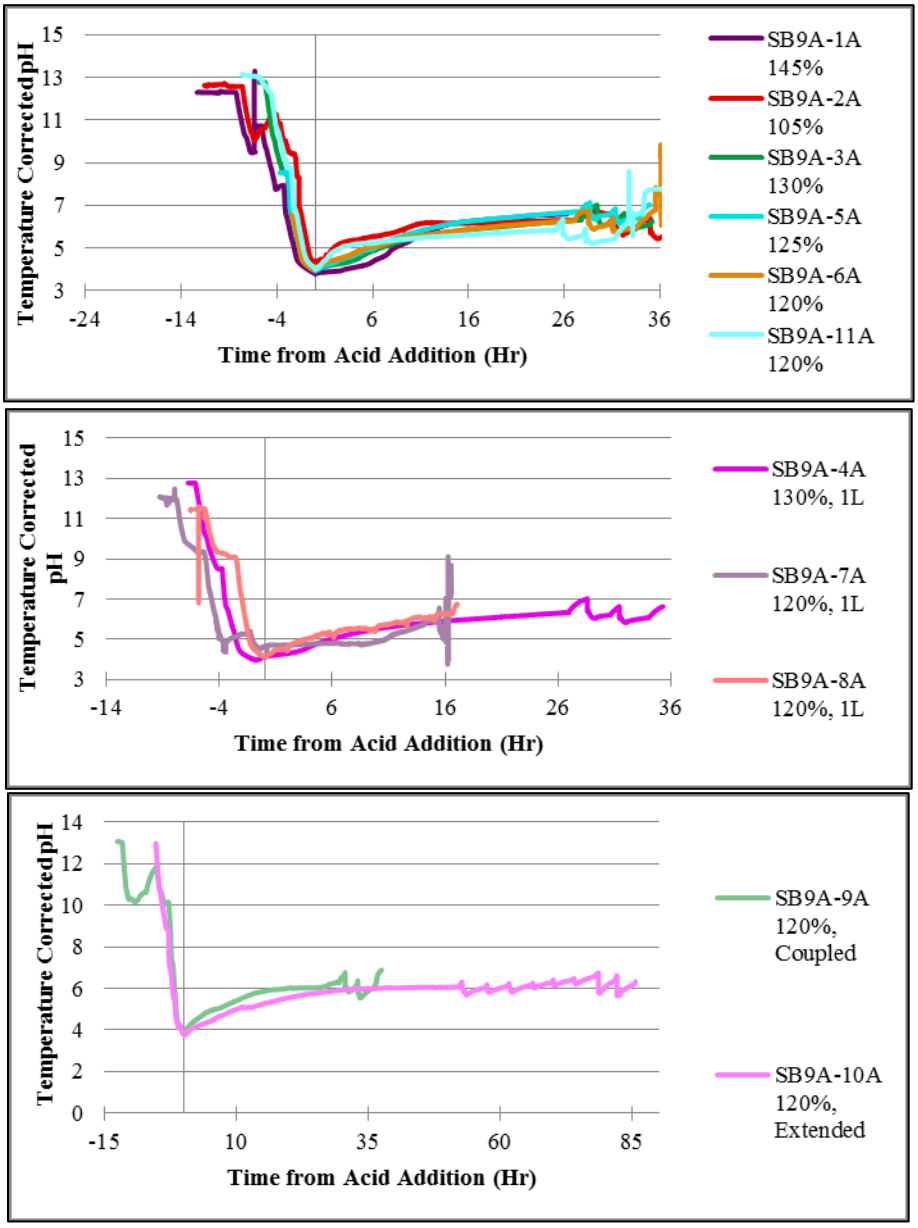


**Figure 3-8. pH Trends**

The pH reaches a minimum upon completion of acid addition. The minimum pHs are presented in Table 3-11.

**Table 3-11. Minimum Process pH**

| SB9A-1A | SB9A-2A | SB9A-3A | SB9A-4A | SB9A-5A | SB9A-6A | SB9A-7A | SB9A-8A | SB9A-9A | SB9A-10A | SB9A-11A |
|---|---|---|---|---|---|---|---|---|---|---|
| 3.78 | 4.33 | 3.95 | 3.95 | 3.92 | 4.00 | 3.75 | 4.12 | 3.85 | 3.77 | 4.00 |

All runs passed the final leak check on the system, except SB9A-9A. At some point during the run, an opening was created allowing additional vapor to potentially escape. SB9A-9A SME product was visibly thicker than all other runs. The qualification of off-gas concentrations was not affected by the leak because of how the He tracer is used to convert the data from a volume basis to a mass basis. SB9A-4A SME product was visibly the thinnest due to stopping the final SME dewater short in order to keep the heated regions of the heating rods submerged.

It is important to note that some foaming was observed during all runs. Foam typically consisted of small bubbles. Maximum foaming was observed 5-9 hours after completing acid addition. Slurry never foamed such that it exited the SRAT/SME vessel and was visible in the off-gas lines, thus no foam overs occurred.

### 3.4 Off-gas

$H_2$, $N_2O$, $NO_2$, NO, $CO_2$, CO, and $NH_3$ evolved from the sludge during processing. The maximum concentrations, on a DWPF scale, can be seen in Table 3-12.

**Table 3-12. Maximum Concentration**

| | | SB9A-1A, 145% 4L | SB9A-2A, 105% 4L | SB9A-3A, 130% 4L | SB9A-4A, 130% 1L | SB9A-5A, 125% 4L | SB9A-6A, 120% 4L | SB9A-7A, 120% 1L | SB9A-8A, 120% 1L | SB9A-9A, 120% 4L Coupled[f] | SB9A-10A, 120% 4L Extended | SB9A-11A, 120% 4L $RuCl_3$ |
|---|---|---|---|---|---|---|---|---|---|---|---|---|
| **Max $CO_2$, lb/hr, MS** | **SRAT** | 701.99 | 679.33 | 719.65 | N/A | 748.30 | 710.03 | N/A | N/A | 691.75 | 674.41 | 687.18 |
| | **SME** | 135.11 | 46.63 | 82.72 | | 123.96 | 83.08 | | | 41.24 | 36.96 | 0.00 |
| **Max $CO_2$, lb/hr, FTIR** | **SRAT** | 736.57 | N/A | 751.47 | N/A | 783.05 | N/A | N/A | N/A | 714.59 | N/A | N/A |
| | **SME** | 138.09 | | 82.57 | | 126.93 | | | | N/A | 41.47 | |
| **Max $CO_2$, lb/hr, GC** | **SRAT** | 698.16 | 754.94 | 717.49 | 697.02 | 730.14 | 734.25 | 647.76 | 694.03 | 629.64 | 707.21 | 691.57 |
| | **SME** | 107.71 | 47.97 | 68.74 | 49.61 | 112.94 | 72.25 | N/A | N/A | 35.04 | 38.37 | 0.00 |
| **Max $N_2O$, lb/hr, GC** | **SRAT** | 37.69 | 31.77 | 39.36 | 49.02 | 34.93 | 38.07 | 28.64 | 25.91 | 15.71 | 19.63 | 11.04 |
| | **SME** | 0.00 | 0.00 | 0.00 | 0.00 | 0.00 | 0.00 | N/A | N/A | 3.448 | 0.00 | 0.00 |
| **Max $N_2O$, lb/hr, FTIR** | **SRAT** | 39.44 | N/A | 37.54 | N/A | 35.81 | N/A | N/A | N/A | 16.36 | N/A | N/A |
| | **SME** | 0.04 | | 0.03 | | 0.02 | | | | N/A | 0.00 | |
| **Max $H_2$, lb/hr, MS** | **SRAT** | 1.33 | 0.02 | 0.69 | N/A | 0.48 | 0.33 | N/A | N/A | 0.23 | 0.31 | 0.09 |
| | **SME** | 0.16 | 0.00 | 0.18 | | 0.22 | 0.12 | | | 0.08 | 0.10 | 0.00 |
| **Max $H_2$, lb/hr, GC** | **SRAT** | 1.142 | 0.023 | 0.656 | 0.413 | 0.432 | 0.323 | 0.204 | 0.304 | 0.226 | 0.309 | 0.083 |
| | **SME** | 0.151 | 0.007 | 0.177 | 0.067 | 0.208 | 0.127 | N/A | N/A | 0.070 | 0.096 | 0.000 |
| **Max NO, lb/hr, MS** | **SRAT** | 7.02 | 2.02 | 2.84 | N/A | 3.85 | 1.64 | N/A | N/A | 2.06 | 1.83 | 1.02 |
| | **SME** | 0.08 | 0.10 | 0.09 | | 0.13 | 0.17 | | | 0.36 | 0.05 | 0.00 |
| **Max NO, lb/hr, FTIR** | **SRAT** | 4.15 | N/A | 1.98 | N/A | 2.44 | N/A | N/A | N/A | 2.36 | N/A | N/A |
| | **SME** | 0.01 | | 0.02 | | 0.07 | | | | N/A | 0.00 | |
| **Max $NO_2$, lb/hr, MS** | **SRAT** | 20.99 | 17.12 | 24.83 | N/A | 24.69 | 26.37 | N/A | N/A | 26.36 | 20.58 | 46.88 |
| | **SME** | 0.16 | 0.18 | 0.15 | | 0.21 | 0.20 | | | 0.17 | 0.14 | 0.00 |
| **Max $NO_2$, lb/hr, FTIR** | **SRAT** | 17.09 | N/A | 20.17 | N/A | 18.59 | N/A | N/A | N/A | 21.88 | N/A | N/A |
| | **SME** | 0.01 | | 0.02 | | 0.06 | | | | N/A | 0.01 | |

[f]Failed post run leak check.

*3.4.1 Hydrogen*

Hydrogen generation rates are important for flammability concerns. The current DWPF hydrogen generation limits are 0.65 lb/hr in the SRAT and 0.223 lb/hr in the SME. Hydrogen generation rates on a DWPF scale can be seen in Figure 3-9, Figure 3-10, and Figure 3-12.

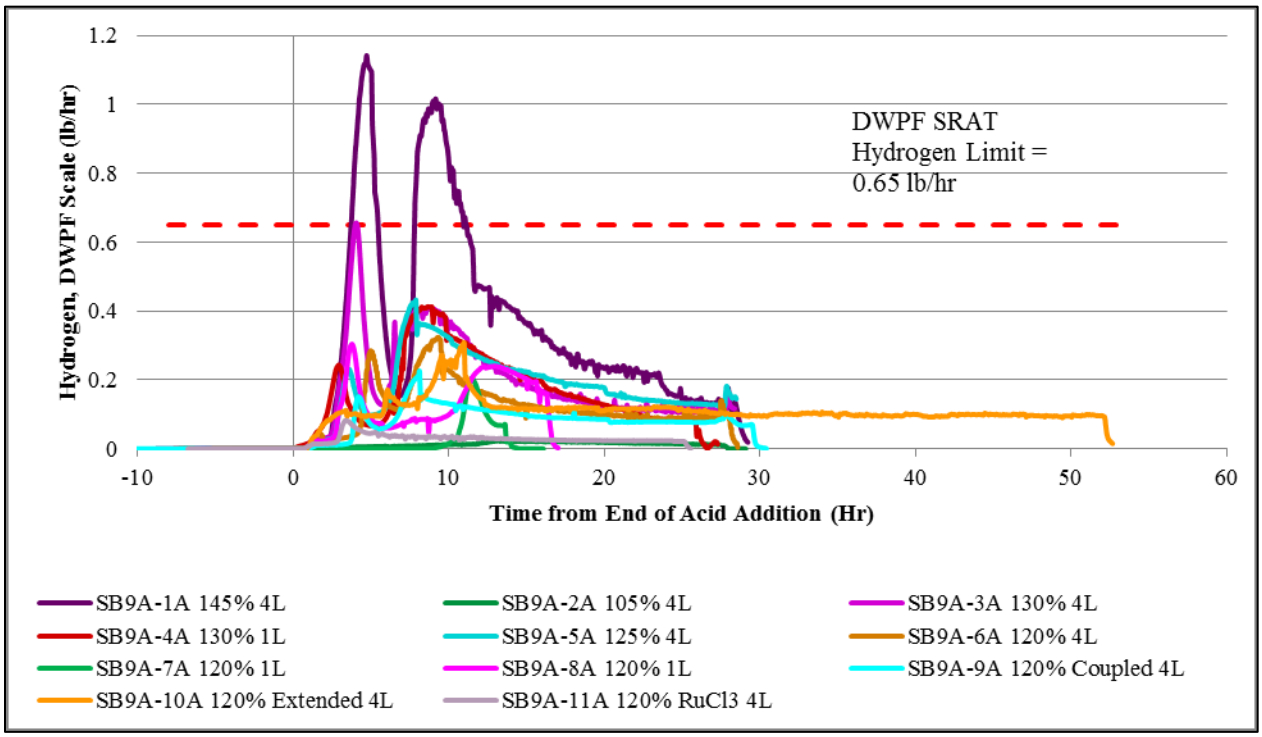


**Figure 3-9. Hydrogen Release during SRAT Cycle**

SB9A-1A and SB9A-3A were above the SRAT limit for hydrogen by about 76% and 0.9%, respectively, measured by GC. The processing delays in SB9A-7A caused the hydrogen peak to occur significantly later. The Rh peak was larger than the Ru peak for SB9A-1A, SB9A-3A, SB9A-8A, and SB9A-11A. The Ru peak in SB9A-11A was level with the sustained release rate. The low acid content in SB9A-2A did not create definitive peaks, which is better seen in Figure 3-10.

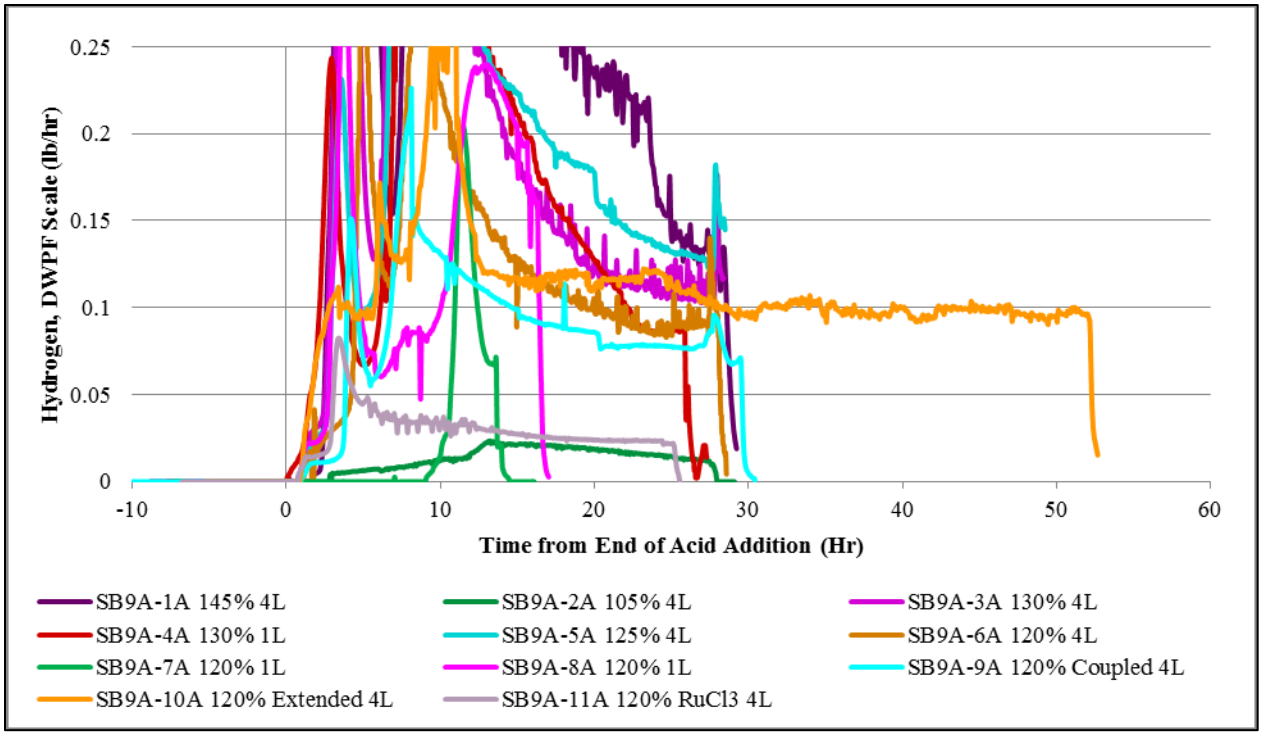


**Figure 3-10. Zoomed SRAT Hydrogen**

The $H_2$ release plotted in Figure 3-9 was aligned with the timing of the $H_2$ peak release associated with Rh for SB9A-3A, see Figure 3-11, to allow for the magnitude and duration of hydrogen generation to be compared. Although variation exists, the hydrogen associated with the Rh and Ru peaks generally scales with acid stoichiometry.

The significant difference in the peak hydrogen release between SB9A-3A (130% 4L) and SB9A-4A (130% 1L) caused SB9A-7A/SB9A-8A (120% 1L) to be performed to collect additional comparison between the 4L and 1L laboratory scale setups. SB9A-6A (120% 4L) and SB9A-8A (120% 4L) align very well, thus indicating that scale is not the primary cause of the variance of hydrogen generation between the runs. SB9A-7A had equipment deviations causing a delay after acid addition, which could affect peak generation rates. However, the variance between SB9A-6A and SB9A-7A is slight and much less significant than the variance between SB9A-3A and SB9A-4A.

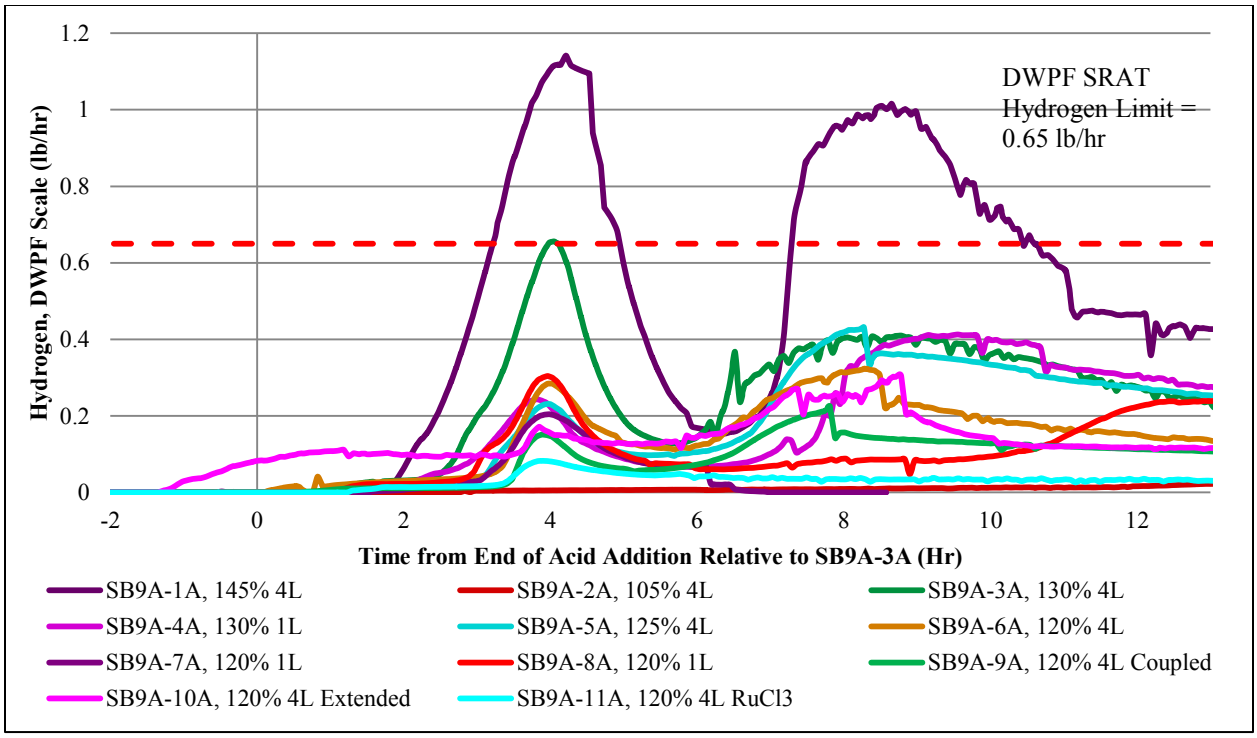


**Figure 3-11. Hydrogen Release Normalized to SB9A-3A Timing**

The SME hydrogen off-gas data can be seen in Figure 3-12.

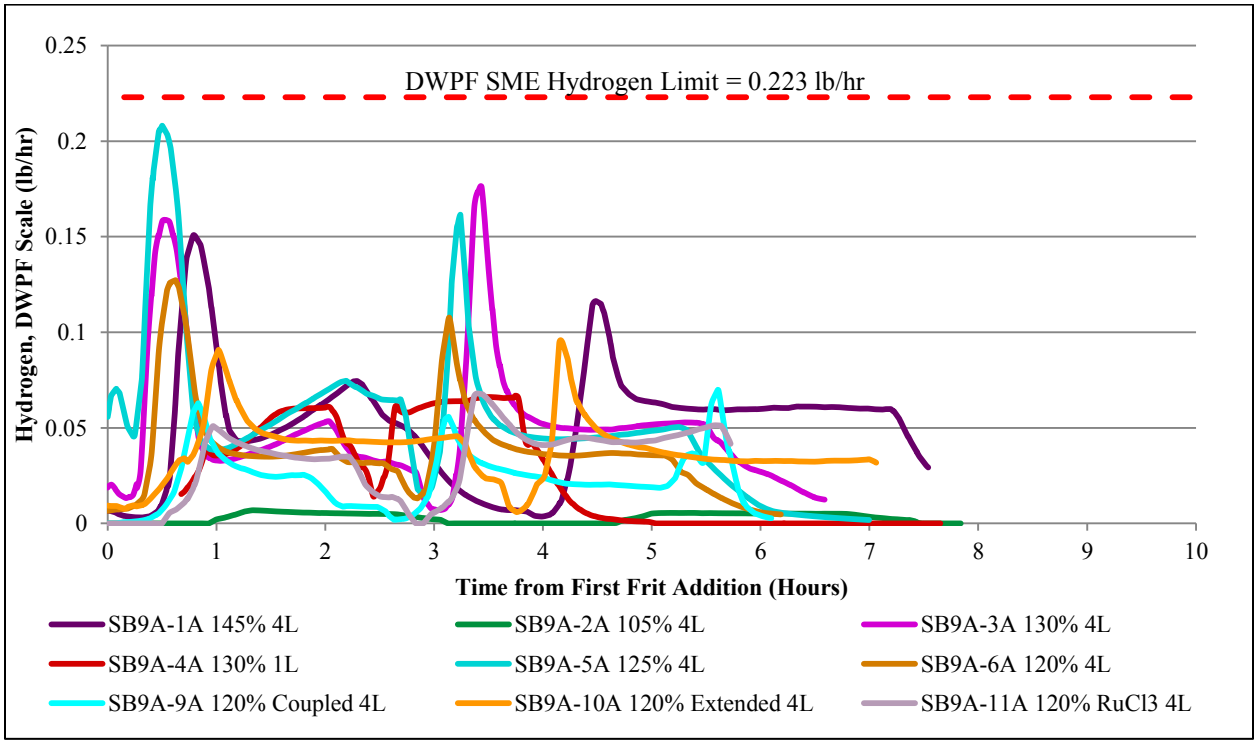


**Figure 3-12. Hydrogen Generation during SME Cycle**

SB9A-5A was 93% of the SME limit recorded by GC and 97% of the limit recorded by MS. Therefore, given the uncertainty associated with the off-gas measurement, the upper end of the acid window is best bounded by 120% of the KMA, SB9A-6A. This drove the extended and coupled run to be performed at 120% of the KMA as well. Hydrogen release in the SME is a result of the decomposition of formic acid. Excess formic acid in the slurry and boil-up rate can impact the amount of hydrogen released. Carbon dioxide is also released simultaneously with hydrogen avulsion due to formic breakdown (see Figure 3-17). Runs SB9A-6A, SB9A-7A, SB9A-8A, SB9A-9A, SB9A-10A, and SB9A-11A were all performed at 120% of the KMA, which can be seen in Figure 3-13.

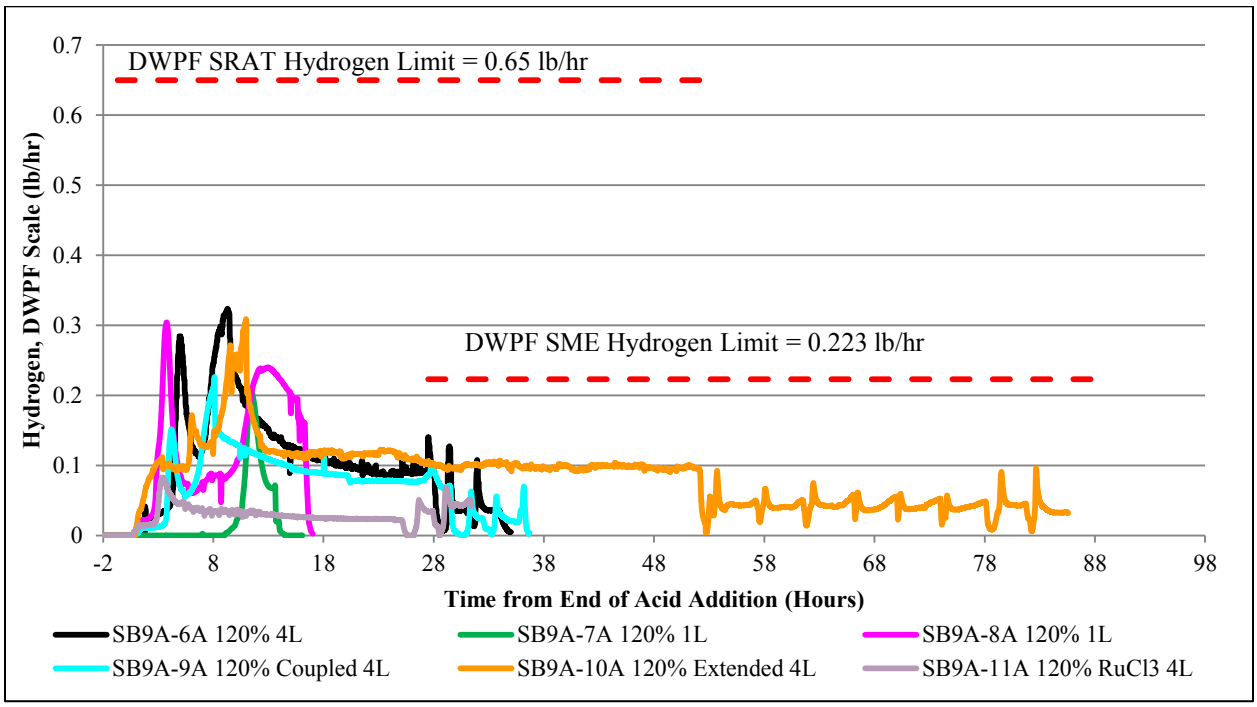


**Figure 3-13. Runs Performed at 120% of the KMA**

The 1L laboratory scale setup resulted in similar peak hydrogen generation rates; however, the hydrogen generated by Ru was delayed compared to the SB9A-6A profile. The shift may be influenced by the fact that the 1L heat transfer coefficient appears to be lower than seen in the 4L laboratory scale setup. Furthermore, head space in the 1L laboratory setup is significantly different than the 4L (see Figure 2-1 and Figure 2-2). The hydrogen released during the coupled run, SB9A-9A, was about half of the amount released during SB9A-6A, which is similar to trends observed in the sludge batch 8 and sludge batch 7 simulant testing [2, 14]. Previous studies indicate that this may be due to the additional oxalate consumption of acid [14]. The hydrogen generated by Rh in SB9A-11A run was approximately a third of the SB9A-6A Rh hydrogen, and the hydrogen associated with Ru does not appear obvious. Additional information on SB9A-11A will be provided in 3.4.4 SB9A-11A Differences. The Rh hydrogen peak in the extended run was dwarfed in comparison to SB9A-6A.

The percentage of the DWPF limit occupied by the maximum hydrogen released can be seen in Table 3-13. Given this data, 120% KMA is the maximum potential acid stoichiometry. Rheology and sample results confirm that 120% is acceptable.

**Table 3-13. Percentage of Hydrogen Limit**

| | | SB9A-1A, 145% | SB9A-2A, 105% | SB9A-3A, 130% | SB9A-4A, 130% | SB9A-5A, 125% | SB9A-6A, 120% | SB9A-7A, 120% | SB9A-8A, 120% | SB9A-9A, 120% Coupled | SB9A-10A, 120% Extended | SB9A-11A, 120% $RuCl_3$ |
|---|---|---|---|---|---|---|---|---|---|---|---|---|
| % of $H_2$ Limit, GC | SRAT | 175.6% | 3.6% | 100.9% | 63.5% | 66.5% | 49.8% | 31.5% | 46.8% | 34.8% | 47.5% | 12.7% |
| | SME | 67.7% | 3.1% | 79.2% | 30.0% | 93.3% | 57.1% | N/A | | 28.1% | 31.4% | 43.0% |
| % of $H_2$ Limit, MS | SRAT | 204.5% | 2.5% | 105.9% | N/A | 73.2% | 50.5% | | | 35.7% | 48.0% | 13.3% |
| | SME | 72.7% | 1.6% | 81.0% | | 97.1% | 56.0% | | | 36.6% | 43.6% | 0.0% |

*3.4.2 Carbon*

During CPC processing, the $CO_2$ release is most significant during neutralization reactions as seen in Figure 3-14.

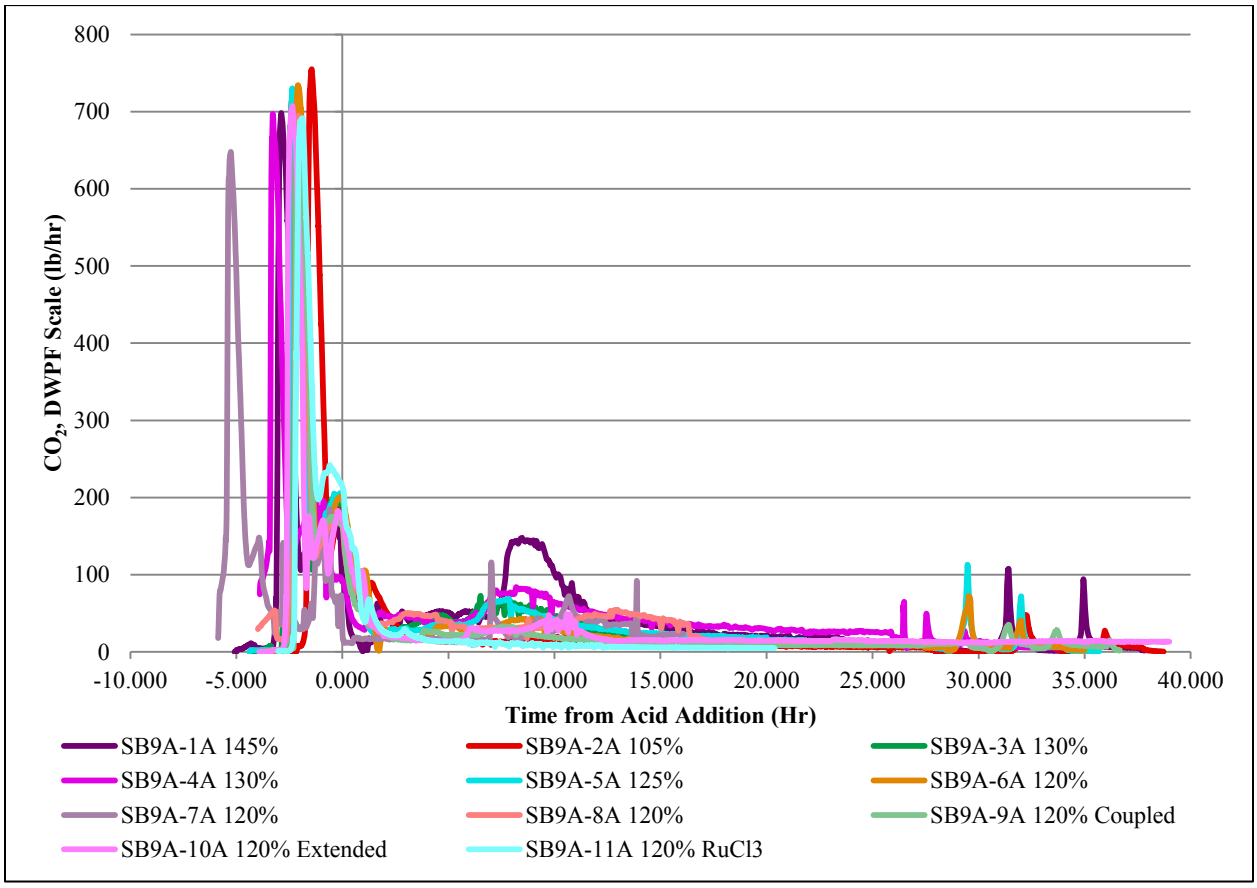


**Figure 3-14. $CO_2$ Release Rate**

The $CO_2$ release plotted in Figure 3-14 was aligned with the timing of the $CO_2$ peak release recorded for SB9A-6A, see Figure 3-15, to allow for the magnitude and duration of carbonate destruction to be compared.

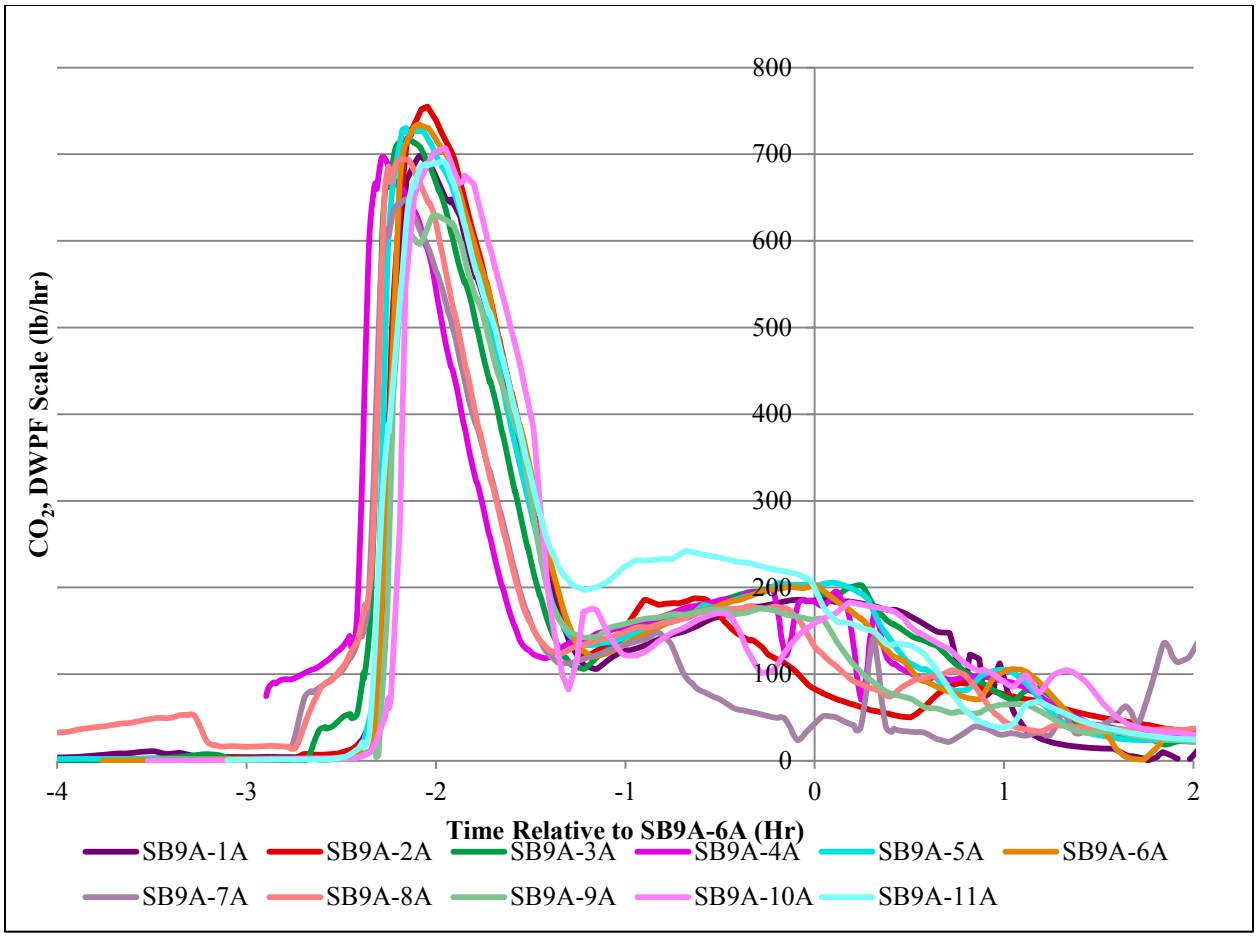


**Figure 3-15. Carbonate Destruction Normalized to SB9A-6A Timing**

The magnitude is fairly close with a peak %RSD of 5.2%, thus there is little difference between the runs outside of the uncertainty and a uniform amount of carbonate was likely destroyed. SB9A-4A, SB9A-7A, and SB9A-9A are about 20% lower than the other runs. The next lowest run is SB9A-8A. The 1L scaling appears to result in a lower carbonate bias. The highest, SB9A-2A, and lowest, SB9A-4A, peak $CO_2$ release caused the total off-gas flow to increase by 41% and 45%, respectively. As the carbonate derived $CO_2$ peak drops off, the $CO_2$ produced during nitrate destruction and Mn reduction begins.

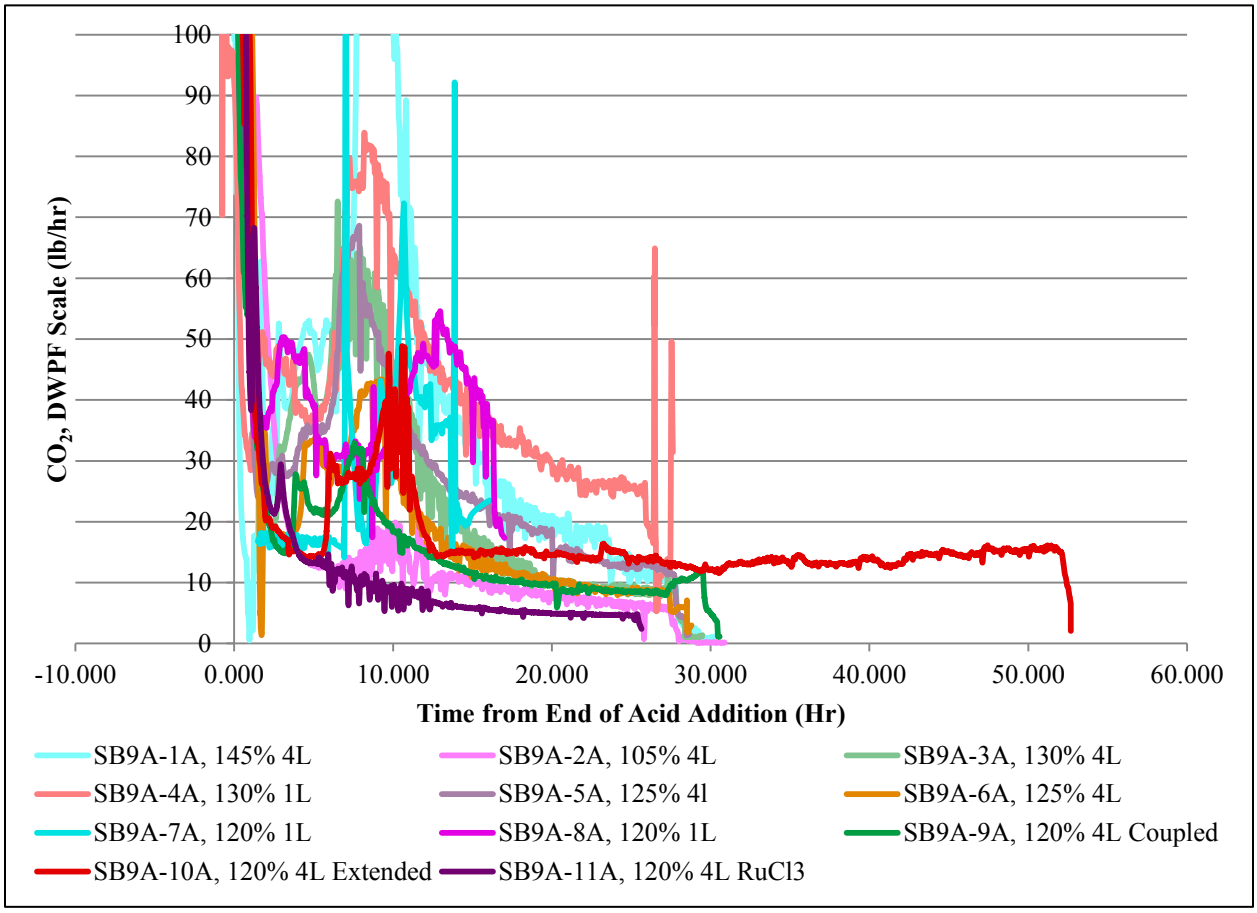


**Figure 3-16. SRAT $CO_2$ Generation after Acid Addition**

After acid addition, the $CO_2$ generation correlates roughly with the acid stoichiometry. The sludge-only runs appear more catalytically active than the coupled run and as a result generate more $CO_2$. The $CO_2$ generated in the SME can be seen in Figure 3-17.

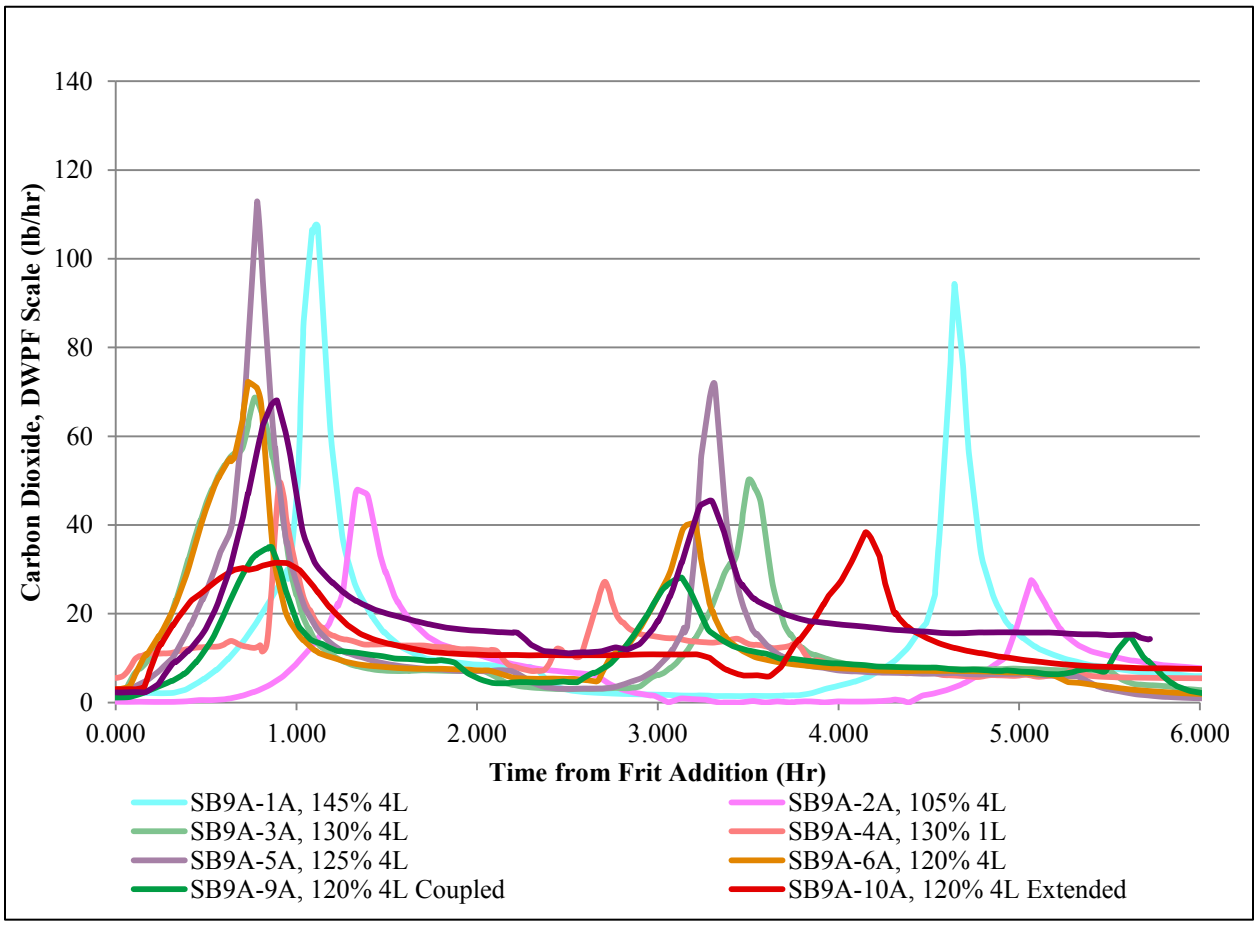


**Figure 3-17. SME $CO_2$ Generation**

The $CO_2$ peak is consistently higher during the first addition than the second addition, except in SB9A-10A. The first SB9A-10A peak does not look as sharp as the typical SME peaks. During the SME cycle little to no nitrogen species were released; however, hydrogen was released during this same period. This is indicative of the catalytic decomposition of formic acid. The dilution of noble metals as a result of the first frit addition may be the cause of the smaller $CO_2$ generation for the second frit addition.

*3.4.3 Nitrogen*

$N_2O$ generation in the SRAT cycle is seen in Figure 3-18.

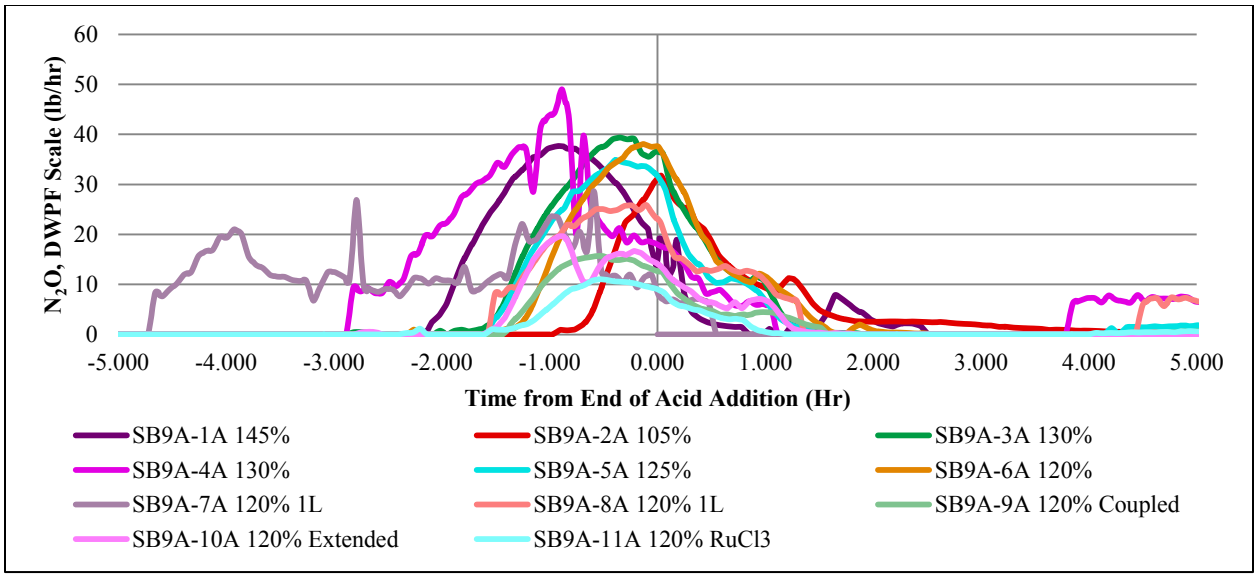


**Figure 3-18. $N_2O$ Generation in the SRAT**

$N_2O$ production in SB9A-4A is the highest, and is significantly larger than the other 1L runs. SB9A-3A generated the next highest $N_2O$ release. Given that both these runs produced more $N_2O$, it can be concluded that the larger amount of formic acid added, due to the assumption that 36% formic acid would be destroyed, was the cause. The $N_2O$ generation was significantly higher than that seen in sludge batch 8 simulant testing, which was about 7 - 15 lb/hr [2]. However, in sludge batch 7 simulant runs $N_2O$ rates were in the 30-33 lb/hr range [2]. Prior to acid addition, SB9A-6A and SB9A-10A were close to replicate tests. The $N_2O$ generation differed by a factor of two. During the SME cycle, $N_2O$ was only seen in SB9A-9A. $N_2O$ formation in the SME could be a result of the drop off in heat transfer as a result of the fouling of one of the heating rods. The change in system energy may shift kinetics.

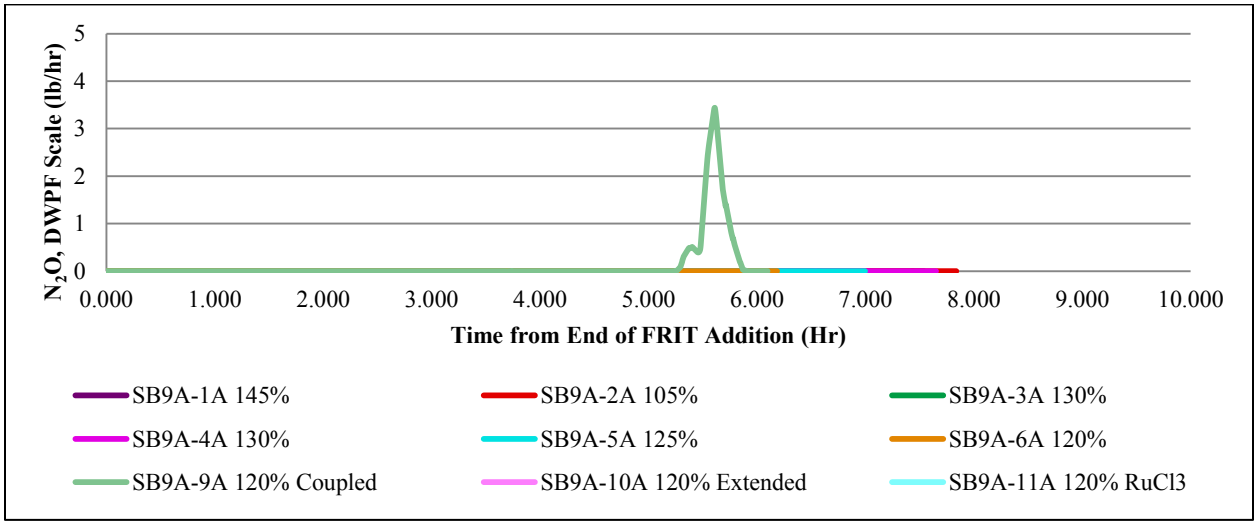


**Figure 3-19. $N_2O$ Generation in the SME**

Except SB9A-11A, the $NO_2$ peak release rate is fairly similar during nitrate destruction. SB9A-11A is significantly higher than the other runs. The delay in processing caused $NO_2$ in SB9A-1A to drop off completely. FTIR data appears to be lower than the MS data.

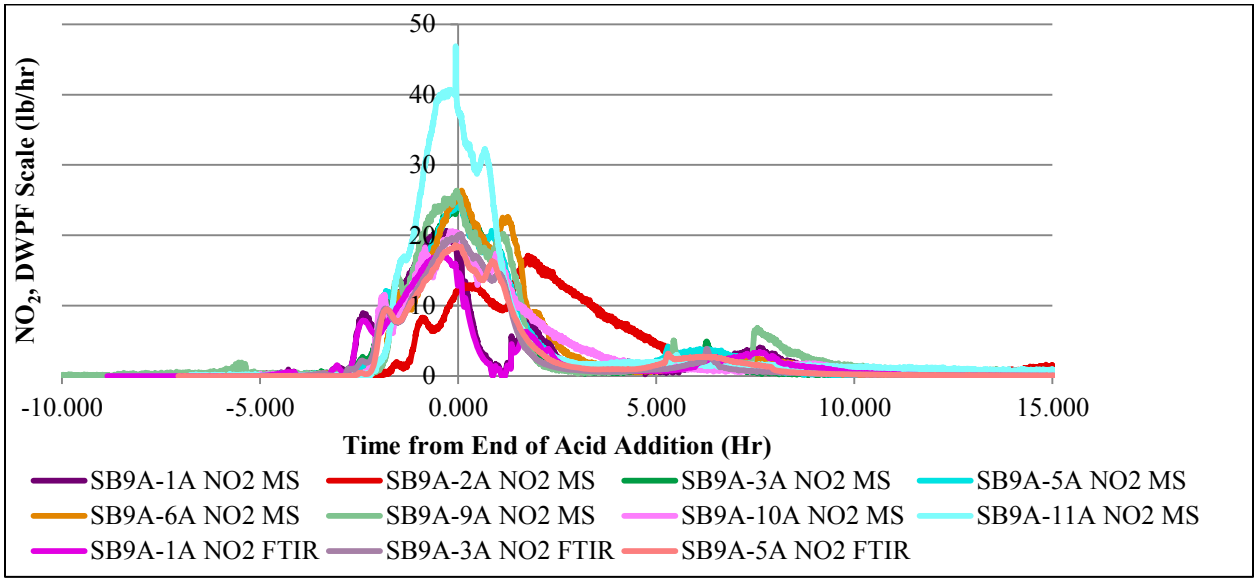


**Figure 3-20. $NO_2$ Off-gas Generated in SRAT**

The small peaks between 5-6 hours correlate to transitioning to reflux, since any accumulated nitric acid in the MWWT was then added back into the sludge where it becomes destroyed.

NO data can be seen in Figure 3-21.

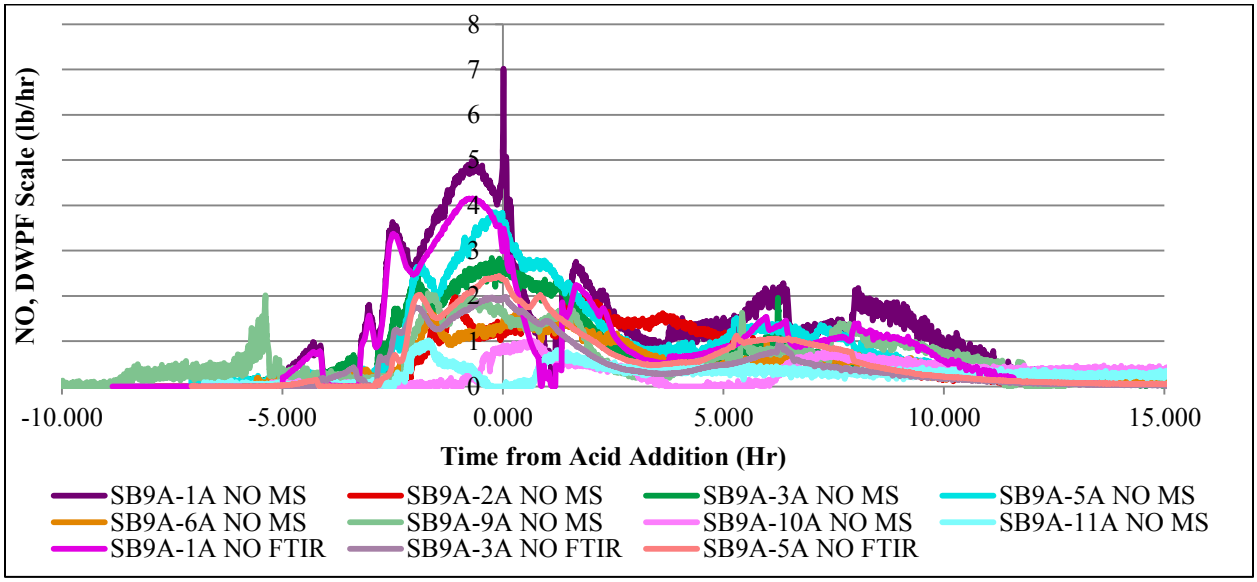


**Figure 3-21. NO Off-gas Generated in SRAT**

The MS data is consistently higher than the FTIR, which may indicate an increased sensitivity to NO or that the FTIR calibration is low. SB9A-10A NO production was delayed. Both SB9A-10A and SB9A-11A appear to be missing the middle hump, which may indicate an increased formation of $NO_2$ as a result of the interactions of NO with $O_2$. There is also a sharp release of NO during the ARP portion of SB9A-

9A. During reflux there is an increase in NO, which correlates to increases in $NO_2$ as well. These are assumed indicators of catalytic attack of nitrate by formic acid that could produce ammonium ions.

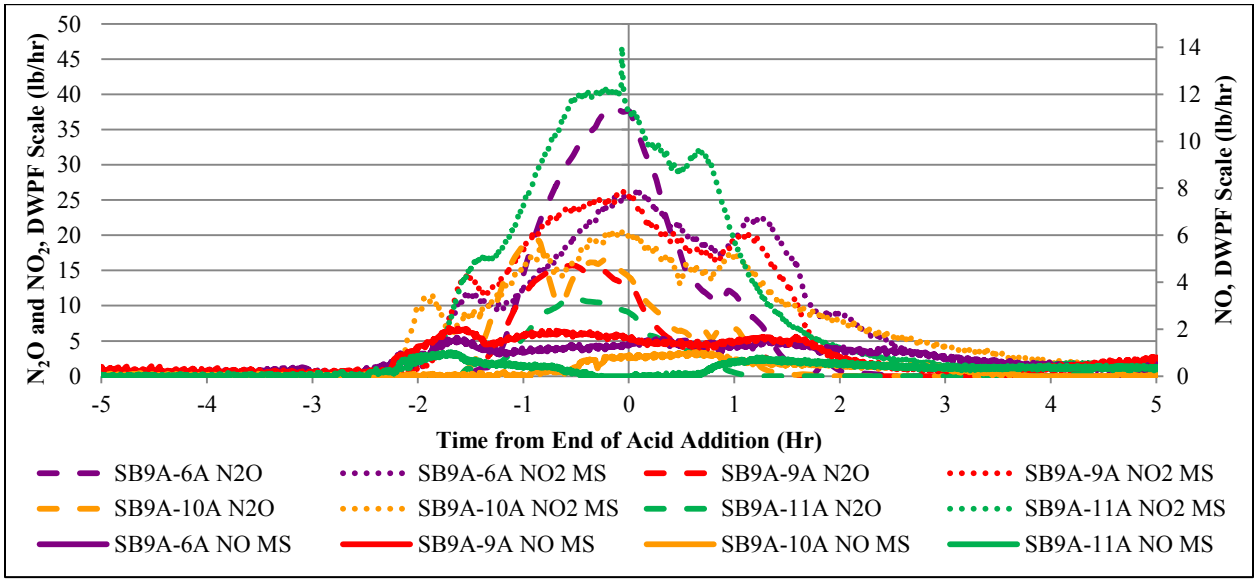


**Figure 3-22. Nitrogen Species Comparison for 4L 120% of KMA Runs**

SB9A-11A appears to have produced more $NO_2$ but less NO and $N_2O$. The differences will be discussed later in 3.4.4 SB9A-11A Differences. Sludge batch 8 simulant studies utilized the $RuCl_3$ catalyst. Testing at 120% of the KMA for sludge batch 8, generated ~8 lb/hr $N_2O$, ~80 lb/hr $NO_2$, and ~14 lb/hr NO, which is higher than SB9A-11A for all except NO. Additional study is required to determine catalyst impacts on nitrogen chemistry and parameters causing increased $N_2O$ production in SB9A.The peak values in the extended and coupled runs are bounded by the sludge-only run, SB9A-6A, expect for NO production. However, NO can be converted to $NO_2$ in the vessel head space. In evaluating the total moles released during the run it becomes more obvious that the coupled and extended flowsheet are comparable or bounded by the sludge-only flowsheet.

**Table 3-14. Comparison of Total Nitrogen Released for Coupled and Extended Flowsheets on a DWPF Scale**

| Species | SB9A-6A, 120% 4L | SB9A-9A, 120% 4L Coupled | SB9A-10A, 120% 4L Extended |
|---|---|---|---|
| N from NO, mol in Off-gas | 195 | 279 | 262 |
| N from NO2, mol in Off-gas | 824 | 860 | 760 |
| N from Sub-Total | 1020 | 1,139 | 1022 |
| N from N2O, mol in Off-gas | 1235 | 600 | 679 |
| Total mol of N Released | 2,255 | 1,739 | 1,701 |
| Mol N from $NO_2$ in Feed | 3102 | 4227 | 3104 |
| Total Mol N Released/mol Feed $NO_2$ | 0.73 | 0.37 | 0.55 |

*3.4.4 SB9A-11A Differences*

SB9A-11A was conducted in a manner that was identical to SB9A-6A, with the exception of ruthenium precursor selection. Experiment SB9A-6A utilized $Ru(NO)(NO_3)_3$, whereas SB9A-11A employed $RuCl_3$ as the ruthenium source.

Table 3-15 gives the supernatant concentration of the noble metals used in CPC simulant runs at various stages throughoutSB9A-6A and SB9A-11A.

**Table 3-15. Concentration of Selected Metals in SB9A-11A and SB9A-6A Supernate**

| | Trimmed Sludge | | Immediately After Acid Addition | | Five hours into Reflux | | SRAT Product | |
|---|---|---|---|---|---|---|---|---|
| | *SB9A-6A* | *SB9A-11A* | *SB9A-6A* | *SB9A-11A* | *SB9A-6A* | *SB9A-11A* | *SB9A-6A* | *SB9A-11A* |
| **Ag, mg/L** | <1.00 | <1.00 | <1.00 | <1.00 | <1.00 | <1.00 | <1.00 | <1.00 |
| **Pd, mg/L** | --- | 2.17 | <1.00 | <1.00 | <1.00 | <1.00 | <1.00 | <1.00 |
| **Ru, mg/L** | <1.00 | <1.00 | 50.0 | 7.40 | 1.74 | <1.00 | <1.00 | <1.00 |
| **Rh, mg/L** | <1.00 | <1.00 | 17.45 | 16.45 | <1.00 | <1.00 | 1.61 | <1.00 |

Predictably, most of the noble metals exhibit no significant difference in supernatant concentration throughout the SRAT process except after acid additions. Immediately following the addition of trim chemicals, silver, ruthenium, and rhodium are undetectable in the supernatant liquid, and palladium is present in only small amounts (2.17 mg/L in SB9A-11A), suggesting a slow rate of dissolution. Upon acid addition, there is a significant change in ruthenium and rhodium concentration, with rhodium increasing to over 16 mg/L in both runs. Interestingly, SB9A-6A exhibits a much larger change in ruthenium concentration upon acid addition compared to SB9A-11A (increase to 50 mg/L in SB9A-6A, versus 7.4 mg/L in SB9A-11A). This is likely due to increased solubility of the ruthenium nitrosyl nitrate species compared to the ruthenium chloride species. After 5 hours of refluxing during the SRAT cycle, the concentration of ruthenium decreased significantly in each run, dropping to 1.74 mg/L in SB9A-6A and below detection limits in SB9A-11A. The lowered concentration of metals in the SRAT product supernate suggests that the metals have undergone chemical transitions to insoluble species.

It is possible that the difference in ruthenium solubility could effect a change in the CPC reaction behavior. In particular, a change in ruthenium concentration has the capacity to influence: 1.) the production of flammable hydrogen gas via metal-catalyzed dehydrogenation of formic acid and 2.) the production of $N_2O$ via the metal-catalyzed reduction of nitrous acid (formed in solution via protonation of nitrite ion with acid).

The combination of noble metal catalysts and formic acid present in the SRAT cycle are believed to lead to the evolution of $H_2$ and $CO_2$ gasses via the metal-catalyzed dehydrogenation of formic acid, shown in Equation 2.

$$HCOOH \xrightarrow{catalyst} H_2 + CO_2 \qquad \text{Equation 2}$$

Given the fact that ruthenium is a known catalyst for dehydrogenation, it is important to evaluate the effects of the ruthenium precursor selection on the production of hydrogen gas. Figure 3-23 shows the hydrogen off-gas data from runs SB9A-6A and S9A-11A.

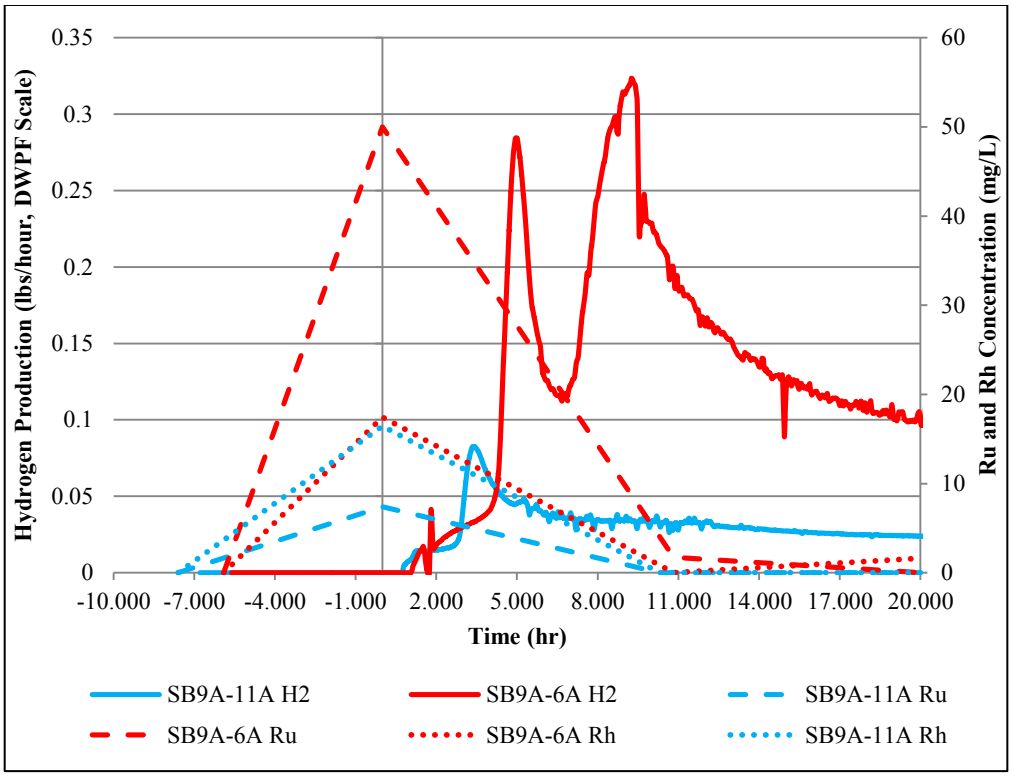


**Figure 3-23. Production of Hydrogen during the SRAT Cycle**

It is evident that significantly more hydrogen is produced when the $Ru(NO)(NO_3)_3$ was used as a precursor, compared to that achieved with $RuCl_3$, with SB9A-6A achieving a peak hydrogen production of 0.32 lbs/hour (solid red line), while SB9A-11A peaks just short of 0.08 lbs/hour (solid blue line). The concentration of rhodium in the supernate is statistically the same. Furthermore, SB9A-6A exhibits two distinct peaks of hydrogen formation, which is characteristic of the typical SRAT simulant process. However, SB9A-11A exhibits only one peak around four hours following acid addition before trailing towards zero. The difference in hydrogen production is likely due to strong differences in ruthenium catalyst solubility (the supernatant concentration of ruthenium is shown in dotted lines for convenience). This is seen more clearly by normalizing the average rate of hydrogen production during the SRAT cycle (total moles of $H_2$ produced during the SRAT cycle, divided by the number of hours during which $H_2$ was being produced within the SRAT cycle) by the moles of $H_2$ that could be formed as a result of formic acid addition, and then plotting the normalized $H_2$ production rate against the measured supernate concentration of Ru immediately after completing acid addition (maximum Ru concentration) as shown in Figure 3-24.

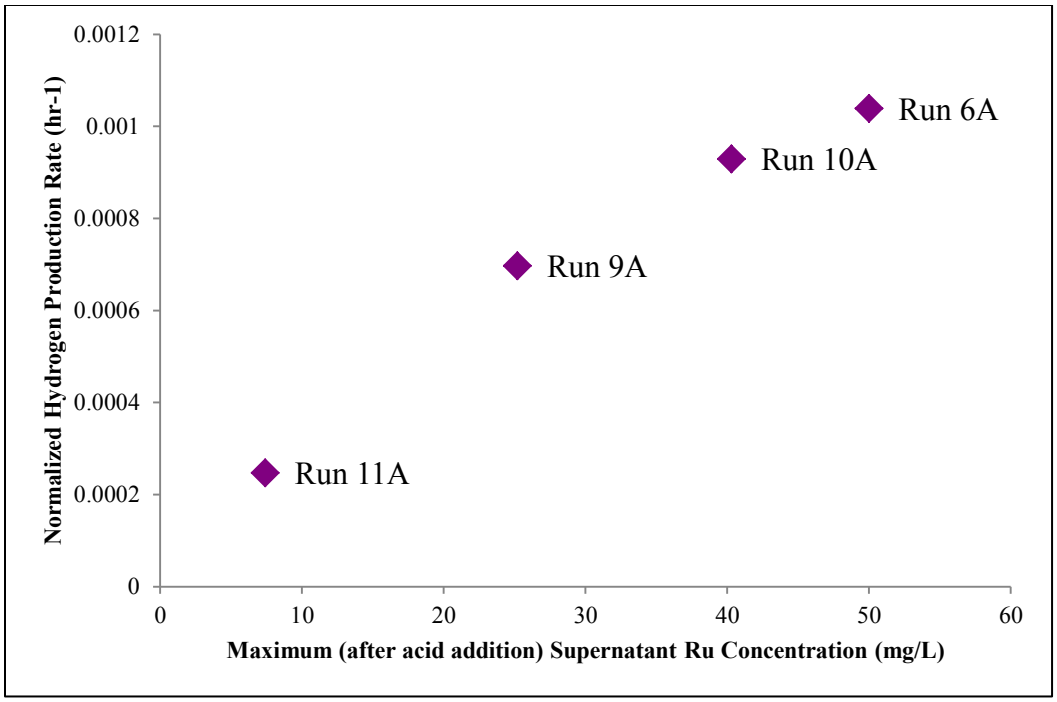


**Figure 3-24. Normalized 4L 120% KMA SRAT Cycle Hydrogen Production Rate**

There is a direct relationship between catalyst solubility and the production of hydrogen gas, as is shown by the monotonic increase in normalized hydrogen production rate as ruthenium concentration is increased. Although the normalized hydrogen generation accounts for other generators of hydrogen, Ru is the greatest mass of noble metals added (see Table 2-1), and the heat transfer coefficient was similar or less than SB9A-11A (see Figure 3-6). Of the runs conducted at 120% KMA stoichiometry, SB9A-11A ($RuCl_3$) exhibits the lowest normalized $H_2$ production rate (0.0002 $hr^{-1}$) at a ruthenium concentration of 7.4 mg/L, and SB9A-6A ($Ru(NO)(NO_3)_3$) exhibits the highest normalized $H_2$ production rate (0.001 $hr^{-1}$) at a ruthenium concentration of 50.0 mg/L.

**Table 3-16. Ruthenium Concentration in Supernate after Acid Addition**

| | SB9A-3A | SB9A-5A | SB9A-6A | SB9A-9A | SB9A-10A | SB9A-11A |
|---|---|---|---|---|---|---|
| Ru Supernate Concentration after acid addition mg/L | 51.35 | 44.86 | 49.99 | 25.16 | 40.3 | 7.4 |

Nitrite destruction has the capacity to produce a variety of gaseous compounds, including $N_2O$, NO, and $NO_2$, during the SRAT cycle. The disproportionation of $NO_2$ to $NO_3$, NO, and water is believed to account for the majority (~75%) of catalyst-free nitrite reduction during the SRAT cycle. This is shown in Equation 3.

$$3HNO_2 \rightarrow HNO_3 + 2NO + H_2O \qquad \text{Equation 3}$$

Figure 3-25 shows the production of NO during the SRAT cycles in SB9A-6A and SB9A-11A.

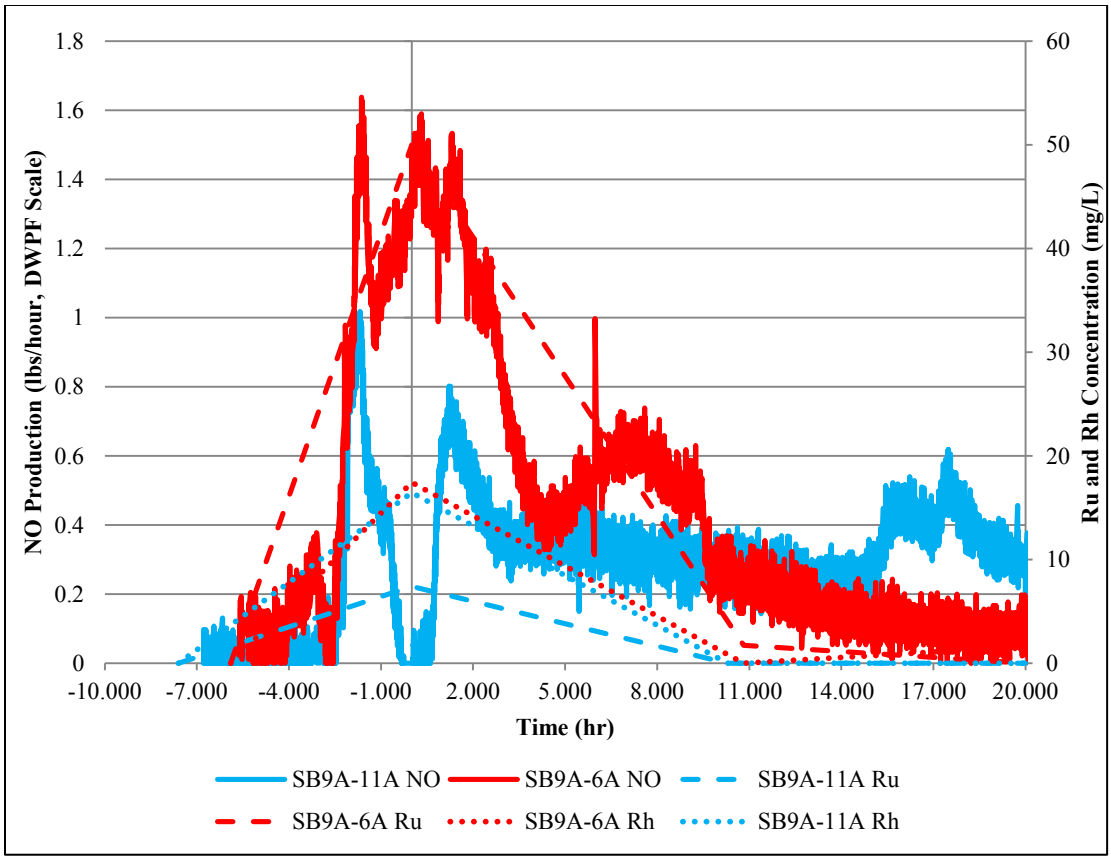


**Figure 3-25. Production of NO during the SRAT Cycle**

NO off-gas appears to spike in SB9A-6A as acid addition is completed, reaching approximately 1.6 lbs/hour at hour 0. By comparison, NO production from 11A drops to nearly zero at the same time. The peak NO generations for SB9A-11A is ~1 lbs/hr and occurs during acid addition. It is known that NO reacts rapidly with air to form $NO_2$, as shown in Equation 4.

$$O_2 + 2NO \rightarrow 2NO_2 \qquad \text{Equation 4}$$

Given this, Equation 2 can be re-written to express the disproportionation of nitrous acid in the presence of air, shown in Equation 5

$$O_2 + 3HNO_2 \rightarrow HNO_3 + 2NO_2 + H_2O \qquad \text{Equation 5}$$

Figure 3-26 shows the off-gas measurement of $NO_2$ during the SRAT cycles of SB9A-6A and SB9A-11A.

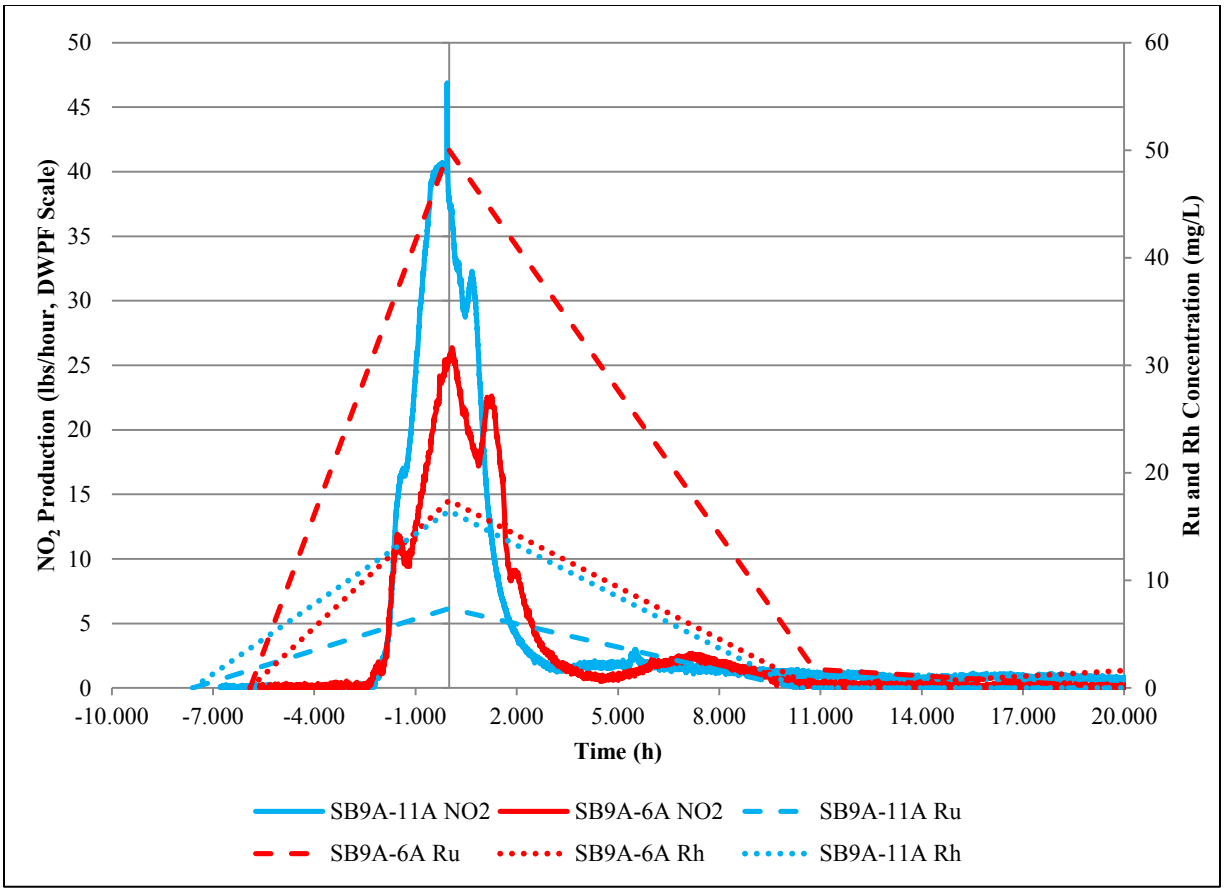


**Figure 3-26. Production of $NO_2$ during the SRAT Cycle**

More $NO_2$ is produced in both SB9A-6A (26 lbs/hour at hour 0) and SB9A-11A (47 lbs/hour at hour 0) compared to NO (1.6 lbs/hour and 0 lbs/hour at hour 0, respectively). SB9A-11A exhibited an $NO_2$ production rate that is significantly higher than SB9A-6A. The reason for this difference is unclear, but might suggest alternate pathways of nitrite reduction available in SB9A-6A, due to heightened catalyst presence.

In addition to the reaction described in Equations 3 and 5, a second reaction pathway for nitrite destruction has been previously proposed, describing the destruction of nitrite in the presence of formic acid to form $N_2O$, water, and $CO_2$. This reaction is believed to account for the balance of metal-free nitrite destruction (~25%), and is shown in Equation 6.

$$2HNO_2 + 2HCOOH \rightarrow N_2O + 3H_2O + 2CO_2 \qquad \text{Equation 6}$$

Figure 3-27 shows the production of $N_2O$ during the SRAT cycles of SB9A-6A and SB9A-11A.

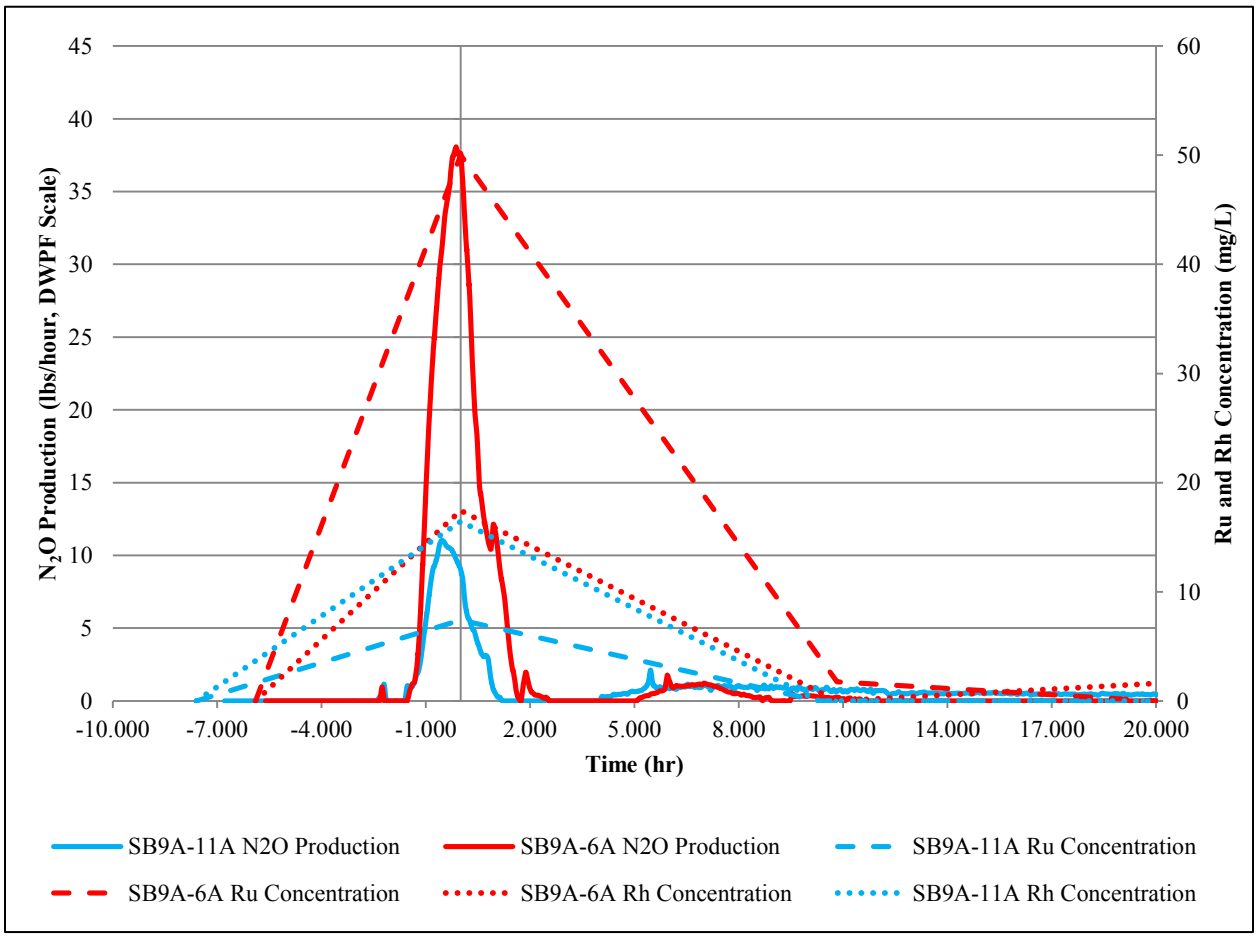


**Figure 3-27. Production of $N_2O$ during the SRAT Cycle**

SB9A- 6A generates more $N_2O$ than SB9A-11A, with SB9A-6A $N_2O$ production peaking at 42 lbs/hour compared to the peak $N_2O$ production of 12 lbs/hour achieved in SB9A-11A. Additionally, when compared to the available ruthenium concentration data, it seems that the production of $N_2O$ may be proportional to the concentration of available catalyst. This may suggest the presence of a catalytic pathway for the destruction of nitrite, as shown in Equation 7.

$$HNO_2 + reducing\ agent \xrightarrow{catalyst} N_2O + side\ products \qquad \text{Equation 7}$$

Assuming the possibility of this alternate nitrite destruction pathway, the rates of $N_2O$ production, relative to those of $NO_x$ gases, can be plotted against catalyst concentration in order to observe the effects of catalyst solubility on nitrite destruction chemistry, as shown in Figure 3-28.

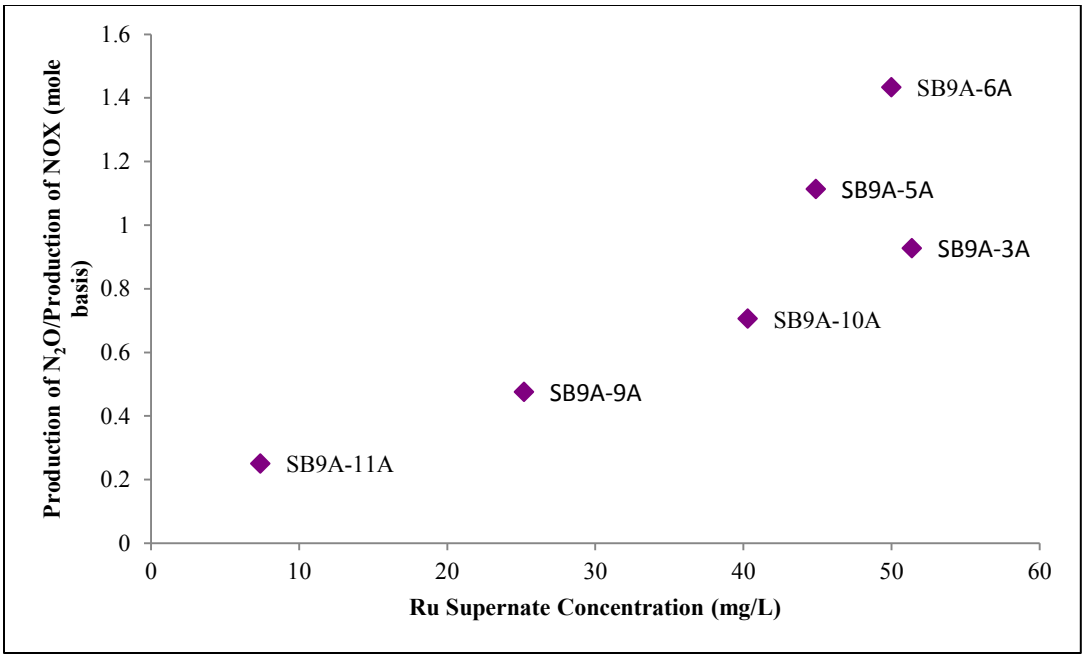


**Figure 3-28. $N_2O$ Release Rate at Completion of Acid Addition vs. Ruthenium Concentration**

The data in Figure 3-28 agrees with the hypothesis of an alternate catalytic pathway for nitrite destruction, exhibiting preference for forming $NO_x$ gases at lower catalyst concentrations. This is clearly demonstrated in SB9A-11A and SB9A-9A, where 4 moles and 2.1 moles of $NO_x$ are produced per mole of $N_2O$ at catalyst concentrations of 7.4 and 25.2 mg/L, respectively. The production of $N_2O$ appears to dominate at higher catalyst concentrations, as seen in SB9A-5A and SB9A-6A (1.1 and 1.4 moles of $N_2O$ produced per mole of $NO_x$ at catalyst concentrations of 44.9 and 50 mg/L, respectively).

The $Ru(NO)(NO_3)_3$ catalyst was used to avoid formation of mercury chloride compounds, such as calomel, that interfere with the ability to determine the flowsheet's ability to strip mercury, and to better simulate the expected chemical forms of mercury in DWPF. The change in Ru precursor may have led to the overly conservative formation of hydrogen in simulant experiments. Independent of the catalyst type, SRNL adds excess noble metals to ensure hydrogen generation bounds standard DWPF processing conditions. Therefore, when the evaluation of hydrogen generation in the nitric-formic CPC flowsheet simulant testing is of more interest than mercury studies, the $RuCl_3$ precursor should be used. Additional study/evaluation should also be performed using the $Ru(NO)(NO_3)_3$ catylyst to better understand the effects, if any, on nitrogen off-gas species.

## 3.5 Mercury Removal

Mercury was added to the sludge at 2.48wt.% as a slurry of HgO. HgO is a reddish orange color because it likely contains two crystalline phases that are red and yellow [14]. The sample, pulled after mixing a minimum of thirty minutes, consistently shows that mercury is well below 2.48 wt.% in the sludge indicating that the sample is not representative of the sludge, the HgO has not solubilized, or the analysis is biasing low. Unrepresentative sampling is unlikely because samples are taken in duplicate from the vessel about 1/3 from the bottom while mixing. During some of the runs, an orange–yellow film would accumulate on the off-gas lines to the condenser and MWWT, in addition to the sludge interface. Figure 3-29 illustrates the film seen at the interface in the 1L pH probe port about an hour after starting the run. The port is located below the starting sludge level (see Figure 2-2) in an area of low mixing. As acid

addition proceeds, off-gas and condensate became more acidic which caused the orange-yellow film to disappear in every case.

**Figure 3-29. Mercury Undissolved in Sludge**

These observations indicate that initial analysis results are low likely due to unsolubilized HgO. Literature shows that HgO increases in solubility under acidic conditions and as temperature increases [14]. Analytical balances used are M&TE equipment with an error of +/- 0.02%; thus, there is high confidence that the expected amount of mercury was added. All analytical results for mercury were normalized to a starting result of 2.48 wt.% (see Figure 3-30). While this could arbitrarily inflate the mercury concentration at points during mercury stripping, it is conservative when evaluating the flowsheet's ability to reduce and strip mercury.

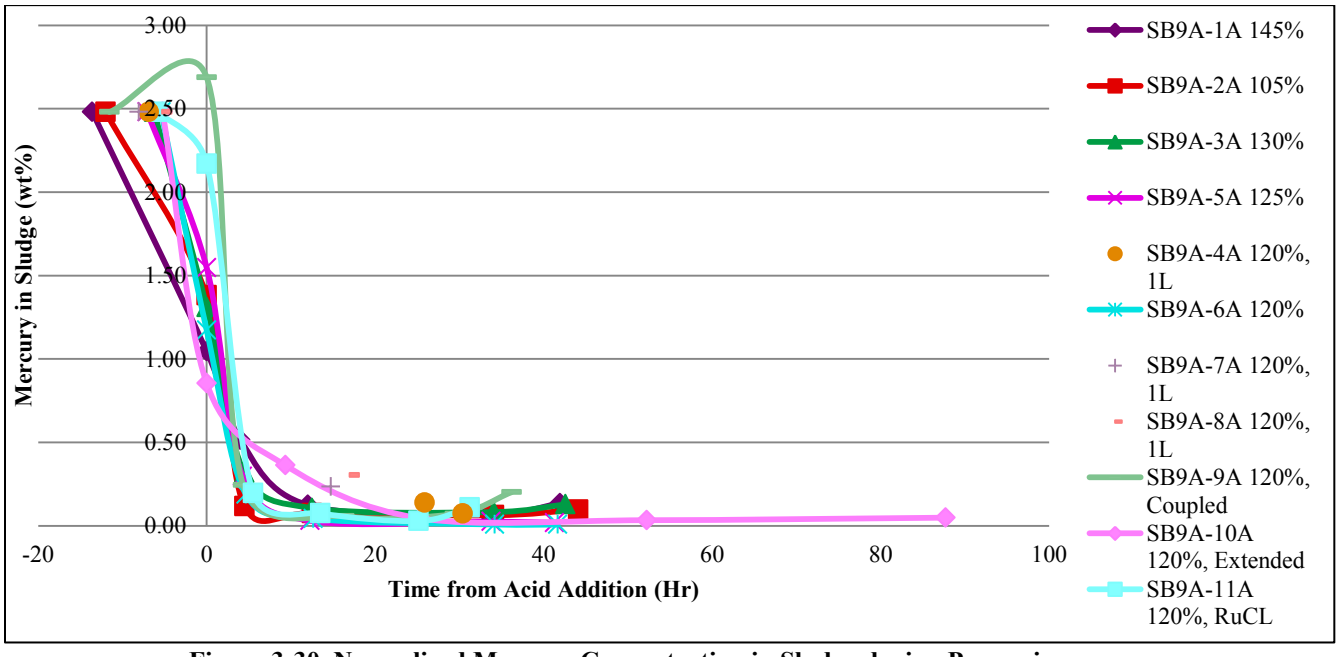


**Figure 3-30. Normalized Mercury Concentration in Sludge during Processing**

During the SME cycle, further volume reduction of the slurry causes the level of mercury in the sludge to appear to rise. Comparing the normalized SRAT product mercury concentration to the DWPF design basis mercury limit indicates that all runs meet the DWPF design basis limit, 0.45 wt.% total solids, except SB9A-4A (see Table 3-17). Both SB9A-3A and SB9A-4A were performed at 130% of the KMA, and assumed higher conversion of nitrite to nitrate, along with assumed greater formate destruction. However, SB9A-3A met the DWPF mercury limit. Although, it is possible that the normalization biased the SRAT product concentration high, it is more likely that differences in the heat transfer to the system and off-gas pathway caused deviations in mercury stripping. The 1L off-gas leg is made of 316, whereas the 4L is made of glass. Although both are insulated with foam, the thermal conductivity of 316 is significantly higher than glass. In addition, both off-gas legs are about the same size. Therefore, it is feasible that elemental mercury could drop out and be transferred back to the 1L vessel at a higher rate than in the 4L laboratory scale setup.

**Table 3-17. Mercury in SRAT Product**

| | **SB9A-1A, 145%** | **SB9A-2A, 105%** | **SB9A-3A, 130%** | **SB9A-4A, 130%** | **SB9A-5A, 125%** | **SB9A-6A, 120%** | **SB9A-9A, 120%** | **SB9A-10A, 120%** | **SB9A-11A, 120%** |
|---|---|---|---|---|---|---|---|---|---|
| Normalized Hg in SRAT Product, mg/Kg Slurry | 658 | 630 | 821 | 1376 | 252 | 77 | 713 | 334 | 284 |
| TS in SRAT Product | 22.65% | 24.31% | 24.33% | 22.76% | 24.33% | 24.94% | 27.38% | 24.19 % | 24.64% |
| Hg wt.% Total Solids | 0.29% | 0.26% | 0.34% | 0.60% | 0.10% | 0.03% | 0.26% | 0.14% | 0.12% |
| DWPF Hg Limit wt.% Total Solids | 0.45% | | | | | | | | |

The actual, non-normalized, mercury concentration in the sludge can be seen in Table 7-4. Using mercury samples taken periodically during the SRAT process (see Figure 3-29), the percent removal can be tracked as seen Table 3-18.

**Table 3-18. Mercury Removal**

| **Mercury Removed** | **SB9A-1A** | **SB9A-2A** | **SB9A-3A** | **SB9A-4A** | **SB9A-5A** | **SB9A-6A** | **SB9A-9A** | **SB9A-10A** | **SB9A-11A** |
|---|---|---|---|---|---|---|---|---|---|
| *by Completion of Dewater* | 79.3% | 95.3% | 87.2% | N/A | 88.1% | 92.4% | 90.2% | 85.4% | 92.1% |
| *at End of SRAT Cycle* | 97.3% | 97.5% | 96.7% | 94.5% | 99.0% | 99.7% | 97.1% | 98.7% | 98.9% |

Mercury is collected in the MWWT. At the end of the SRAT cycle, the material is collected, dried, and weighed. The total mass collected in the MWWT can be found in Table 3-19. Elemental mercury was found at the bottom of various SME products and within REDOX samples after drying. Thus, the mercury mass balance is not considered closed.

**Table 3-19. Mercury Mass Balance**

| *Mercury Removed* | SB9A -1A | SB9A -2A | SB9A -3A | SB9A -4A | SB9A -5A | SB9A -6A | SB9A -7A | SB9A -8A | SB9A -9A | SB9A-10A | SB9A-11A |
|---|---|---|---|---|---|---|---|---|---|---|---|
| Mass in MWWT (Removed), g | 2.444 | 1.268 | 4.773 | 1.403 | 2.310 | 2.299 | 0.628 | 1.777 | 2.597 | 1.627 | 2.998 |
| Mass Hg Added, g | 13.517 | 13.529 | 13.425 | 5.606 | 13.585 | 13.587 | 5.236 | 5.237 | 13.577 | 13.579 | 13.579 |
| % Removed | 18.1% | 9.4% | 35.6% | 25.0% | 17.0% | 16.9% | 12.0% | 33.9% | 19.1% | 12.0% | 22.1% |

3.6 SRAT and SME Cycle Anions

Slurry anion data are given in Table 3-20 and Table 3-21 for SRAT and SME products.

**Table 3-20. SRAT Product Anion Results on a Slurry Basis**

| Slurry | SB9A-1A, 145% | SB9A-2A, 105% | SB9A-3A, 130% | SB9A-4A, 130% | SB9A-5A, 125% | SB9A-6A, 120% | SB9A-7A, 120% | SB9A-8A, 120% | SB9A-9A, 120% Coupled | SB9A-10A, 120%, Extended | SB9A-11A, 120% $RuCl_3$ |
|---|---|---|---|---|---|---|---|---|---|---|---|
| Nitrite, mg/kg | <100 | <100 | <100 | <100 | <500 | <500 | <500 | <500 | <500 | <500 | <500 |
| Nitrate, mg/kg | 25,000 | 23,450 | 19,600 | 19,450 | 24,800 | 25,700 | 27,150 | 26,700 | 30,150 | 26,050 | 23,500 |
| Sulfate, mg/Kg | 1,530 | 1,690 | 1,765 | 1,530 | 1,650 | 1,670 | 1,470 | 1,530 | 1,960 | 1,655 | 1,655 |
| Oxalate, mg/kg | 4,140 | 4,420 | 4,460 | 4,325 | 4,440 | 4,175 | 3,970 | 4,195 | 5,820 | 4,535 | 4,545 |
| Formate, mg/kg | 40,350 | 46,650 | 54,750 | 50,400 | 42,100 | 48,800 | 50,100 | 46,600 | 59,050 | 43,000 | 51,400 |

**Table 3-21. SME Product Anion Results on a Slurry Basis**

| Slurry | SB9A-1A, 145% | SB9A-2A, 105% | SB9A-3A, 130% | SB9A-4A, 130% | SB9A-5A, 125% | SB9A-6A, 120% | SB9A-7A, 120% | SB9A-8A, 120% | SB9A-9A, 120% Coupled | SB9A-10A, 120%, Extended | SB9A-11A, 120% $RuCl_3$ |
|---|---|---|---|---|---|---|---|---|---|---|---|
| Nitrite, mg/kg | <100 | <100 | <100 | <100 | <500 | <500 | N/A | | <500 | <500 | <500 |
| Nitrate, mg/kg | 20,200 | 17,300 | 14,900 | 14,400 | 19,500 | 21,200 | | | 24,300 | 18,900 | 19,900 |
| Sulfate, mg/kg | 1,280 | 1,300 | 1,500 | 1,120 | 1,360 | 1,390 | | | 1,750 | 1,400 | 1,340 |
| Oxalate, mg/kg | 3,530 | 3,470 | 3,890 | 3,200 | 3,620 | 3,300 | | | 5,320 | 3,490 | 3,220 |
| Formate, mg/kg | 33,900 | 38,400 | 44,800 | 40,600 | 35,500 | 41,700 | | | 46,600 | 30,100 | 42,500 |

Nitrite can be destroyed during formic acid addition via the major mechanisms [15]:

$$3NaNO_2 + 3HCOOH \rightarrow 3HNO_2 + 3HCOONa \rightarrow HNO_3 + 2NO + H2O + 3HCOONa \quad \text{Equation 8}$$

$$2NaNO_2 + 3HCOOH \rightarrow 2HCOONa + 2NO + CO_2 + 2H2O \quad \text{Equation 9}$$

$$2NaNO_2 + 4HCOOH \rightarrow N_2O + 2HCOONa + 3H_2O + 2CO_2 \quad \text{Equation 10}$$

The reactions were written for sodium nitrite, since that is the primary nitrite species in the sludge. The second and third reactions could also be written for $HNO_2$ instead, since that species probably dominates

at the pH ranges seen for nitrite destruction. $NO_2$ is formed by the reaction of NO and $O_2$ in the vapor space.

$$2NO + O_2 \rightarrow 2NO_2 \quad \text{Equation 11}$$

Nitrate and nitrite can be converted to ammonia via the mechanisms below.

$$5HCO_2H + NO_3 \rightarrow NH_3 + HCO_2 + 4CO_2 + 3H_2O \quad \text{Equation 12}$$
$$4HCO_2H + NO_2 \rightarrow NH_3 + HCO_2 + 3CO_2 + 2H_2O \quad \text{Equation 13}$$

Alternatively the following nitrogen reactions could also exist.

$$5HCO_2H + 2NO \rightarrow 2NH_3 + 5CO_2 + 2H_2O \quad \text{Equation 14}$$
$$2HCO_2 + 2NO \rightarrow N_2 + 2CO_2 + 2H_2O \quad \text{Equation 15}$$

The neutralization reactions of soluble hydroxides produce water. Neutralization of insoluble carbonate produces water and $CO_2$. The following REDOX equations also result in $CO_2$ formation.

$$MnO_2 + 3HCO_2H \rightarrow Mn(COOH)_2 + 2H_2O + CO_2 \quad \text{Equation 16}$$
$$HgO + HCO_2H \rightarrow Hg + H_2O + CO_2 \quad \text{Equation 17}$$

While the gas analyzer monitors nitrogen, the air purge makes it difficult to detect small changes in $N_2$ concentration due to $N_2$ formation. Mass balances were performed using the off-gas, analytical, and process data to evaluate the nitrite, nitrate, and formate consumption. The nitrogen and carbon balances can be seen in Table 3-22 and Table 3-23. Analytical results that are less than the detection limit are treated as a zero in the mass balance to be conservative. As seen in Table 2-7, the 1L scaled runs only utilize the GC; therefore, NO, $NO_2$, and $N_2O$ were not analyzed for. This is noted by an "N/A" in Table 3-22. Lack of analysis causes the percent variance and unanalyzed nitrogen species to be greater than the 4L runs.

**Table 3-22. Laboratory Scale Nitrogen Mass Balance**

| | SB9A-1A, 145% | SB9A-2A, 105% | SB9A-3A, 130% | SB9A-4A, 130% | SB9A-5A, 125% | SB9A-6A, 120% | SB9A-7A, 120% | SB9A-8A, 120% | SB9A-9A, 120% Coupled | SB9A-10A, 120%, Extended | SB9A-11A, 120% $RuCl_3$ |
|---|---|---|---|---|---|---|---|---|---|---|---|
| N from $NO_2$ in Feed, mol | 0.73 | 0.73 | 0.73 | 0.30 | 0.73 | 0.73 | 0.34 | 0.28 | 0.78 | 0.73 | 0.73 |
| N from $NO_3$ in Feed, mol | 0.32 | 0.32 | 0.32 | 0.13 | 0.31 | 0.31 | 0.12 | 0.12 | 0.52 | 0.32 | 0.31 |
| N from $NO_3$ Added as Acid, mol | 0.84 | 0.47 | 0.46 | 0.19 | 0.65 | 0.61 | 0.25 | 0.25 | 0.57 | 0.56 | 0.60 |
| **TOTAL N IN** | 1.89 | 1.51 | 1.51 | 0.62 | 1.70 | 1.65 | 0.71 | 0.66 | 1.87 | 1.61 | 1.64 |
| N from NO gas, mol | 0.06 | 0.03 | 0.04 | N/A | 0.05 | 0.03 | N/A | N/A | 0.04 | 0.04 | 0.02 |
| N from $NO_2$ gas, mol | 0.09 | 0.11 | 0.10 | N/A | 0.11 | 0.11 | N/A | N/A | 0.13 | 0.10 | 0.15 |
| N from $N_2O$ gas, mol | 0.19 | 0.14 | 0.19 | N/A | 0.07 | 0.17 | N/A | N/A | 0.09 | 0.09 | 0.11 |
| N from $NO_3$ Loss in Dewater, mol | 0.01 | 0.05 | 0.01 | 0.02 | 0.03 | 0.01 | 0.00 | 0.02 | 0.11 | 0.02 | 0.05 |
| N from $NO_3$ Removed in Samples, mol | 0.13 | 0.13 | 0.12 | 0.07 | 0.17 | 0.19 | 0.10 | 0.11 | 0.22 | 0.16 | 0.15 |
| N from $NO_3$ in SME Product, mol | 0.80 | 0.64 | 0.54 | 0.23 | 0.72 | 0.76 | 0.21 | 0.20 | 0.72 | 0.67 | 0.74 |
| N from $NH_4$ in SME, mol | 0.04 | 0.00 | 0.07 | 0.03 | 0.02 | 0.02 | 0.00 | 0.01 | 0.02 | 0.01 | 0.01 |
| N from $NH_4$ in Scrubber, mol | 0.00 | 0.00 | 0.00 | 0.00 | 0.02 | 0.00 | 0.00 | 0.00 | 0.00 | 0.01 | 0.00 |
| **TOTAL N OUT** | 1.23 | 1.04 | 0.97 | 0.36 | 1.15 | 1.22 | 0.31 | 0.34 | 1.29 | 1.06 | 1.18 |
| Variance | 34.7% | 31.6% | 35.7% | 42.3% | 32.5% | 26.5% | 56.7% | 47.4% | 31.0% | 33.9% | 28.0% |
| Unanalyzed Nitrogen Species, mol | 0.66 | 0.48 | 0.54 | 0.26 | 0.55 | 0.44 | 0.40 | 0.31 | 0.58 | 0.55 | 0.46 |

**Table 3-23. Laboratory Scale Carbon Mass Balance**

| | SB9A-1A, 145% | SB9A-2A, 105% | SB9A-3A, 130% | SB9A-4A, 130% | SB9A-5A, 125% | SB9A-6A, 120% | SB9A-7A, 120% | SB9A-8A, 120% | SB9A-9A, 120% Coupled | SB9A-10A, 120%, Extended | SB9A-11A, 120% $RuCl_3$ |
|---|---|---|---|---|---|---|---|---|---|---|---|
| TIC in Sludge, mol | 0.44 | 0.44 | 0.44 | 0.18 | 0.44 | 0.44 | 0.17 | 0.17 | 0.49 | 0.44 | 0.44 |
| Formate Added in SRAT, mol | 4.68 | 3.54 | 4.46 | 1.86 | 4.10 | 3.96 | 1.58 | 1.57 | 4.46 | 3.99 | 3.97 |
| Formate Added in SME, mol | 0.19 | 0.19 | 0.19 | 0.07 | 0.19 | 0.19 | 0.00 | 0.00 | 0.17 | 0.17 | 0.19 |
| **TOTAL IN** | **5.32** | **4.17** | **5.09** | **2.11** | **4.74** | **4.59** | **1.75** | **1.74** | **5.12** | **4.61** | **4.60** |
| TIC Removed in Dewater, mol | 0.00 | 0.00 | 0.00 | 0.00 | 0.00 | 0.00 | 0.00 | 0.00 | 0.00 | 0.00 | 0.00 |
| Formate Removed in Dewater | 0.09 | 0.01 | 0.05 | 0.01 | 0.03 | 0.02 | 0.01 | 0.02 | 0.02 | 0.00 | 0.00 |
| TIC in SME Product, mol | 0.15 | 0.13 | 0.07 | 0.02 | 0.12 | 0.07 | 0.00 | 0.00 | 0.08 | 0.14 | 0.00 |
| Formate in SME Product, mol | 1.85 | 1.95 | 2.23 | 0.91 | 1.80 | 2.07 | 0.87 | 0.80 | 1.90 | 1.48 | 2.17 |
| Formate Removed in Samples | 0.30 | 0.35 | 0.45 | 0.25 | 0.40 | 0.50 | 0.25 | 0.26 | 0.60 | 0.37 | 0.46 |
| $CO_2$ gas, mol | 2.87 | 1.62 | 2.32 | 1.25 | 2.39 | 2.03 | 0.70 | 0.83 | 1.89 | 2.89 | 1.77 |
| **TOTAL OUT** | **5.25** | **4.07** | **5.11** | **2.30** | **4.75** | **4.68** | **1.83** | **1.90** | **4.50** | **4.88** | **4.40** |
| Variance | 1.3% | 2.5% | -0.4% | -15.8% | -0.2% | -1.9% | -4.7% | -9.3% | 12.2% | -5.9% | 4.3% |
| Unanalyzed Carbon Species, mol | 0.07 | 0.11 | -0.02 | -0.19 | -0.01 | -0.09 | -0.08 | -0.16 | 0.62 | -0.27 | 0.20 |

The nitrogen mass balance does not include any nitrogen species the MWWT, scrubber, and FAVC. Previous studies have found that nitrate in the condensate and ammonia scrubber accounted for approximately 50% of the feed nitrogen [12]. Furthermore, small fluctuations in $N_2$ (as a result of formation) cannot be distinguished from the nitrogen in the air purge. The carbon mass balance is closed within analytical uncertainty. Deviations are likely a result of analytical and instrumental uncertainty. Analytical results (see Table 3-20 and Table 3-21) indicated that in all runs nitrite was completely destroyed. Given the total carbon and nitrogen balance it is expected that nitrite destruction was the source of the unanalyzed nitrogen species.

Formate loss, nitrite loss, and nitrate gain following acid addition and after the SRAT cycle are presented in Table 3-24. Post SRAT and SME cycle data was corrected for loss associated with sampling and SRAT dewater. These numbers were presented on a product basis only in previous reports because dewater data was not previously available. Increasing nitrate (positive nitrate gain) is a result of conversion of nitrite to nitrate.

**Table 3-24. Change in Anion Composition Post Acid Addition and SRAT Product**

| | SB9A-1A, 145% | SB9A-2A, 105% | SB9A-3A, 130% | SB9A-4A, 130% | SB9A-5A, 125% | SB9A-6A, 120% | SB9A-7A, 120% | SB9A-8A, 120% | SB9A-9A, 120% Coupled | SB9A-10A, 120%, Extended | SB9A-11A, 120% $RuCl_3$ |
|---|---|---|---|---|---|---|---|---|---|---|---|
| Nitrite Loss, post acid Addition | 100.0% | 46.9% | 91.0% | N/A[g] | 82.8% | 77.2% | N/A[g] | N/A[g] | 84.0% | 87.6% | 84.8% |
| Nitrate Gain, post Acid Addition | 7.9% | -3.9% | -1.7% | N/A[g] | 23.7% | 23.9% | N/A[g] | N/A[g] | 32.8% | 43.3% | 6.1% |
| Formate loss, post Acid Addition | 16.7% | 23.6% | 29.9% | N/A[g] | 15.1% | 14.7% | N/A[g] | N/A[g] | 11.9% | 9.7% | 16.4% |
| Nitrite Loss, End of SRAT | 100% | 100% | 100% | 100% | 100% | 100% | 100% | 100% | 100% | 100% | 100% |
| Nitrate Gain, End of SRAT | -13.3% | 14.4% | -7.4% | 4.7% | 4.1% | 4.7% | -7.2% | -11.3% | 7.6% | 4.8% | 4.5% |
| Formate Loss, End of SRAT | 51.8% | 35.1% | 38.4% | 40.5% | 43.9% | 36.9% | 44.4% | 52.2% | 36.5% | 48.8% | 32.3% |
| Nitrate Loss, End of SME | 7.5% | 10.0% | 8.6% | 0.5% | 10.4% | 0.0% | N/A | | 9.6% | 8.7% | 0.0% |
| Formate Loss, End of SME | 12.5% | 8.3% | 9.2% | 0.1% | 13.0% | 5.2% | | | 20.3% | 19.8% | 10.0% |

[g]Sample not taken to conserve processing mass in 1L.

Post acid nitrite loss increases with increasing acid stoichiometry, in general. Upon completion of the SRAT cycle all nitrite was destroyed to below the detection limit of IC. For the sludge-only flowsheet, nitrate gain generally decreases with increased stoichiometry. The coupled and extended runs appear to gain more nitrate initially than the sludge-only flowsheet. SB9A-3A and SB9A-4A were performed based on higher assumptions for the conversion of nitrite to nitrate and the destruction of formate. This influenced the amount of each acid added, with less nitric acid and more formic acid added. It is expected that if the same assumptions had been used for all runs, the destruction of formate would have increased with increasing acid stoichiometry. Interestingly, SB9A-3A and SB9A-4A resulted in significantly more ammonium formation as evident in the SRAT products. Given reactions described in Equation 12 through Equation 14 it is likely that the over addition of formate caused the increased formation of the ammonium ion. It is also possible that the nitrate loss in some SRAT products is actually being converted to ammonium.

SB9A-4A formate loss appears less than other runs for the SME. This is likely due to uncertainty in the measurements.

**Table 3-25. Ammonium Content during CPC Processing**

| mg/mL | SB9A-1A, 145% | SB9A-2A, 105% | SB9A-3A, 130% | SB9A-4A, 130% | SB9A-5A, 125% | SB9A-6A, 120% | SB9A-7A, 120% | SB9A-8A, 120% | SB9A-9A, 120% Coupled | SB9A-10A, 120%, Extended | SB9A-11A, 120% $RuCl_3$ |
|---|---|---|---|---|---|---|---|---|---|---|---|
| SRAT Post Acid | <0.0 10 | < 0.010 | - | - | - | - | - | - | - | - | - |
| Scrubber Post acid | - | - | < 0.010 | - | 0.109 | < 0.025 | - | - | 0.012 | 0.015 | <0.010 |
| Dewater | - | - | - | < 0.010 | - | - | < 0.025 | < 0.025 | - | - | - |
| SRAT Product | - | - | 0.973 | 0.827 | 0.463 | 400 | < 0.025[h] | 0.456[h] | 0.186 | 0.481 | 0.073 |
| Scrubber end of SRAT | - | - | < 0.010 | - | 0.311 | 0.046 | - | - | - | - | - |
| SME Product | 0.428 | 0.030 | 0.782 | 0.633 | 0.157 | 0.252 | - | - | 0.214 | 0.065 | 0.076 |
| Scrubber end of SME | - | - | < 0.010 | - | 0.406 | 0.083 | - | - | - | 0.380 | < 0.010 |

[h]Run was not a full SRAT cycle.

## 3.7 SRAT and SME Elemental Solids Content

Total solids determined in the SRAT and SME products were near the targets. Total solids, calcined solids, insoluble solids, and soluble solids measured in the SRAT and SME products can be seen in Table 3-26 below. Total solids were near the targeted values.

**Table 3-26. Product Solids Content in SB9A-1A through SB9A-6A**

| | | SB9A-1A, 145% | SB9A-2A, 105% | SB9A-3A, 130% | SB9A-4A, 130% | SB9A-5A, 125% | SB9A-6A, 120% |
|---|---|---|---|---|---|---|---|
| **SRAT** | *Target Total Solids, wt.%* | 25.0% | | | | | |
| | *Total Solids, wt.%* | 22.6% | 24.3% | 24.3% | 22.8% | 24.3% | 24.9% |
| | *Calcined Solids, wt.%* | 15.3% | 16.5% | 16.4% | 15.1% | 15.8% | 16.1% |
| | *Insoluble Solids, wt.%* | 13.7% | 13.9% | 13.7% | 12.9% | 13.5% | 12.5% |
| | *Soluble Solids, wt.%* | 9.0% | 10.5% | 10.6% | 9.8% | 10.8% | 12.5% |
| **SME** | *Target Total Solids, wt.%* | 48.0% | | | | | |
| | *Total Solids, wt.%* | 45.7% | 47.5% | 47.6% | 41.6% | 46.6% | 48.9% |
| | *Calcined Solids, wt.%* | 40.1% | 41.7% | 41.5% | 36.2% | 39.9% | 41.3% |
| | *Insoluble Solids, wt.%* | 38.1% | 39.2% | 38.9% | 34.3% | 37.0% | 38.9% |
| | *Soluble Solids, wt.%* | 7.6% | 8.2% | 8.7% | 7.3% | 9.7% | 10.0% |

**Table 3-27. Product Solids Content in SB9A-7A through SB9A-11A**

| | | SB9A-7A, 120% | SB9A-8A, 120% | SB9A-9A, 120% | SB9A-10A, 120% | SB9A-11A, 120% |
|---|---|---|---|---|---|---|
| **After SEFT Addition** | *Total Solids, wt.%* | N/A | | 27.8% | N/A | |
| | *Calcined Solids, wt.%* | | | 18.4% | | |
| | *Insoluble Solids, wt.%* | | | 14.6% | | |
| | *Soluble Solids, wt.%* | | | 13.1% | | |
| **SRAT** | *Target Total Solids, wt.%* | 25.0% | | | | |
| | *Total Solids, wt.%* | 21.6% | 21.3% | 27.4% | 24.2% | 24.6% |
| | *Calcined Solids, wt.%* | 14.3% | 14.5% | 18.1% | 16.4% | 16.1% |
| | *Insoluble Solids, wt.%* | 11.0% | 11.2% | 13.9% | 13.6% | 12.8% |
| | *Soluble Solids, wt.%* | 10.6% | 10.1% | 13.5% | 10.6% | 11.8% |
| **SME** | *Target Total Solids, wt.%* | 48.0% | | | | |
| | *Total Solids, wt.%* | N/A | | 49.3% | 45.0% | 47.2% |
| | *Calcined Solids, wt.%* | | | 42.5% | 39.4% | 40.0% |
| | *Insoluble Solids, wt.%* | | | 38.4% | 36.5% | 37.4% |
| | *Soluble Solids, wt.%* | | | 10.9% | 8.5% | 9.8% |

The SRAT product elemental composition is listed in Table 3-28 on a calcined solids basis; the SME product results are listed in Table 3-29.

**Table 3-28. Calcined Solids Content in SRAT Product**

| Element wt.% | SB9A-1A, 145% | SB9A-2A, 105% | SB9A-3A, 130% | SB9A-4A, 130% | SB9A-5A, 125% | SB9A-6A, 120% | SB9A-7A, 120% | SB9A-8A, 120% | SB9A-9A, 120% Coupled | SB9A-10A, 120%, Extended | SB9A-11A, 120% $RuCl_3$ |
|---|---|---|---|---|---|---|---|---|---|---|---|
| Al | 9.78 | 9.76 | 9.81 | 9.78 | 9.38 | 9.11 | 9.38 | 9.89 | 9.17 | 9.70 | 9.58 |
| B | < 0.10 | < 0.10 | < 0.10 | < 0.10 | < 0.10 | < 0.10 | < 0.10 | < 0.10 | 0.21 | < 0.10 | < 0.10 |
| Ba | < 0.10 | < 0.10 | < 0.10 | < 0.10 | < 0.10 | < 0.10 | < 0.10 | < 0.10 | < 0.10 | < 0.10 | < 0.10 |
| Ca | 1.36 | 1.41 | 1.45 | 1.50 | 1.49 | 1.35 | 1.49 | 1.52 | 1.36 | 1.48 | 1.52 |
| Cr | 0.15 | 0.15 | 0.13 | 0.13 | 0.12 | 0.12 | 0.13 | 0.13 | 0.11 | 0.12 | 0.12 |
| Cu | < 0.10 | < 0.10 | < 0.10 | < 0.10 | < 0.10 | < 0.10 | < 0.10 | < 0.10 | < 0.10 | < 0.10 | < 0.10 |
| Fe | 24.1 | 24.1 | 24.8 | 24.7 | 23.9 | 23.2 | 23.9 | 24.6 | 22.5 | 24.1 | 23.7 |
| K | < 0.10 | < 0.10 | < 0.10 | < 0.10 | < 0.10 | < 0.10 | < 0.10 | < 0.10 | < 0.10 | < 0.10 | < 0.10 |
| La | < 0.10 | < 0.10 | N/A | N/A | N/A | N/A | N/A | N/A | N/A | N/A | N/A |
| Li | < 0.10 | < 0.10 | < 0.10 | < 0.10 | < 0.10 | < 0.10 | < 0.10 | < 0.10 | < 0.10 | < 0.10 | < 0.10 |
| Mg | 0.22 | 0.22 | 0.28 | 0.27 | 0.27 | 0.27 | 0.29 | 0.29 | 0.26 | 0.29 | 0.27 |
| Mn | 8.29 | 8.33 | 8.28 | 8.22 | 7.75 | 7.70 | 8.51 | 8.33 | 7.77 | 8.32 | 8.14 |
| Na | 15.6 | 15.8 | 16.3 | 16.3 | 14.6 | 14.4 | 15.6 | 15.7 | 20.2 | 16.8 | 16.6 |
| Ni | 1.75 | 1.73 | 1.78 | 1.76 | 1.69 | 1.64 | 1.70 | 1.74 | 1.68 | 1.81 | 1.75 |
| P | < 0.10 | < 0.10 | < 0.10 | < 0.10 | < 0.10 | < 0.10 | < 0.10 | < 0.10 | < 0.10 | < 0.10 | < 0.10 |
| Pd | < 0.10 | < 0.10 | < 0.10 | < 0.10 | < 0.10 | < 0.10 | < 0.10 | < 0.10 | < 0.10 | < 0.10 | < 0.10 |
| Rh | 0.17 | 0.24 | < 0.10 | < 0.10 | < 0.10 | < 0.10 | < 0.10 | < 0.10 | < 0.10 | < 0.10 | < 0.10 |
| Ru | < 0.10 | < 0.10 | < 0.10 | < 0.10 | < 0.10 | < 0.10 | < 0.10 | < 0.10 | < 0.10 | < 0.10 | < 0.10 |
| S | 0.39 | 0.38 | 0.31 | 0.31 | 0.32 | 0.33 | 0.35 | 0.34 | 0.33 | 0.34 | 0.32 |
| Si | 1.81 | 1.86 | 2.05 | 2.04 | 1.93 | 1.87 | 1.74 | 1.84 | 2.05 | 2.09 | 1.87 |
| Sn | < 0.10 | < 0.10 | < 0.10 | < 0.10 | < 0.10 | < 0.10 | < 0.10 | < 0.10 | < 0.10 | < 0.10 | < 0.10 |
| Ti | < 0.10 | < 0.10 | < 0.10 | < 0.10 | < 0.10 | < 0.10 | < 0.10 | < 0.10 | < 0.10 | < 0.10 | < 0.10 |
| Zn | < 0.10 | < 0.10 | < 0.10 | < 0.10 | < 0.10 | < 0.10 | < 0.10 | < 0.10 | < 0.10 | < 0.10 | < 0.10 |
| Zr | < 0.10 | < 0.10 | 0.11 | 0.11 | < 0.10 | < 0.10 | < 0.10 | < 0.10 | < 0.10 | 0.11 | < 0.10 |

**Table 3-29. Calcined Solids Content in SME Product**

| Element wt.% | SB9A-1A, 145% | SB9A-2A, 105% | SB9A-3A, 130% | SB9A-4A, 130% | SB9A-5A, 125% | SB9A-6A, 120% | SB9A-9A, 120% Coupled | SB9A-10A, 120%, Extended | SB9A-11A, 120% $RuCl_3$ |
|---|---|---|---|---|---|---|---|---|---|
| Al | 3.11 | 3.09 | 3.16 | 2.85 | 3.27 | 3.21 | 3.61 | 3.21 | 3.31 |
| B | 1.61 | 1.67 | 1.80 | 1.76 | 1.86 | 1.90 | 1.66 | 3.74 | 1.74 |
| Ba | < 0.10 | < 0.10 | < 0.10 | < 0.10 | < 0.10 | < 0.10 | < 0.10 | < 0.10 | < 0.10 |
| Ca | 0.42 | 0.44 | 0.40 | 0.36 | 0.41 | 0.40 | 0.43 | 0.41 | 0.40 |
| Cr | 0.04 | 0.04 | 0.04 | 0.04 | < 0.10 | < 0.10 | 0.05 | 0.04 | 0.04 |
| Cu | < 0.10 | < 0.10 | < 0.10 | < 0.10 | < 0.10 | < 0.10 | < 0.10 | < 0.10 | < 0.10 |
| Fe | 7.45 | 7.36 | 7.11 | 6.72 | 7.64 | 7.47 | 8.28 | 7.35 | 7.88 |
| K | < 0.10 | < 0.10 | < 0.10 | < 0.10 | < 0.10 | < 0.10 | < 0.10 | < 0.10 | < 0.10 |
| Li | 1.88 | 1.88 | 1.92 | 1.92 | 1.99 | 2.00 | 1.75 | 2.54 | 1.86 |
| Mg | 0.08 | 0.08 | < 0.10 | < 0.10 | < 0.10 | < 0.10 | < 0.10 | < 0.10 | < 0.10 |
| Mn | 2.58 | 2.57 | 2.56 | 2.27 | 2.82 | 2.78 | 2.96 | 2.59 | 2.73 |
| Na | 8.68 | 8.91 | 9.13 | 8.70 | 8.95 | 9.16 | 9.33 | 8.59 | 9.11 |
| Ni | 0.50 | 0.49 | 0.48 | 0.44 | 0.51 | 0.50 | 0.53 | 0.48 | 0.46 |
| P | < 0.10 | < 0.10 | < 0.10 | < 0.10 | < 0.10 | < 0.10 | < 0.10 | < 0.10 | < 0.10 |
| Pd | < 0.10 | < 0.10 | < 0.10 | < 0.10 | < 0.10 | < 0.10 | < 0.10 | < 0.10 | < 0.10 |
| Rh | 0.21 | 0.17 | < 0.10 | < 0.10 | < 0.10 | < 0.10 | < 0.10 | < 0.10 | < 0.10 |
| Ru | < 0.10 | < 0.10 | < 0.10 | < 0.10 | < 0.10 | < 0.10 | < 0.10 | < 0.10 | < 0.10 |
| S | < 0.10 | < 0.10 | < 0.10 | < 0.10 | 0.11 | < 0.10 | 0.11 | < 0.10 | 0.11 |
| Si | 25.0 | 25.1 | 25.5 | 26.2 | 26.6 | 26.8 | 24.0 | 25.4 | 25.6 |
| Sn | < 0.10 | < 0.10 | < 0.10 | < 0.10 | < 0.10 | < 0.10 | < 0.10 | < 0.10 | < 0.10 |
| Ti | < 0.10 | < 0.10 | < 0.10 | < 0.10 | < 0.10 | < 0.10 | < 0.10 | < 0.10 | < 0.10 |
| Zn | < 0.10 | < 0.10 | < 0.10 | < 0.10 | < 0.10 | < 0.10 | < 0.10 | < 0.10 | < 0.10 |

Using the equivalent oxide form, the data can be converted to waste loadings as seen in Table 3-30. The standard waste loading calculation uses $Fe_2O_3$. However, $Li_2O$ and $Al_2O_3$ were also included. All waste loadings are low except in SB9A-9A. Although the proper amount of frit was added based on the inputs and assumptions discussed in 2.3 Experimental Run Parameters, the resulting data indicates that less frit should be added in future experiments.

**Table 3-30. Waste Loadings**

| | SB9A-1A | SB9A-2A | SB9A-3A | SB9A-4A | SB9A-5A | SB9A-6A | SB9A-9A | SB9A-10A | SB9A-11A |
|---|---|---|---|---|---|---|---|---|---|
| $Fe_2O_3$ | 30.94% | 30.51% | 28.62% | 27.26% | 31.96% | 32.17% | 36.75% | 30.45% | 33.29% |
| $Li_2O$ | 29.32% | 29.28% | 27.75% | 27.69% | 24.80% | 24.46% | 34.13% | 4.25% | 29.74% |
| $Al_2O_3$ | 31.85% | 31.67% | 32.24% | 29.10% | 34.88% | 35.26% | 39.37% | 33.10% | 34.54% |

## 3.8 SRAT and SME Supernate Content

The elemental composition of the supernate sampled from the SRAT and SME products can be seen in Table 3-31.

**Table 3-31. Supernate Content in SRAT Product**

| mg/L | SB9A-1A, 145% | SB9A-2A, 105% | SB9A-3A, 130% | SB9A-4A, 130% | SB9A-5A, 125% | SB9A-6A, 120% | SB9A-7A, 120% | SB9A-8A, 120% | SB9A-9A, 120% Coupled | SB9A-10A, 120%, Extended | SB9A-11A, 120% $RuCl_3$ |
|---|---|---|---|---|---|---|---|---|---|---|---|
| Ag | < 1.00 | < 1.00 | < 1.00 | < 1.00 | < 1.00 | < 1.00 | < 1.00 | < 1.00 | < 1.00 | < 1.00 | < 1.00 |
| Al | 0.325 | 0.328 | 0.125 | 0.134 | < 1.00 | < 1.00 | 5.91 | < 1.00 | < 1.00 | < 1.00 | 1.04 |
| B | 27.0 | 26.7 | 30.2 | 24.7 | 17.2 | 24.3 | 76.8 | 37.7 | 139 | 37.2 | 35.3 |
| Ba | 0.48 | 0.386 | 0.152 | 0.163 | < 1.00 | < 1.00 | < 1.00 | < 1.00 | < 1.00 | < 1.00 | < 1.00 |
| Ca | 1460 | 812 | 439 | 385 | 986 | 449 | 733 | 406 | 271 | 375 | 450 |
| Cr | < 0.10 | < 0.10 | 0.179 | 0.154 | < 0.10 | < 0.10 | 0.688 | 0.328 | < 0.10 | < 0.10 | 0.230 |
| Cu | < 1.00 | < 1.00 | < 1.00 | < 1.00 | < 1.00 | < 1.00 | 12.7 | 0.125 | 0.142 | 0.154 | < 0.100 |
| Fe | < 0.100 | < 0.100 | < 0.100 | < 0.100 | < 1.000 | < 1.00 | 742 | < 1.00 | < 1.00 | < 1.00 | < 1.00 |
| K | 190 | 166 | 177 | 142 | 166 | 167 | 126 | 124 | 218 | 193 | 174 |
| Li | 82.2 | 84.1 | 63.0 | 55.8 | 56.2 | 57.0 | 72.2 | 74.0 | 54.5 | 54.0 | 67.2 |
| Mg | 197 | 243 | 396 | 347 | 242 | 374 | 314 | 338 | 304 | 365 | 335 |
| Mn | 1420 | 2290 | 7740 | 7050 | 2290 | 7780 | 13900 | 9995 | 5740 | 3370 | 10600 |
| Na | 31600 | 36250 | 35250 | 33100 | 32300 | 33600 | 27950 | 29150 | 47800 | 35500 | 34100 |
| Ni | 0.293 | 0.223 | 2.27 | 1.81 | < 1.00 | 1.99 | 672 | 14.2 | 0.976 | 2.98 | 8.93 |
| P | <10.0 | <10.0 | <10.0 | <10.0 | <10.0 | <10.0 | <10.0 | <10.0 | <10.0 | <10.0 | <10.0 |
| Pd | < 1.00 | < 1.00 | < 1.00 | < 1.00 | < 1.00 | < 1.00 | < 1.00 | < 1.00 | < 1.00 | < 1.00 | < 1.00 |
| Rh | 1.99 | < 1.00 | 1.96 | 1.36 | 1.97 | 1.61 | 1.40 | < 1.00 | < 1.00 | < 1.00 | < 1.00 |
| Ru | 10.91 | < 1.00 | 2.92 | 3.24 | 3.22 | < 1.00 | 2.07 | 1.35 | 1.01 | < 1.00 | < 1.00 |
| S | 301 | 360 | 526 | 441 | 364 | 464 | 493 | 425 | 723 | 454 | 470 |
| Si | 97.2 | 250 | 90.1 | 76.4 | 30.9 | 36.1 | 48.5 | 63.7 | 34.9 | 79.6 | 68.1 |
| Sn | 1.03 | 1.44 | 4.10 | 3.72 | < 1.00 | 3.54 | 7.70 | 5.46 | < 1.00 | < 1.00 | 6.52 |
| Ti | < 1.00 | < 1.00 | < 1.00 | < 1.00 | < 0.10 | < 0.10 | < 0.10 | < 0.10 | < 0.10 | < 0.10 | < 0.10 |
| Zn | < 1.00 | < 1.00 | < 1.00 | < 1.00 | < 0.10 | < 0.10 | 4.73 | < 0.10 | < 0.10 | < 0.10 | < 0.10 |
| Zr | < 1.00 | < 1.00 | < 1.00 | < 1.00 | < 0.10 | < 0.10 | < 0.10 | < 0.10 | < 0.10 | < 0.10 | < 0.10 |

Data from SB9A-7A is higher than all other runs. The increased presence of metals in the supernate could be a result of sludge solids in the filtered supernate sample or perhaps a result of the increased time exposed to acid. Mn solubility seemed to be increased in SB9A-11A in the SRAT products. There is a loose correlation to the amount of Mn in solution, and the amount of formic acid remaining at the end of the SRAT, which is reasonable given the reduction mechanism occurs via the interaction of Mn and formic acid.

**Table 3-32. Supernate Content in SME Product**

| mg/L | SB9A-1A, 145% | SB9A-2A, 105% | SB9A-3A, 130% | SB9A-4A, 130% | SB9A-5A, 125% | SB9A-6A, 120% | SB9A-9A, 120% Coupled | SB9A-10A, 120%, Extended | SB9A-11A, 120% $RuCl_3$ |
|---|---|---|---|---|---|---|---|---|---|
| Ag | < 1.00 | < 1.00 | < 1.00 | < 1.00 | < 1.00 | < 1.00 | < 1.00 | < 1.00 | < 1.00 |
| Al | 0.422 | 0.395 | 0.199 | 0.161 | < 1.00 | < 1.00 | 1.10 | < 1.00 | < 1.00 |
| B | 56.3 | 56.8 | 56.0 | 60.6 | 33.7 | 56.9 | 229 | 101 | 97.0 |
| Ba | 0.394 | 0.319 | 0.154 | 0.170 | < 1.00 | < 1.00 | < 1.00 | < 1.00 | < 1.00 |
| Ca | 1140 | 485 | 488 | 428 | 779 | 555 | 122 | 304 | 549 |
| Cr | 0.210 | 0.370 | 0.318 | 0.268 | < 0.10 | < 0.10 | < 0.10 | < 0.10 | 0.33 |
| Cu | < 1.00 | < 1.00 | < 1.00 | < 1.00 | < 1.00 | < 1.00 | 0.50 | 0.17 | 0.14 |
| Fe | 0.19 | 0.12 | < 0.10 | < 0.10 | < 1.00 | < 1.00 | 2.89 | 1.79 | < 1.00 |
| K | 211 | 174 | 189 | 131 | 193 | 185 | 243 | 201 | 191 |
| Li | 265 | 278 | 212 | 154 | 188 | 217 | 197 | 284 | 220 |
| Mg | 311 | 373 | 438 | 346 | 337 | 444 | 380 | 339 | 370 |
| Mn | 3891 | 5646 | 9770 | 8780 | 4820 | 10600 | 7730 | 539 | 12300 |
| Na | 36600 | 37600 | 38800 | 28500 | 36100 | 38500 | 53000 | 39100 | 38400 |
| Ni | 3.51 | 3.58 | 6.54 | 10.8 | 1.07 | 7.45 | 11.3 | 2.62 | 43.2 |
| P | <10.0 | <10.0 | <10.0 | <10.0 | <10.0 | <10.0 | <10.0 | <10.0 | <10.0 |
| Pd | < 1.00 | < 1.00 | < 1.00 | < 1.00 | < 1.00 | < 1.00 | < 1.00 | < 1.00 | < 1.00 |
| Rh | 2.39 | < 1.00 | 1.93 | 1.20 | 2.14 | 1.71 | < 1.00 | < 1.00 | < 1.00 |
| Ru | 4.03 | < 1.00 | < 1.00 | 2.06 | < 1.00 | < 1.00 | < 1.00 | < 1.00 | < 1.00 |
| S | 519 | 545 | 594 | 457 | 504 | 602 | 895 | 563 | 582 |
| Si | 417 | 485 | 77.1 | 104 | 34.0 | 45.7 | 46.5 | 704 | 161 |
| Sn | 2.37 | 3.30 | 5.64 | 4.93 | 2.15 | 5.20 | < 1.00 | < 1.00 | 7.47 |
| Ti | < 1.00 | < 1.00 | < 1.00 | < 1.00 | < 0.10 | < 0.10 | < 0.10 | < 0.10 | < 0.10 |
| Zn | < 1.00 | < 1.00 | < 1.00 | < 1.00 | < 0.10 | < 0.10 | < 0.10 | <0.10 | < 0.10 |
| Zr | < 1.00 | < 1.00 | < 1.00 | < 1.00 | < 0.10 | < 0.10 | < .010 | < 0.10 | < 0.10 |

Evaluating the elemental composition of the calcined solids and the supernate, on a per mass of slurry basis, allows the solubility of the elements to be determined. These can be seen in Table 3-33 and Table 3-34. It is important to note that SB9A-7A and SB9A-8A were stopped early after viewing the Rh and Ru hydrogen peaks. Zirconium, titanate, cadmium are often below detection limits in SRAT supernate samples. Sodium and potassium are generally fully soluble. Other cations like Ba, Ca, Cu, Mg, Mn, Ni, S, Si, and Zn exhibit a range of solubility during processing. When an element was fully in the supernate the result is listed as greater than (>), whereas if an element was not soluble it is listed as less than (<). Elements that are below detection limits in both the supernate and the slurry are listed as N/A. The difference between Table 3-33 and Table 3-34 is the addition of insoluble frit.

**Table 3-33. SRAT Product Elemental Solubility**

| | SB9A-1A, 145% | SB9A-2A, 105% | SB9A-3A, 130% | SB9A-4A, 130% | SB9A-5A, 125% | SB9A-6A, 120% | SB9A-7A, 120% | SB9A-8A, 120% | SB9A-9A, 120% Coupled | SB9A-10A, 120%, Extended | SB9A-11A, 120% $RuCl_3$ |
|---|---|---|---|---|---|---|---|---|---|---|---|
| Al | < | < | < | < | < | < | < | < | < | < | < |
| B | > | > | > | > | > | > | > | > | 28% | > | > |
| Ba | > | > | > | > | N/A | N/A | N/A | N/A | N/A | N/A | N/A |
| Ca | 56% | 28% | 15% | 14% | 34% | 17% | 28% | 15% | 9% | 12% | 15% |
| Cr | < | < | < | < | < | < | < | < | < | < | < |
| Cu | N/A | N/A | N/A | N/A | N/A | N/A | > | > | > | > | N/A |
| Fe | < | < | < | < | < | < | 2% | < | < | < | < |
| K | > | > | > | > | > | > | > | > | > | > | > |
| Li | > | > | > | > | > | > | > | > | > | > | > |
| Mg | 46% | 53% | 70% | 68% | 46% | 70% | 62% | 65% | 51% | 62% | 61% |
| Mn | 9% | 13% | 45% | 46% | 15% | 51% | 94% | 68% | 32% | 20% | 65% |
| Na | 107% | 112% | 105% | 109% | 113% | 117% | 103% | 106% | 102% | 103% | 103% |
| Ni | 0% | < | 0% | 0% | < | 0% | 23% | 0% | 0% | 0% | 0% |
| Rh | 5% | < | 5% | 5% | 5% | 5% | 6% | N/A | N/A | N/A | N/A |
| Ru | 1% | N/A | 0% | 1% | 1% | N/A | 1% | 1% | 0% | N/A | N/A |
| S | 1% | 0% | 1% | 1% | 1% | 1% | 1% | 1% | 0% | 0% | 0% |
| Si | 6% | 0% | 1% | 2% | 2% | 1% | 1% | 1% | 0% | 0% | 0% |
| Sn | > | > | > | > | > | N/A | > | > | N/A | N/A | > |

N/A denotes both supernate and calcined solids are below detection limit
> denotes calcined solids are below detection limit
< denotes supernate is below detection limit.

**Table 3-34. SME Product Elemental Solubility**

| | SB9A-1A, 145% | SB9A-2A, 105% | SB9A-3A, 130% | SB9A-4A, 130% | SB9A-5A, 125% | SB9A-6A, 120% | SB9A-9A, 120% Coupled | SB9A-10A, 120%, Extended | SB9A-11A, 120% $RuCl_3$ |
|---|---|---|---|---|---|---|---|---|---|
| Al | 0% | 0% | 0% | 0% | < | < | 0% | < | < |
| B | 1% | 0% | 0% | 1% | 0% | 0% | 2% | 0% | 1% |
| Ba | > | > | > | > | N/A | N/A | N/A | N/A | N/A |
| Ca | 39% | 15% | 17% | 20% | 28% | 19% | 4% | 11% | 19% |
| Cr | < | < | 0% | 0% | N/A | N/A | < | < | < |
| Cu | N/A | N/A | N/A | N/A | N/A | N/A | > | > | > |
| Fe | 0% | 0% | < | < | < | < | 0% | 0% | < |
| K | > | > | > | > | > | > | > | > | > |
| Li | 2% | 2% | 1% | 1% | 1% | 1% | 1% | 2% | 2% |
| Mg | 54% | 59% | 59% | 58% | > | > | > | > | > |
| Mn | 22% | 30% | 51% | 65% | 25% | 51% | 34% | 3% | 64% |
| Na | 61% | 57% | 57% | 55% | 59% | 57% | 74% | 68% | 60% |
| Ni | 0% | 0% | 0% | 0% | 0% | 0% | 0% | 0% | 1% |
| Rh | 1% | < | > | > | > | > | N/A | N/A | N/A |
| Ru | > | N/A | N/A | > | N/A | N/A | N/A | N/A | N/A |
| S | > | > | > | > | 0% | > | 0% | > | 0% |
| Si | 1% | 0% | 0% | 0% | 0% | 0% | 0% | 0% | 0% |
| Sn | > | > | > | > | > | > | N/A | N/A | > |

N/A denotes both supernate and calcined solids are below detection limit
> denotes calcined solids are below detection limit
< denotes supernate is below detection limit.

## 3.9 Scaling Differences

SB9A-4A was performed at the same time and using the same inputs as SB9A-3A. A significant difference between the peak hydrogen generation rates was seen; SB9A-3A produced 0.66 lb/hr, whereas SB9A-4A produced 0.41 lb/hr. (Both peak hydrogen generation rates occurred in the SRAT.) Correspondingly, the $CO_2$ was also 20.48 lb/hr different between the peak release rates. $N_2O$ generation rates were similar between the runs. There was also a slight (0.5 $W/cm^{2\circ}C$) difference in the heat transfer coefficients of the systems. Total mercury was considerably higher in SB9A-4A than SB9A-3A.

Given the differences, additional data was needed to better understand if scaling was impacting the results. Therefore, SB9A-7A was performed. Equipment issues caused a delay in the SB9A-7A processing that could adversely impact hydrogen release rates; therefore, the decision was made to repeat the experiment as SB9A-8A. SB9A-8A was performed at 120% and has identical inputs as SB9A-6A. The peak hydrogen generation rates between the runs were similar. The $CO_2$ release rate had a difference of 40.23 lb/hr, which is a slightly greater variance than seen in SB9A-3A and SB9A-4A. There was also a difference (38.1 lb/hr SB9A-6A and 28.6 lb/hr SB9A-8A) seen in peak $N_2O$ generation rates between the runs. The comparisons in off-gas conclude that the scaling of the vessel is not the significant cause of variation between off-gas results. The heat transfer coefficient in SB9A-8A was lower than SB9A-6A. Although SB9A-7A and SB9A-8A were stopped after viewing the hydrogen generation rate, the mercury results are higher than the 4L mercury sample results taken at a similar processing time indicating the 4L is superior at stripping mercury from the system. This is likely a combination of decreased heat transfer and the differences in the off-gas legs. The 1L off-gas leg is constructed of stainless steel, which has a

different heat transfer rate than glass in the 4L. Furthermore, the off-gas legs are of similar length. Thus, from a scaling standpoint, the path to the MWWT is longer for the 1L, which provides additional time for cooling and dropping out of mercury prior to reaching the condenser.

### 3.10 Rheology

Rheological properties of slurries are known to depend on particle size, insoluble solids content, pH, and ionic strength. Simulant development is performed to target slurry that is chemically representative of the sludge batch; therefore, the resulting rheological properties should be viewed for trends between the various acid additions. There is generally a yield stress maximum somewhere in or near the middle pH region (pH 6 - 8). Flow curves were obtained on SRAT product slurry samples and the SME product slurry samples from the flowsheet runs. Measurements were made at 25ºC. Weight percent insoluble solids, pH, and supernate sodium molarity, the major soluble cation and representative of the magnitude of ionic strength, were also included in Table 3-35.

**Table 3-35. Rheology**

| | | **SB9A-1A, 145%** | **SB9A-2A, 105%** | **SB9A-3A, 130%** | **SB9A-4A, 130%** | **SB9A-5A, 125%** | **SB9A-6A, 120%** | **SB9A-7A, 120%** | **SB9A-8A, 120%** | **SB9A-9A, 120% Coupled** | **SB9A-10A, 120%, Extended** | **SB9A-11A, 120% $RuCl_3$** |
|---|---|---|---|---|---|---|---|---|---|---|---|---|
| SRAT | Yield Stress, Pa (Up) | 1.11 | 2.27 | 1.45 | 1.25 | 1.28 | 1.39 | 0.41 | 0.78 | 5.97 | 2.06 | 1.50 |
| | Consistency, cP (Up) | 8.13 | 14.96 | 8.73 | 9.06 | 7.84 | 8.35 | 4.84 | 5.63 | 5.33 | 10.48 | 7.80 |
| | Yield Stress, Pa (down) | 0.85 | 1.93 | 1.10 | 0.85 | 1.05 | 1.05 | 0.35 | 0.65 | 5.23 | 1.49 | 1.14 |
| | Consistency, cP (down) | 6.01 | 10.90 | 7.37 | 6.87 | 6.94 | 7.28 | 4.83 | 5.29 | 4.57 | 7.31 | 6.56 |
| | wt.% Insoluble Solids | 13.7% | 13.9% | 13.7% | 12.9% | 13.5% | 12.5% | 11.0% | 11.2% | 13.9% | 13.6% | 12.8% |
| | Supernate Na, M | 1.37 | 1.58 | 1.53 | 1.44 | 1.41 | 1.46 | 1.22 | 1.27 | 2.08 | 1.54 | 1.48 |
| | pH | 8.29 | 8.12 | 7.65 | 7.66 | 8.08 | 7.82 | 5.09 | 7.00 | 7.85 | 7.25 | 7.26 |
| SME | Yield Stress, Pa (Up) | 7.13 | 8.99 | 8.25 | 3.15 | 7.38 | 8.31 | N/A | | 51.03 | 10.09 | 11.22 |
| | Consistency, cP (Up) | 24.83 | 41.61 | 35.81 | 19.97 | 31.16 | 38.48 | | | 91.98 | 51.62 | 38.94 |
| | Yield Stress, Pa (down) | 7.13 | 16.13 | 14.60 | 3.53 | 10.71 | 15.49 | | | 56.28 | 14.98 | 16.47 |
| | Consistency, cP (down) | 27.37 | 23.34 | 20.28 | 15.90 | 24.37 | 21.42 | | | 76.64 | 37.36 | 26.21 |
| | wt.% Insoluble Solids | 38.1% | 39.2% | 38.9% | 34.3% | 37.0% | 38.9% | | | 38.4% | 36.5% | 37.4% |
| | Supernate Na, M | 1.59 | 1.63 | 1.69 | 1.24 | 1.57 | 1.67 | | | 2.31 | 1.70 | 1.48 |
| | pH | 7.44 | 7.41 | 7.23 | 7.03 | 7.65 | 7.34 | | | 7.14 | 7.30 | 6.62 |

The SRAT design basis for yield stress and consistency is 1.5 - 5 Pa and 5 - 12 cP, whereas the SME design basis is 2.5 - 15 Pa and 10 - 40 cP. SB9A-7A and SB9A-8A were stopped early, thus they have not undergone complete conflux and are still thin sludge. As expected the high acid has the smallest yield stress and consistency of the actual SRAT products. The second thinnest sludge is SB9A-4A, which was also stopped slightly early (100 grams of water not removed) to prevent exposure of the heating rods. However, the equivalent 4L run, SB9A-3A, was thicker than both the 120% and 125% KMA runs. The

rheological parameters of SB9A-9A SRAT and SME products were above the DWPF design basis. The measured rheology of the SB9 qualification sample, HTF-51-15-81, (which contains the insoluble sodium) was 4.6 Pa and 6.9 cP [16]. The shielded cells SB9 SRAT and SME product rheology was 4.2 Pa/7.2 cP and 43 Pa/93 cP, respectively [16]. The SME product yield stress roughly decreases with increasing acid concentration, as expected. SB9A-6A is a little higher than expected for this trend. SB9A-4A is abnormally low and visibly thinner, which may be a result of the additional water, lower heat transfer and/or off-gas train.

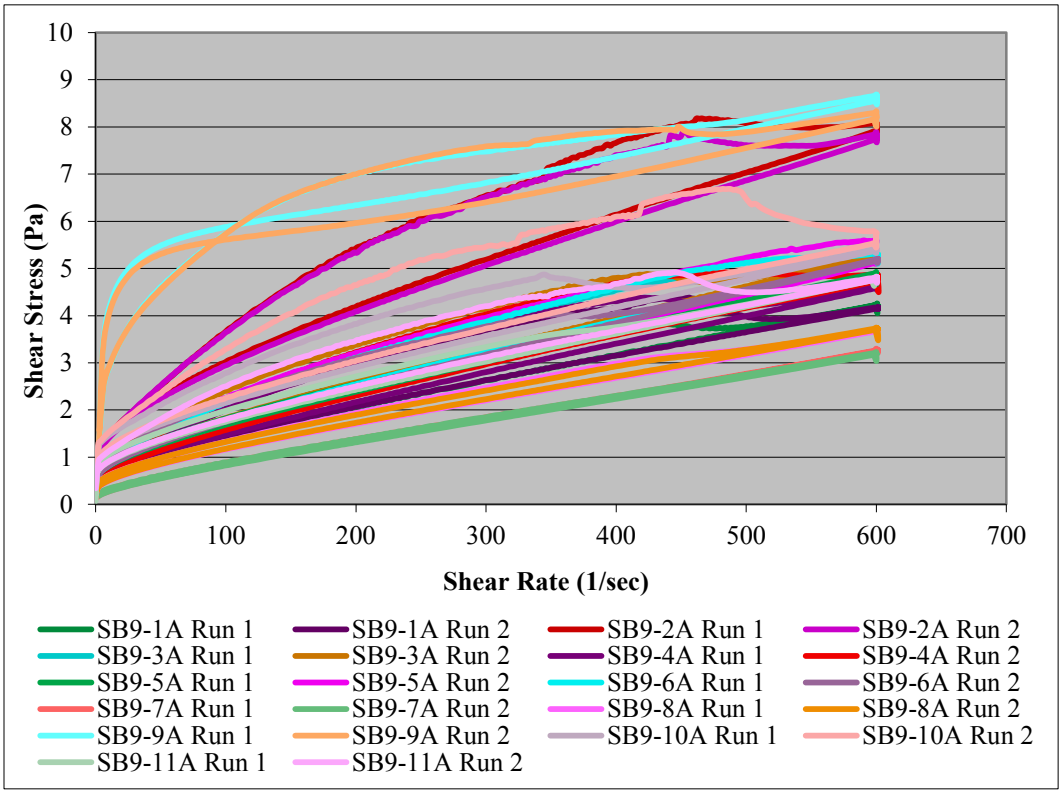


**Figure 3-31. Effective Viscosity of SRAT Product**

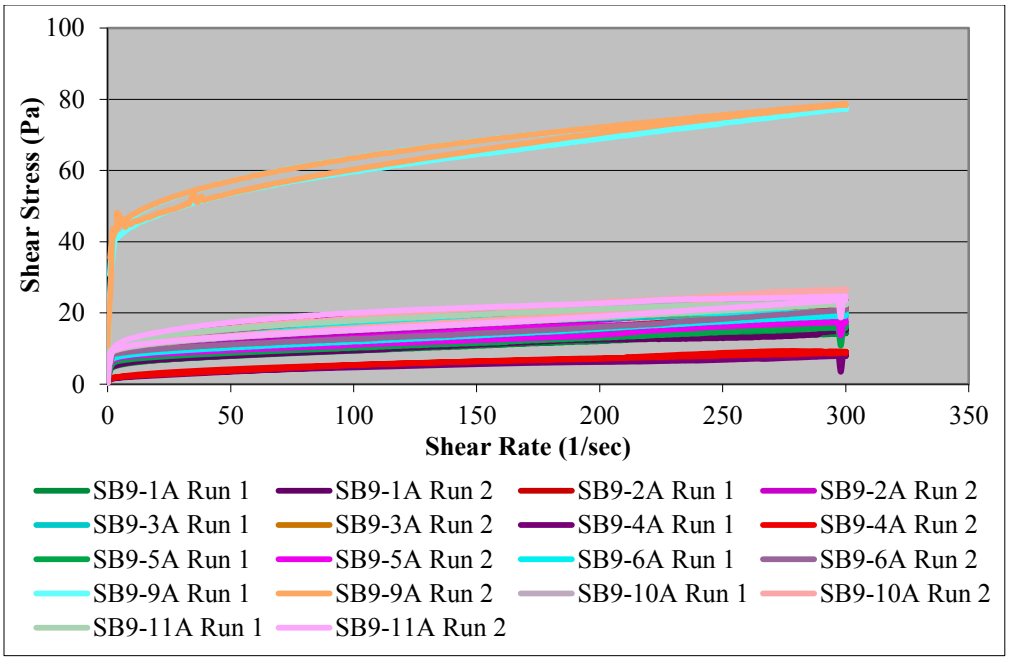


**Figure 3-32. Effective Viscosity of SME Product**

The SRAT product rheological measurements (see Figure 3-31) are fairly consistent, except in the case of SB9A-1A and SB9A-9A. There is also negligible hysteresis. The SME rheograms (see Figure 3-32) showed evidence of radial segregation (probably of the frit) leading to apparent hysteresis (down flow curves above up flow curves). The SME down portion of SB9A-9A run 2 shows some erratic behavior, which may be mild clumping of frit. SB9A-9A run 1 and run 2 exhibit a much higher shear stress than all other runs. The combination of higher sodium content and over concentration in the SME may have impacted rheology. Rheology was performed without the addition of 14 g of Na per kg slurry (added as sodium hydroxide), which was added to REDOX samples to mimic the insoluble sodium content in SB9. In the case of SB9A-9A this would have increased the SME product sodium to 2.32 M (a 0.24 M increase). Therefore, it is assumed that shear stress would be somewhat higher for SB9.

## 3.11 REDOX

The target REDOX was 0.15. The measured REDOX is compared to the calculated REDOX. The calculated REDOX equation can be seen in Equation 18. The concentration of $HCO_2$, $C_2O_2$, $NO_3$, Mn, and carbon from antifoam (AF C) used in the equation are in moles per kilogram of slurry. Total solids (TS) are in weight percent.

$$\frac{Fe^{+2}}{\sum Fe} = 0.2353 + 0.1999(2[HCO_2] + 4[C_2O_2] + 2.8815[\text{AF C}] - 5[NO_3] - X * Mn)\frac{45}{TS} \quad \text{Equation 18}$$

Note that the equation above has been abbreviated, and that the full equation includes additional terms for coal and the nitrite ion; these two species were negligible in SB9A simulant melter feed. The current Mn Electron Equivalent (EE) term in the DWPF REDOX equation is 5 (i.e. X = 5). Historically, this term has also been equal to 2 (i.e. Mn EE = 2). A separate memorandum will be issued formally evaluating the REDOX equation fit.

**Table 3-36. REDOX Results**

| | SB9A-1A, 145% | SB9A-2A, 105% | SB9A-3A, 130% | SB9A-4A, 130% | SB9A-5A, 125% | SB9A-6A, 120% | SB9A-9A, 120% | SB9A-10A, 120% | SB9A-11A, 120% |
|---|---|---|---|---|---|---|---|---|---|
| Measured | < 0.023 | 0.153 | 0.210 | 0.373 | 0.094 | 0.169 | 0.152 | 0.021 | 0. 181 |
| Calculated Mn EE = 5 | 0.08 | 0.17 | 0.26 | 0.27 | 0.09 | 0.10 | 0.16 | 0.08 | 0.14 |
| Calculated Mn EE = 2 | 0.19 | 0.27 | 0.36 | 0.36 | 0.20 | 0.22 | 0.24 | 0.20 | 0.25 |

Measured values and calculated values are fairly close except in SB9A-10A and SB9A-11A. The acceptable range for REDOX is 0.09 - 0.33. In SB9A-10A, the presence of additional $Fe^{+2}$ in the REDOX sample would indicate that the sludge was overly reduced. Analytical results indicate that it was slightly higher in formate and lower in nitrate than expected. SB9A-10A was performed at half the DWPF design basis boil-up rate. This caused the run to take about twice as long. As a result the equivalent amount of acid that was added for SB9A-6A was not sufficient enough to maintain REDOX control. The conversion and destruction inputs for SB9A-3A and SB9A-4A were different than the other runs, which resulted in an overly reduced glass, causing the assumed inputs to be changed back to the set used in SB9A-1A and SB9A-2A.

## 4.0 Recommendations

Based on testing results and observations, SRNL recommends the following future testing to better align simulant studies with the facility. These recommendations are not tied to the implementation of SB9.

1. Perform additional testing on the $Ru(NO)(NO_3)_3$ catalyst to evaluate impacts, if any, on nitrogen chemistry.
2. SRNL issue a white paper evaluating the optimal selection of noble metals based on impact of mercury stripping and gas chemistry.
3. Perform experiments in which SRR prioritizes evaluation of hydrogen generation, over the study of mercury stripping, with $RuCl_3$ for the nitric-formic CPC flowsheet.
4. Perform shielded cells qualification, or slurry chemistry focused experiments in the 4L vessel to increase flexibility. Increased volume decreases sensitivity to small fluctuations in processing.
5. For simulant testing during the next sludge batch, analyze selected mercury samples (2-3 condensate and 2 -3 slurry samples) by the digestion/CvAA Hg method and ICPES to compare method sensitivity, and evaluate path forward for future testing.

## 5.0 Conclusions

Eleven runs have been completed ranging from 105% to 145% KMA. One coupled flowsheet and one extended run was performed. Hydrogen exceeded, or was near the DWPF limits for runs above 120% (SB9A-1A 145%, SB9A-3A/SB9A-4A 130%, and SB9A-5A 125%). The results from the experiments show the use of a different Ru precursor, used to improve the evaluation of mercury stripping, have an impact on hydrogen, leading to increased formation of hydrogen in simulant experiments. The experimental plan calls for excess noble metals, independent of the catalyst type, to ensure hydrogen generation bounds standard DWPF processing conditions. Therefore, when the evaluation of hydrogen generation in the nitric-formic CPC flowsheet simulant testing is of more interest than mercury studies, the $RuCl_3$ precursor should be used. REDOX was acceptable for SB9A-6A 120%. **Based on nitrite decomposition, REDOX, and hydrogen generation the sludge batch 9 acid window is 105% to 120% of the KMA, which is equivalent to 109.7% - 125.4 % of the Hsu minimum acid factor**.

Nitrogen off-gas species, particularly $N_2O$, were significantly higher than seen in SB8. In all experiments nitrite was destroyed to less than detection. Mercury appears to have reached below 0.45 wt.% within the given conflux time for the 4L laboratory scale setup. The coupled run processing was bounded by the sludge-only flowsheet; however, the rheology was above the DWPF design basis. The rheology of SB9A-9A (SRAT: 5.97 Pa, 5.33 cP; SME: 51.03 Pa, 91.98 cP) was higher than the DWPF design basis, but significantly less than that of the shielded cells qualification run performed with real waste.

Separate memoranda will be issued providing the SRNL recommendation on the DWPF REDOX equation and starting operational conditions.

## 6.0 References


1. Bannochie, C.J., SRNL-STI-2013-00504, Revision 0. *Tank 40 Final Sludge Batch 8 Chemical Characterization Results,* September 2013.
2. Koopman, D.C. and J.R. Zamecnik, SRNL-STI-2013-00106, Revision 0. *DWPF Simulant CPC Studies for SB8,* June 2013.
3. Clark, M.C., X-TTR-S-00005, Revision 2. *Sludge Batch 9 Flow Sheet Studies,* November 3, 2015.
4. Martino, C.J., SRNL-RP-2014-01059, Revision 1. *Task Technical and Quality Assurance Plan for Sludge Batch 9 Simulant Flowsheet Studies,* November 4, 2015.
5. Smith, T.E., SRNL-L3100-2015-00224, Revision 0. *Recomendation for Sludge Batch 9 Qualification Processing Under the Nitric-Formic Flowsheet in the Sheilded Cells,* January 2016.
6. Johnson, F.C., T.B. Edwards, and D.K. Peeler, SRNL-MS-2015-00175, Revision 0. *SB9 Frit Development: MAR Results Based on the August 26-27, 2015 Projections*. 2015, Savannah River National Laboratory: Aiken, SC. August 31, 2015.
7. Shah, H.B. and M.A. Rios-Armstrong, SRR-LWP-2015-00037, Revision 0. *Sludge Batch 9 Qualification Blend Recommendation,* October 22, 2015.
8. Johnson, F.C., T.B. Edwards, and D.K. Peeler, SRNL-L3100-2015-00155, Revision 0. *Confirmation of Frit 803 for Sludge Batch 9,* October 23, 2015.
9. Thoman, D.C., S-CLC-S-00102, Revision 2. *ARP/DWPF with MCU-SE Coupled Operations Leaks and Spills (U),* April 2013.
10. Barrett, J.A., G-SYD-S-00054, Revision 13. *Sludge Feed Preparation System,* February 23, 2015.
11. Zamecnik, J.R. and D.C. Koopman, SRNL-STI-2012-00051, Revision 0. *Behavior of Mercury During DWPF Chemical Process Cell Processing,* January 2012.
12. Lambert, D.P., et al., SRNL-STI-2012-00018, Revision 1. *Glycolic-Nitric Acid Flowsheet Demonstration of the DWPF Chemical Process Cell with Sludge and Supernate Simulants,* August 2012.
13. Peters, T.B., SRNL-STI-2015-00372, Revision 0. *Tris(isodecyl)guanidine Degradation in the MCU System,* June 2016.
14. *International Union of Pure and Applied Chemistry Analytical Chemistry Division Commission on Solubility Data: Solubility Data Series*. ed. A.S. Kertes. Volume 23. Mercury(II) Oxide, ed. T.P. Dirkse. p. 307-317. Office of Data and Informatics of the National Institute of Standards and Technology (NIST) 2015.
15. Koopman, D.C., D.R. Best, and B.R. Pickenheim, WSRC-STI-2008-00131, Revision 0. *SRAT Chemistry and Acid Consumption during Simulated DWPF Melter Feed Preparation,* December 2008.
16. Pareizs, J.M. and C.J. Martino, SRNL-L3100-2016-00088, Revision 1. *Sludge Batch 9 SME Offgas, Weight Percent Solids, Density, and SRAT and SME Rheology,* May 19, 2016.

# 7.0 Appendix

## 7.1 Appendix A: Sludge Batch 9 Projections

**Table 7-1. SB9 Washed Elemental Projection**

| STATION | SB9 Tk 51 | SB9 Tk 40 |
|---|---|---|
| **DESCRIPTION** | **SB9 Assembled in Tank 51** | **SB9 Blend in Tank 40** |
| Calcine Solids Mass, kg | 165,079 | 316,565 |
| wt.%, Al | 8.95 | 9.00 |
| B | - | 0.02 |
| Ba | - | 0.06 |
| Ca | 1.33 | 1.29 |
| Ce | 0.23 | 0.25 |
| Cr | - | 0.05 |
| Cu | - | 0.05 |
| Fe | 22.96 | 22.37 |
| K | 0.14 | 0.14 |
| La | - | 0.04 |
| Li | - | 0.01 |
| Mg | 0.28 | 0.29 |
| Mn | 7.51 | 7.15 |
| Na | 18.88 | 18.87 |
| Ni | 0.99 | 1.62 |
| Pb | - | 0.02 |
| S | 0.21 | 0.34 |
| Si | 2.23 | 1.78 |
| Th | 1.01 | 1.04 |
| Ti | - | 0.01 |
| U | 3.96 | 4.45 |
| Zn | - | 0.02 |
| Zr | - | 0.05 |
| Hg | 3.40 | 2.48 |

**Table 7-2. SB9 Anion Projection**

| Tank 51 SB9 10/13/15 | SB9 End |
|---|---|
| Initial tank Level (in) | 68.24 |
| liquid volume (gal) | 191,159 |
| sludge volume (gal) | 13,270 |
| settled sludge level (in) | |
| kg insol. solids | 122,639 |
| wt.% insol solids | 13.90 |
| | |
| SpG, mol/L | 1.050 |
| Na, mol/L | 1.020 |
| NO2, mol/L | 0.324 |
| NO3, mol/L | 0.141 |
| OH, mol/L | 0.304 |
| Cl, mol/L | 0.001 |
| SO4, mol/L | 0.007 |
| F, mol/L | 0.001 |
| CO3, mol/L | 0.034 |
| AlO2, mol/L | 0.060 |
| C2O4, mol/L | 0.049 |
| PO4, mol/L | 0.000 |
| K, mol/L | 0.003 |

## 7.2 Appendix B: Off-gas Run Data

The off-gas trends for the individual runs can be seen below.

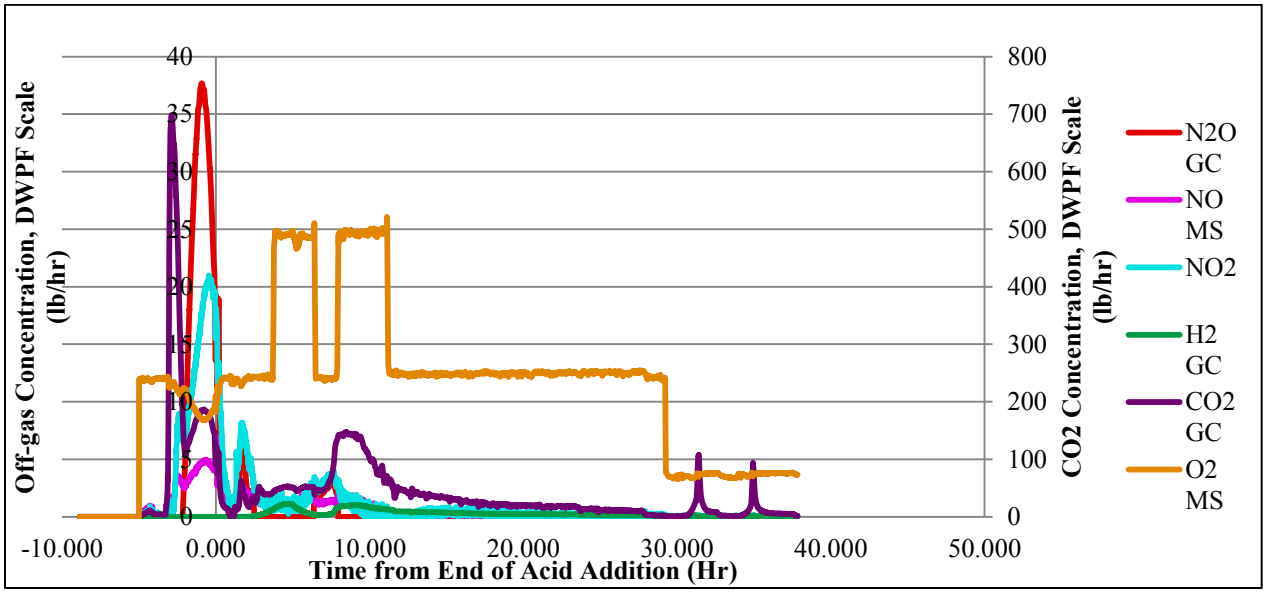


**Figure 7-1. Off-gas Spectra of SB9A-1A**

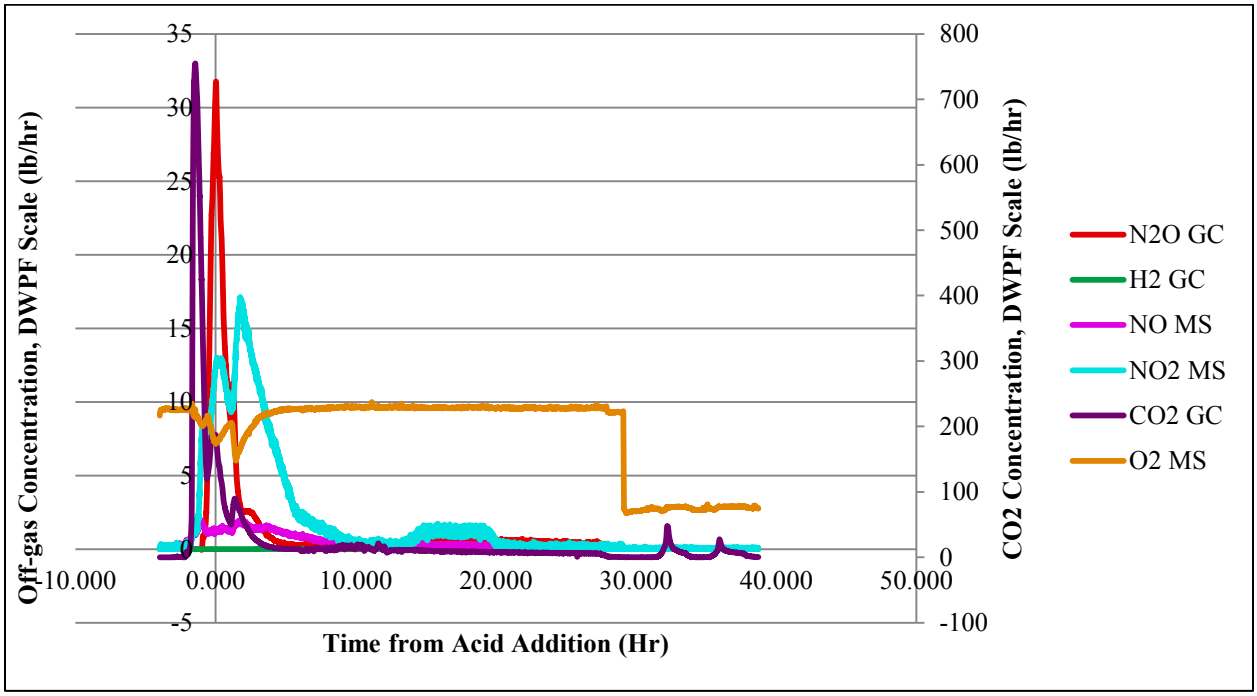


**Figure 7-2. Off-gas Spectra of SB9A-2A**

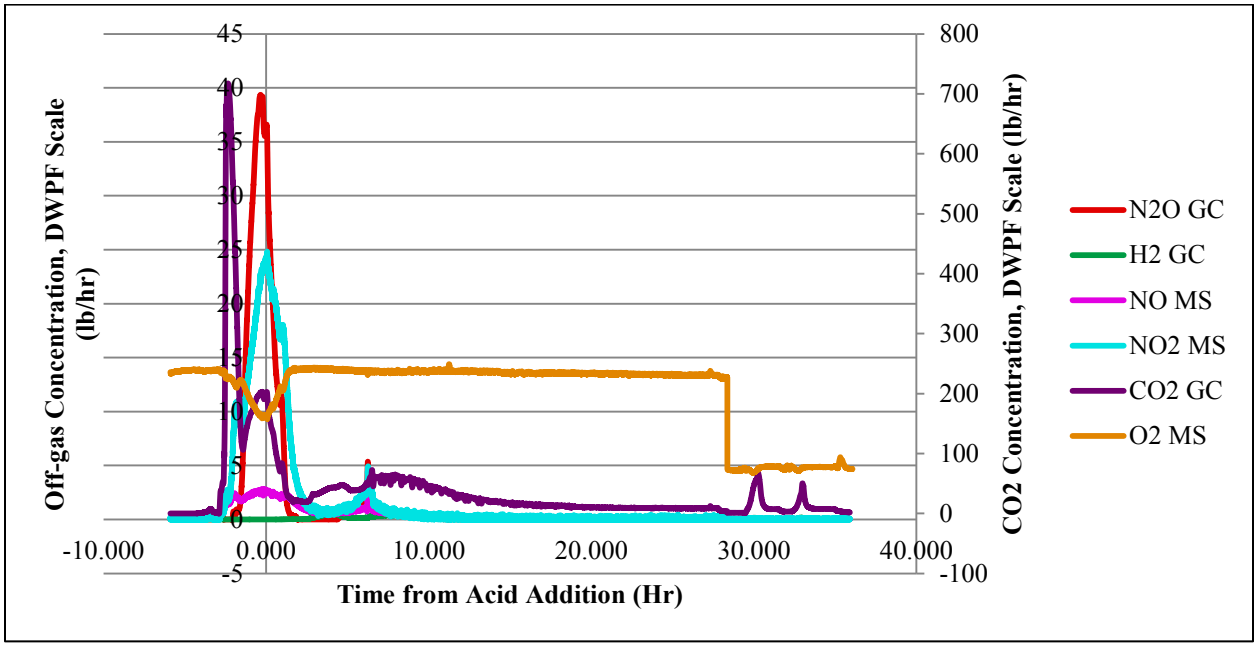


**Figure 7-3. Off-gas Spectra of SB9A-3A**

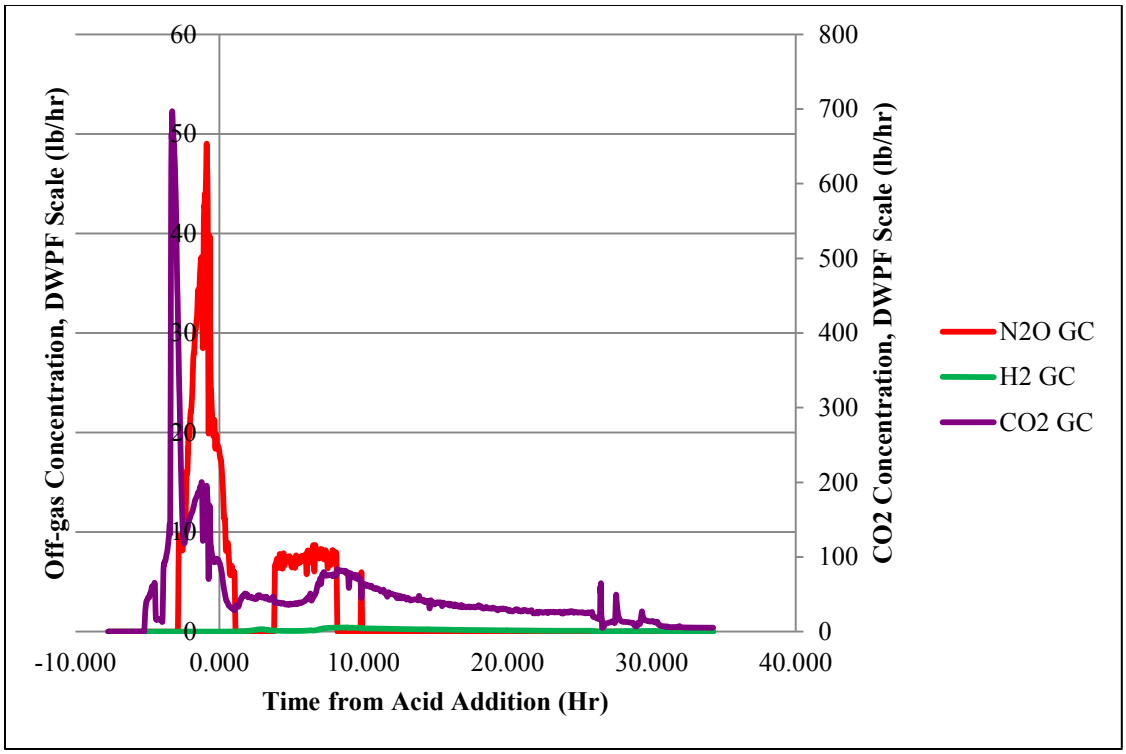


**Figure 7-4. Off-gas Spectra of SB9A-4A**

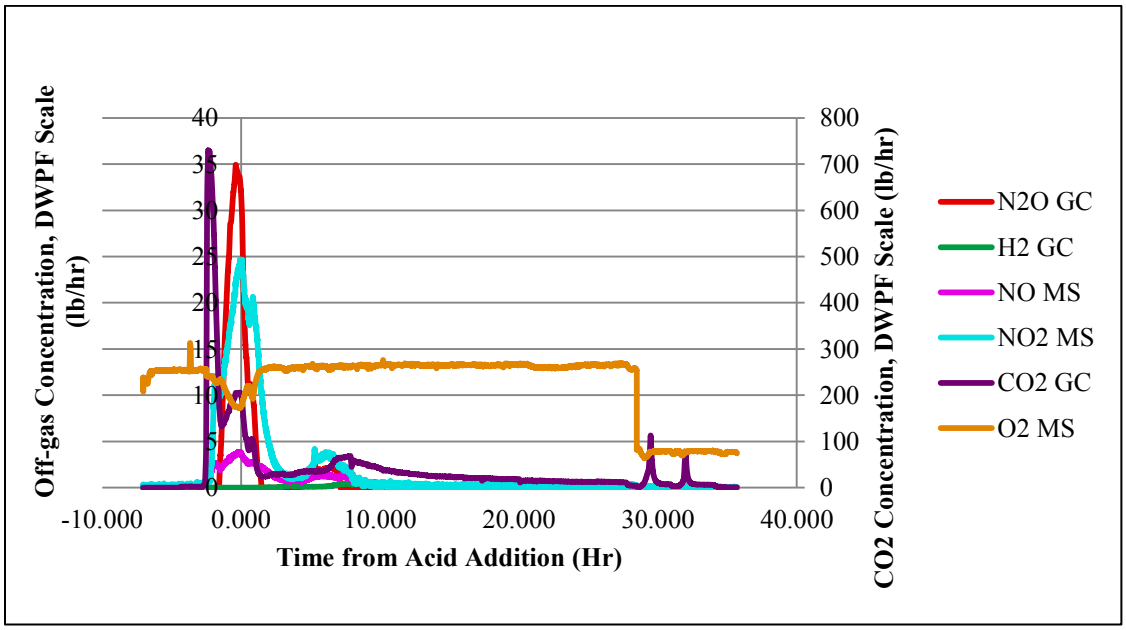


**Figure 7-5. Off-gas Spectra of SB9A-5A**

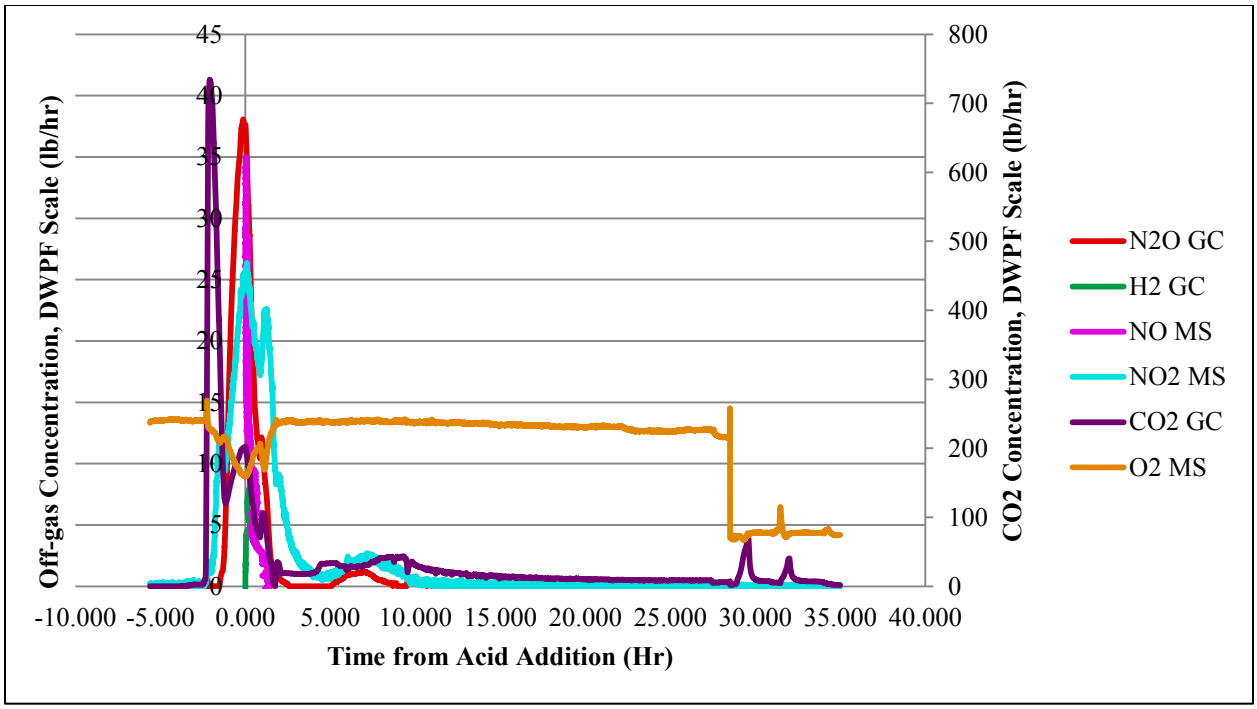


**Figure 7-6. Off-gas Spectra of SB9A-6A**

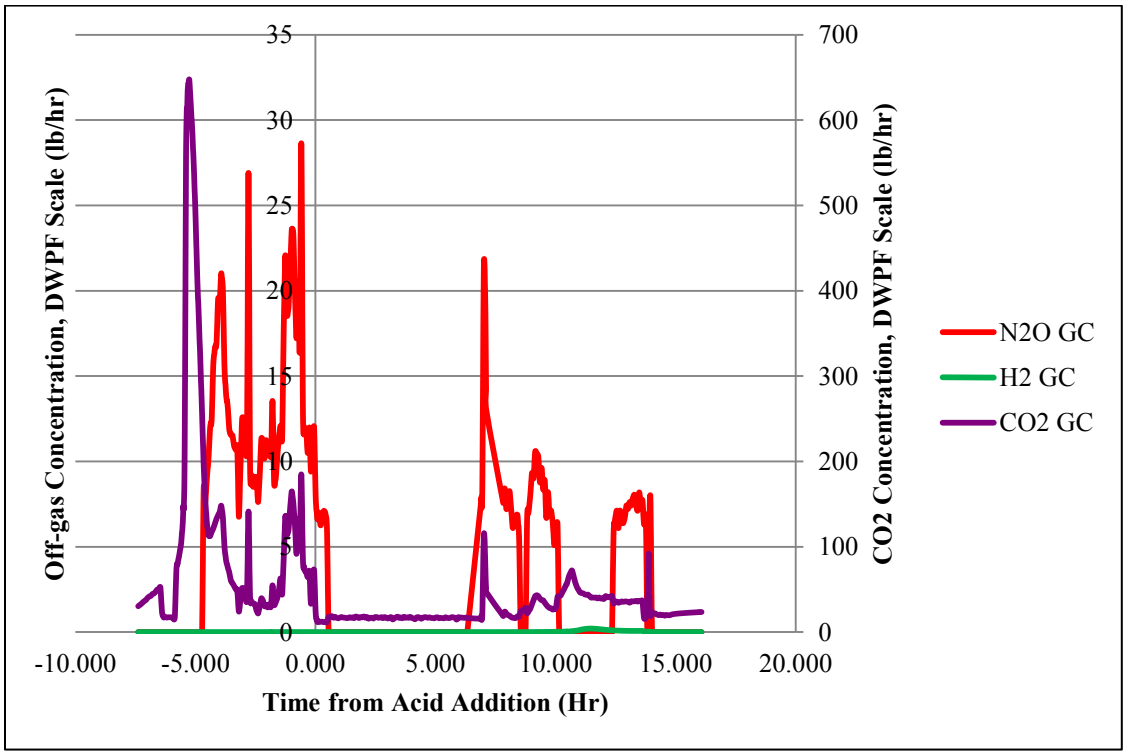


**Figure 7-7. Off-gas Spectra of SB9A-7A**

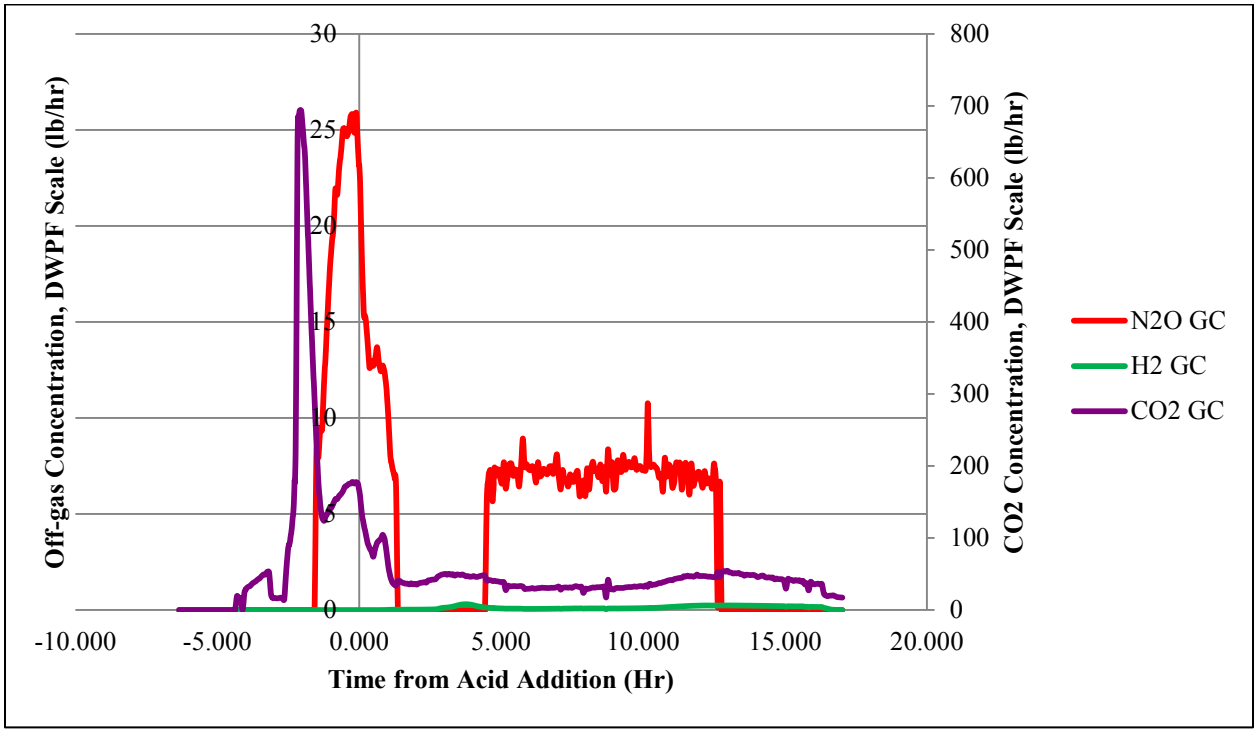


**Figure 7-8. Off-gas Spectra of SB9A-8A**

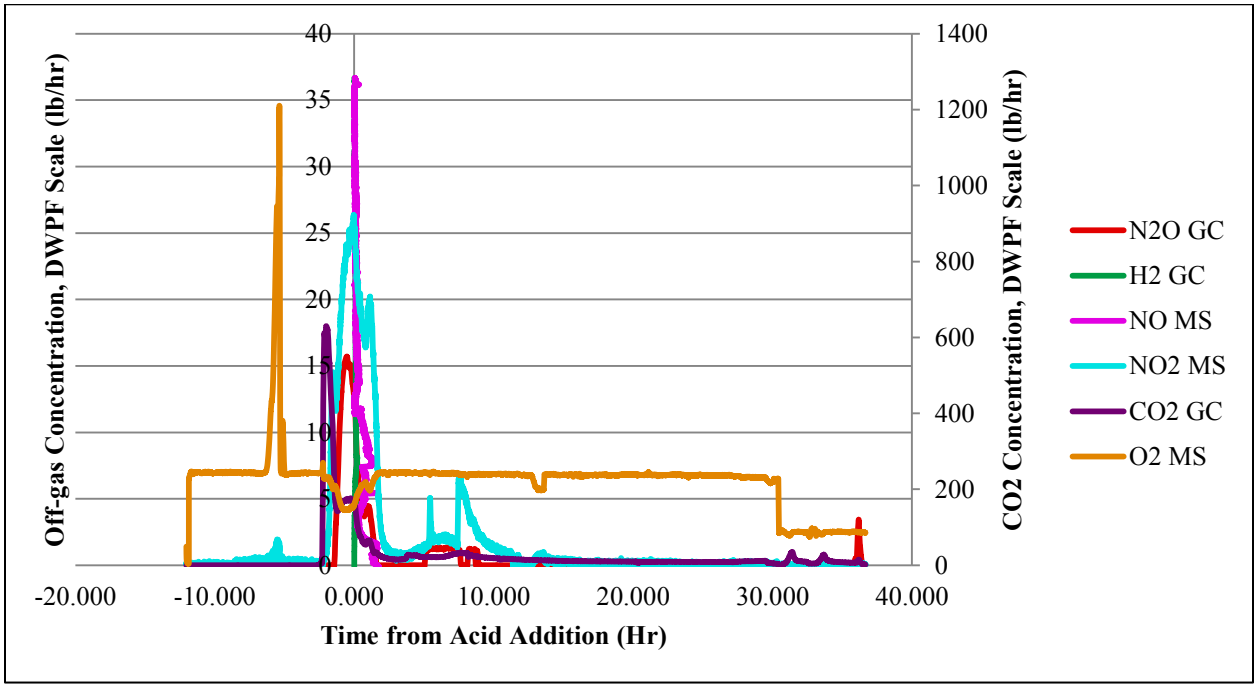


**Figure 7-9. Off-gas Spectra of SB9A-9A**

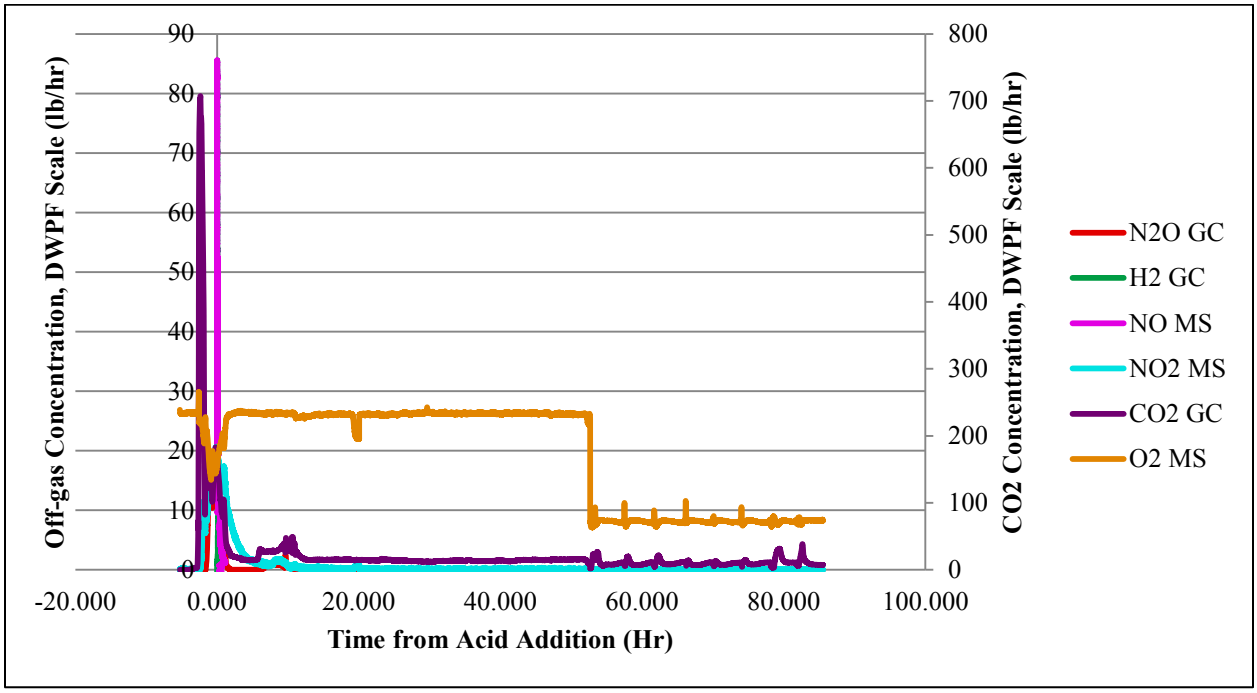


**Figure 7-10. Off-gas Spectra of SB9A-10A**

**Table 7-3. TIC and Ammonium Analytical Results**

| | | SB9A-1A | SB9A-2A | SB9A-3A | SB9A-4A | SB9A-5A | SB9A-6A | SB9A-7A | SB9A-8A | SB9A-9A | SB9A-10A | SB9A-11A |
|---|---|---|---|---|---|---|---|---|---|---|---|---|
| TIC, g C/kg | Dewater | 1.80E-02 | 1.16E-02 | < 0.004 | N/A | < 0.004 | < 0.004 | < 0.004 | < 0.004 | < 0.004 | < 0.004 | N/A |
| | SRAT | 1.01 | 1.63 | 6.48E-01 | N/A | 9.05E-01 | 6.45E-01 | N/A | N/A | 9.81E-01 | 1.13E+00 | < 3.53E-02 |
| | SME | 0.72 | 0.68 | 0.35 | 0.20 | 0.65 | 0.38 | N/A | N/A | 0.54 | 0.76 | < 3.53E-02 |
| Ammonium g $NH_4$/kg | Scrubber Post Acid Addition | N/A | N/A | < 0.01 | N/A | 1.09E-01 | < 2.5E-02 | N/A | N/A | 1.20E-02 | 1.50E-02 | < 1.00E-02 |
| | Dewater | N/A | N/A | N/A | < 0.01 | N/A | N/A | < 2.5E-02 | < 2.5E-02 | N/A | N/A | N/A |
| | SRAT Product | N/A | N/A | 8.25E-01 | 6.92E-01 | 4.09E-01 | 3.43E-01 | < 2.13E-02 | 3.86E-01 | 1.59E-01 | 4.29E-01 | 6.02E-02 |
| | Scrubber Post SRAT cycle | N/A | N/A | < 1.00E-02 | N/A | 3.11E-01 | 4.60E-02 | N/A | N/A | N/A | N/A | N/A |
| | SME Product | 3.10E-01 | 2.13E-02 | 5.61E-01 | 5.06E-01 | 1.25E-01 | 1.88E-01 | N/A | N/A | 1.57E-01 | 5.64E-02 | 5.51E-02 |
| | Scrubber Post SME Cycle | N/A | N/A | < 1.00E-02 | N/A | 4.06E-01 | 8.30E-02 | N/A | N/A | N/A | 3.80E-01 | < 1.00E-02 |

**Table 7-4. Concentration of Mercury in Sludge**

| | SB9A-1A | SB9A-2A | SB9A-3A | SB9A-4A | SB9A-5A | SB9A-6A | SB9A-7A | SB9A-8A | SB9A-9A | SB9A-10A | SB9A-11A |
|---|---|---|---|---|---|---|---|---|---|---|---|
| Starting mg/Kg | 2960.0 | 2910.0 | 2627.5 | 3065.0 | 2477.5 | 2830.0 | 3320.0 | 4245.0 | 3757.5 | 3602.5 | 5037.5 |
| After Acid Addition mg/Kg | 1247.5 | 1620.0 | 1387.5 | | 1.55 | 1337.5 | | | 4072.5 | 1240.0 | 4407.5 |
| During Reflux mg/Kg | 613.00 | 137.25 | 335.75 | - | 295.50 | 214.75 | - | - | 368.50 | 526.50 | 397.75 |
| | 148.25 | 88.85 | 112.50 | | 30.00 | 48.53 | | | 86.85 | 64.93 | 152.38 |
| SRAT Product mg/Kg | 78.58 | 73.98 | 87.00 | 170.00 | 25.13 | 8.76 | 313.50 | 519.00 | 108.05 | 48.45 | 57.65 |
| SME Product mg/Kg | 160.25 | 113.50 | 136.03 | 112.50 | 18.00 | 8.10 | | | 305.25 | 70.33 | 220.50 |

**Distribution:**

M. E. Cercy, 773-42A
D. A. Crowley, 773-43A
D. E. Dooley, 773-A
A. P. Fellinger. 773-42A
S. D. Fink, 773-A
C. C. Herman, 773-A
D. T. Hobbs, 773-A
E. N. Hoffman, 999-W
J. E. Hyatt, 773-A
K. M. Kostelnik, 773-42A
F. M. Pennebaker, 773-42A
G. N. Smoland, 773-42A
W. R. Wilmarth, 773-A
Records Administration (EDWS)
J. S. Contardi, 704-56H
M. C. Clark 773-67A
T. L. Fellinger, 766-H
E. J. Freed, 704-S
J. M. Gillam, 766-H
B. A. Hamm, 766-H
E. W. Holtzscheiter, 766-H
J. F. Iaukea, 704-27S
V. Jain, 766-H
C. J. Martino, 999-W
J. W. Ray, 704-27S
M. A. Rios-Armstrong, 766-H
H. B. Shah, 766-H
A. Samadi-Dezfouli, 704-27S
J.M. Pareizs, 773-A
R.J. Mcnew, 766-H
P. R. Jackson, DOE-SR, 703-46A
J. A. Crenshaw, 703-46A